ACKNOWLEDGEMENT

The author wishes to express his graditude and deep appreciation to his thesis supervisors, Dr. J. Svoboda and DR. C.K. Kwok for initiating the project and providing continued guidance throughout the investigation.

The author appreciates the cooperation of Ritepro Inc. and the technical assistance given. The author also wishes to express his thanks to Mr. R. Blakely and Mr. H. Hong for preparing the manuscripts. Thanks is also extended to Mr. N. Krouglicof and Mr. W. Fitch for their assistance.

This work is supported by the Natural Sciences and Engineering Research Council of Canada under a grant for Project Research Applicable in Industry.

TABLE OF CONTENTS

LIST OF FIGURES

LIST OF TABLES

NOMENCLATURE

A_{cx}	=	close plunger discharge area, in^2
A_{ox}	=	open plunger discharge area, in^2
A_o	=	effective orifice area, in^2
A_p	=	piston side piston area, in^2
A_r	=	rod side piston area, in^2
A_v	=	needle valve orifice area, in^2
B	=	viscous damping coefficient, $in\text{-}lb_f/sec$
C_d	=	discharge coefficient
C_e	=	external leakage coefficient, $in^3/sec/psi$
C_i	=	internal leakage coefficient, $in^3/sec/psi$
C_1	=	close plunger straight length, in
C_2	=	close plunger tapper length, in
C_3	=	close plunger clearance, in
D_1	=	plunger piston diameter, in
D_2	=	plunger diameter, in
F	=	force generated or developed by piston, lb_f
F_f	=	friction force, lb_f
I	=	lumped inertia, $slug\text{-}in^2$
K	=	load spring gradient, lb_f/in
M_t	=	total mass of piston and load, $lb_f\text{-}sec^2/in$
O_1	=	open plunger straight length, in
O_2	=	open plunger tapper length, in
O_3	=	open plunger clearance, in
$\overline{OA}$	=	torque lever, counter weight lever, in
$\overline{OB}$	=	reference pivot distance, flapper weight lever, in

P = hydraulic pressure, psi

P_a = accumulator pressure, psi

P_{atm} = atmospheric pressure, psi

P_{ao} = initial accumulator pressure, psi

P_{af} = final accumulator pressure, psi

P_p = piston end pressure, psi

P_r = rod end pressure, psi

P_1 = upstream pressure, psi

P_2 = downstream pressure, psi

Q = fluid flow, in^3/sec

Q_1 = rod end fluid flow, in^3/sec

Q_2 = piston end fluid flow, in^3/sec

Q_a = accumulator fluid flow, in^3/sec

R = equivalent fluid resistance, $lb\text{-}sec^2/in^8$

R_c = check valve resistance coefficient, $lb\text{-}sec^2/in^8$

R_p = pinion radius, in

R_l = lower cushion resistance coefficient, $lb\text{-}sec^2/in^8$

R_u = upper cushion resistance coefficient, $lb\text{-}sec^2/in^8$

R_v = needle valve resistance coefficient, $lb\text{-}sec^2/in^8$

T_{ao} = initial accumulator temperature, °R

T_{af} = final accumulator temperature, °R

T_{cy} = torque generated by actuator, $lb_f\text{-}in$

T_o = valve opening torque, $lb_f\text{-}in$

U_1 = upstream fluid velocity, in/sec

U_2 = downstream fluid velovity, in/sec

V_a = accumulator volume, in^3

V_{af} = final accumulator volume, in^3

V_{ao} = initial accumulator volume, in^3

V_{ro} = initial rod side chamber volume, in^3

V_p = piston end chamber volume, in^3

V_r = rod end chamber volume, in^3

W_b = counter weight, lb_f

W_f = flapper weight, lb_f

X = plunger displacement, in

X_p = piston displacement, in

$\dot{X}_p$ = piston velocity, in/sec

Y = actuator displacement, in

$\dot{Y}$ = actuator velocity, in/sec

Y_{lc} = actuator lower cushion limit, in

Y_{uc} = actuator upper cushion limit, in

α = torque angle, counter weight angle, rad

β_e = effective bulk modulus, psi

θ = valve disk angle, rad

θ_{max} = maximum disk angle, rad

θ_{min} = minimum disk angle, rad

θ_o = initial valve disk displacement, rad

$\dot{\theta}$ = valve disk angular velocity, rad/sec

$\dot{\theta}_o$ = initial valve disk angular velocity, rad/sec

ρ = mass density, $lb\text{-}sec^2/in^4$

CHAPTER 1

INTRODUCTION

1.1 General

Check valves are essential components in fluid pipe lines since they prevent flow reversal. The detrimental effects of reversed flow include water hammer, driving a failed pump in the reverse direction and leakage of downstream fluid from ruptured pipes. Thus the check valve is a safety device. The penalty to achieve safety is the development of a pressure drop across the valve and the possible creation of high pressure transients in the pipe during valve closure. As a result, optimum design for these valves involves minimizing pressure loss and controlling the valve dynamics. At the same time simplicity, compactness and check valve function must be retained.

Aiming at optimal design of wafer-type swing-disk check valves, a research project is currently in progress at Concordia University. It is directed into two major problem areas:

1. A study of energy loses and their minimization
2. A study of valve dynamics to limit pressure surges and mechanical shocks.

The interaction between these effects is shown in figure 1-1.

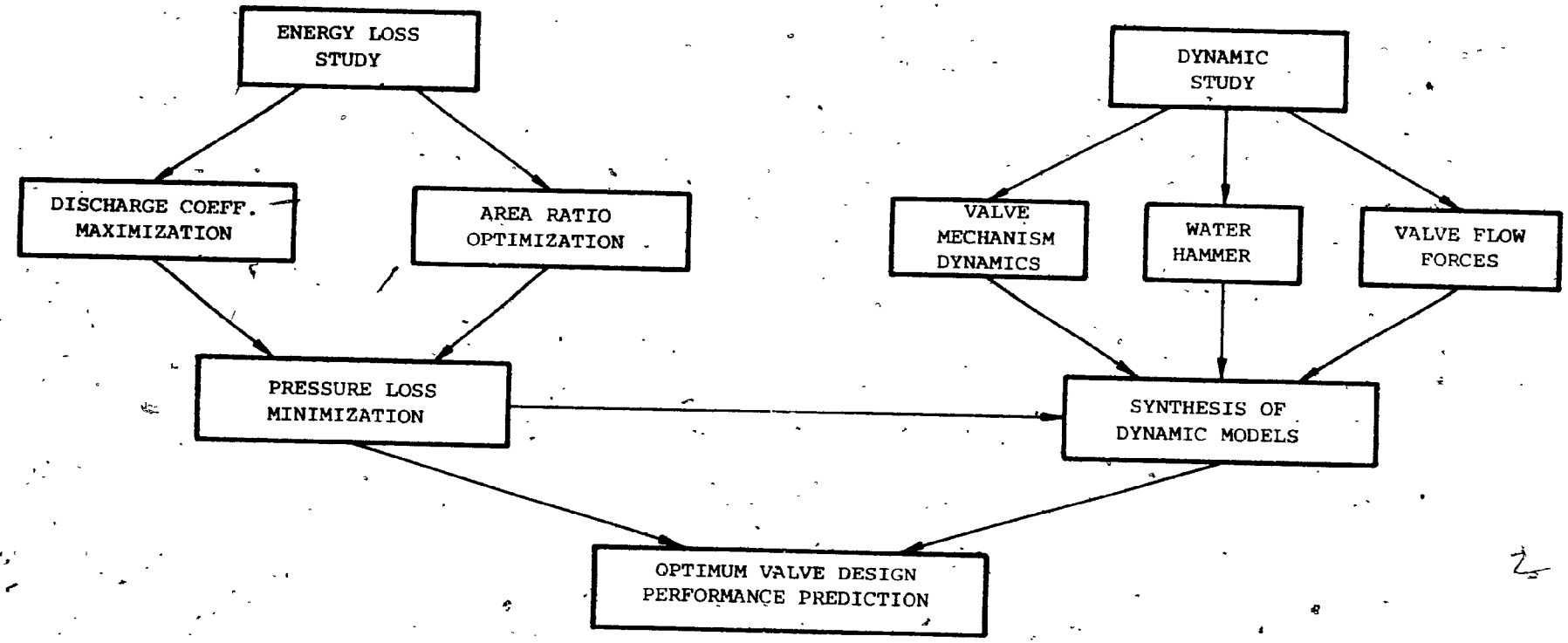

Figure 1-1 Check Valve Design Problem Areas and Their Interactions

There are two main aspects in the energy loss investigation. One aspect is the alteration of the discharge coefficient and the minor loss factors associated with the valve geometry. The other aspect is the passage area ratio effects.

The valve dynamics investigation is divided into three distinct areas. These include the valve mechanism dynamics, the valve flow forces and fluid transients caused by valve closure.

This work is an attempt to obtain adequate analytical models of the valve mechanism - the first step in the valve dynamic study. Analytical models are developed for two check valve mechanisms and programmed for computer solution. Both models relate the angular position of the valve disk to an input torque. One of the check valve mechanisms is based on a hydro-pneumatic closing spring and the other on a counter weight closing system. Experiments are then performed to confirm the adequacy of the models.

The emphasis in this investigation is given to the study of the current wafer-type swing check design so that its advantages can be retained. At the same time the limitations of the present valve are established and design guidelines to improve valve performance are developed.

1.2. Review of Previous Work

Hydraulic performance of check valves has been the subject of several investigations.

Csemniczky [1] showed that the moment acting on the wafer shaft created by the fluid force on a valve disk depends not only upon the disk angle but also on the location of the disk pivot. In his work, a half-empirical formula was developed to determine the influence of the pivot location on the hydraulic parameters such as pressure drop and moment acting on the shaft. The importance of kinematic design has been considered in conjunction with the performance characteristics of the check valve.

Krane and Cho [2] examined the hydraulic performance characteristics of a swing-disk check valve. In particular, design parameters affecting the pressure drop, flow reversal and surge pressure were considered. In their experimental results, the pressure loss was expressed as a function of disk angle and Reynolds' number, A method of calculating fluid torque on a moving disk was described. It was shown that the fluid torque was mainly dependent on the pressure drop across the valve. The friction between moving parts of the valve was expressed as a function of the reverse flow. The surge pressure was estimated by a function of contact angle of the disk together with the known initial pressure

of the dash-pot.

Gwinn's [3] graphical method shows that the estimation for a valve disk closure impact speed under trip loads could assist the piping network design.

Uram [4] presented an interpretation of the valve disk dynamics. The motion of the disk assembly about the wafer shaft was considered to be function of the drag force moment, moment due to disk weight, and the moment due to the pressure differential across the valve. By comparing the order of magnitudes of these three moments, the former two are usually small and can be neglected. Therefore, the motion of valve disk can be estimated if the pressure drop across the valve is known. This is in agreement with Krane and Cho [2].

Esleeck and Rosser [5] investigated the check valve water hammer characteristics. They have shown that the problem of check valve water hammer could be reduced to a second order differential equation of motion. The disk motion was analyzed using a moment equation consisting of the following forces: the disk weight and inertia, the spring torsion, and the reaction between the water and the disk. The last item is similar to the drag force moment and moment due to pressure differential across the valve mentioned by Uram [4]. Esleeck and Rosser [5] concluded that no simple type

of valve could be designed to achieve complete elimination of water hammer effects. However minimization of the effects could be achieved. This is done by intensive tests and calculations to determine the proper combination of disk weight, shape, pivot location etc.

Extensive investigations on check valve related pressure surges have been conducted by Pool [6] and Porwit, Carlton and Pool [7]. They found that it was possible to predict the surge pressure accurately from the basic design parameters of pivoting check valves.

It follows from the above that a well designed check valve should be able to keep surge pressure, pressure loss and reverse flow within acceptable limits.

1.3. General Check Valve Design Factors

Since all valve mechanisms contain a finite amount of inertia and friction, the valve will close sometime after the start of the flow reversal. If the closure is fast, as it would be in quick-action valves, the sudden stoppage of a small amount of reverse flow will produce a large pressure surge which might cause significant damages to the piping system and the valve. On the other hand, if the valve closes too slowly an excessive reverse flow is introduced,

which is not desired either. In addition to the above, there is the problem of the pressure drop across the valve. A close inspection of the valve shows two restrictions in series as shown in figure 1-2. The first restriction is formed by the valve seat orifice. The second restriction depends on the area between the tilted swing-disk and the pipe inside diameter. Obviously, for every piping system, there must exist a certain valve closing pattern resulting in an acceptable pressure surge and reverse flow. To reduce pressure loss, Svoboda, Katz and Fitch [8] used a smooth valve seat orific entrance as well as a favourable valve seat to pipe size ratio.

In general, check valve specifications should include pressure drop across the valve, allowance for the maximum amount of reverse flow during closure as well as the limitations on the maximum amount of surge pressure. The check valve design will then strive to achieve an optimum performance.

The check valve design incorperates a disk which swings on a hinge. The selection of the most suitable pattern and size is determined by the number of parameters, such as working pressure and temperature, velocity of fluid, permissible friction losses etc. Table 1-1 summarizes the applications of various type of check valves.

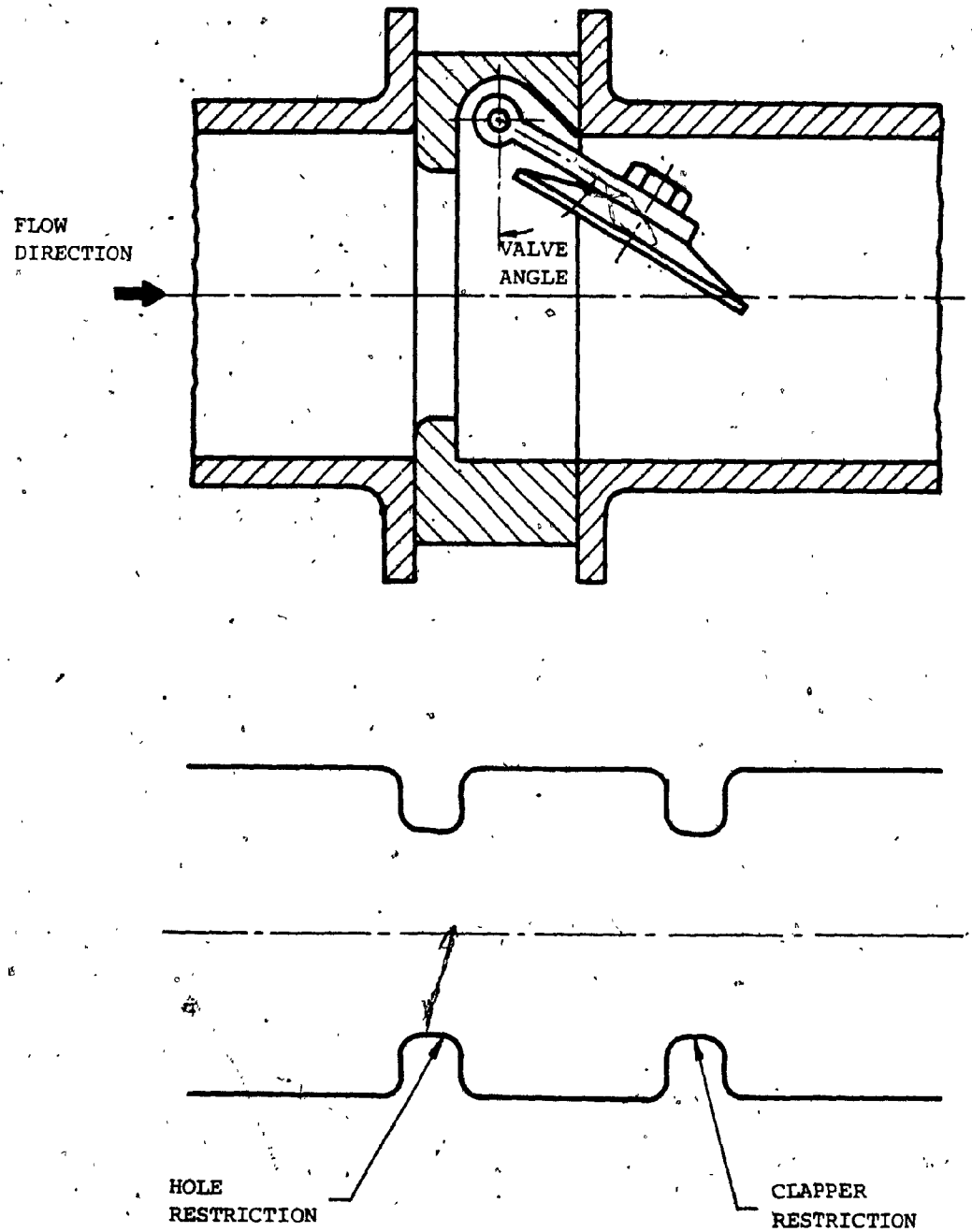

Figure 1-2 Flow Model for Wafer Type Swing Check Valve

	Ball	Butter Fly	Gate	Globe	Pinch	Plug	Poppet	Swing
Check Valve	P	P	P	P	P	P	G	G
Contamination free	G	F	G	G	G	G	F	P
Corrosive Fluid	G	P	F - G	F	F - G	P - F	G	G
Cryogenic Fluid	G	P	P	G	P	P	G	P
Gases	G	G	G	G	G	G	G	G
High ΔP	P	P	F	G	P	F	F	P
High Flow	G	G	G	G	G	G	G	G
High Pressure	G	P	P	G	P	P	G	P
High Temperature	G	G	G	G	P	P	G	P
Leak Tight	G	P	G	G	G	G	G	P
Light Weight	G	G	F	P	F	G	G	G
Low Actuation Force	P	P	P	P	P	P	G	G
Low Cost	G	F - G	G	F - G	G	G	G	G
Low ΔP	G	G	G	P	G	G	G	G
Low Flow Control	G	G	P	G	F	G	G	G
Rapid Opening	G	G	P	F - P	P	G	G	G
Liquids	G	G	G	G	G	G	G	G
Relief	P	P	P	P	P	P	G	P

P = Poor F = Fair G = Good

Table 1-1 Aplication of Various Type of Check Valve

One of the major criteria in check valve design is the regulation of the closure speed and the elimination of the slamming action in the final stages of closure. There are many techniques used in valve design to counteract the slamming action. Some examples include extended hinge shaft with weight and lever, spring loaded or external dash-pot. Ideally every check valve mechanism should be designed in regard to each pipe flow condition

1.4. Objective of the Project

As discussed earlier, the optimal design of the check valve entails the minimization of the pressure loss and a proper control of the valve dynamics. It is important that maximum surging pressure and mechanical shocks must be kept within acceptable limits during the valve closing and opening. This thesis deals with the initial step in the optimal check valve design - the development of a realistic analytical model of two hydraulically damped check valves.

(i) hydro-pneumatic spring closing valve

(ii) counter weight closing valve

These values are selected for their system damping flexibility and control, as well as their wide industrial usage. The models will be used in further investigations of the valve flow forces and the water hammer effects during closure.

To make the models realistic, all system parameters are sized according to actual specifications. Following the mathematical model formulations, computer models are developed using MIMIC, a digital simulation language. With the computer models, the valve dynamic performances and the system parameters effects are studied in detail.

For a qualitative evaluation of the simulated responses, an experiment is set up for the hydro-pneumatic spring closing check valve. Since both valves investigated in this thesis, i.e. hydro-pneumatic type and the counter weight type, are operated on a similar principle, the experimental evaluation of the hydro-pneumatic type valve is sufficient.

CHAPTER 2

SYSTEM DESCRIPTION

2.1. Introduction

The most common mechanism used in check valve design is the spring return mechanism. This mechanism is simple and maintenance free. However, it has several drawbacks. This mechanism can be described as an undamped system when mechanical friction is small and neglegible. As a result of the undamped characteristics, the disk movement has a tendancy of following the fluid flow closely. During any flow reversal or sudden stoppage of flow, the valve will act as a quick-action valve. Mechanical shock can be created by the valve-disk slamming against the valve seat during rapid closure. At the same time, a significant water hammer surge pressure occurs. Both mechanical shocks and surge pressure are very destructive and not desirable. The application of a spring return valve in small size piping networks is generally adequate. The problem of water hammer becomes more acute as the valve size increases. Ignoring these problems may lead to the failure of the entire system. It becomes necessary to control the valve closing and opening. A hydraulic damper is an attractive solution for such a control task.

2.2. System Description of the Hydro-Pneumatic Spring Closing Valve

Figure 2-1 depicts the schematics of the hydro-pneumatic spring closing valve. The valve is closed by a hydraulic accumulator spring (5) via the the actuator (2). Dynamics of the valve closure can be controlled by the viscous resistor (4) which can be adjusted according to the damping requirements. Valve closure can be slowed down in order to reduce surge pressures to acceptable levels. With the actuator's upper cushion adjustment, the slamming of the valve disk against the valve seat during closing can be reduced to a minimum. Valve opening depends on the net force difference between the actuator (2) and the opening torque (T_o). Both upper and lower cushions of the actuator (2) are used to reduce mechanical shocks while valve disk approaches its extreme positions i.e. completely open or closed.

The hydraulic spring closing torque on the disk valve is created in actuator (2) by the area difference between (A_r) and (A_p). Valve opening torque (T_o) is created by fluid flow against the valve disk. When the opening torque (T_o) at the pivot point (0) exceeds the hydraulic spring closing torque, the valve disk will open causing the piston actuator (2) to retract. Due to the difference in area between (A_r) and (A_p), the displaced flow rate (Q_2) will be greater

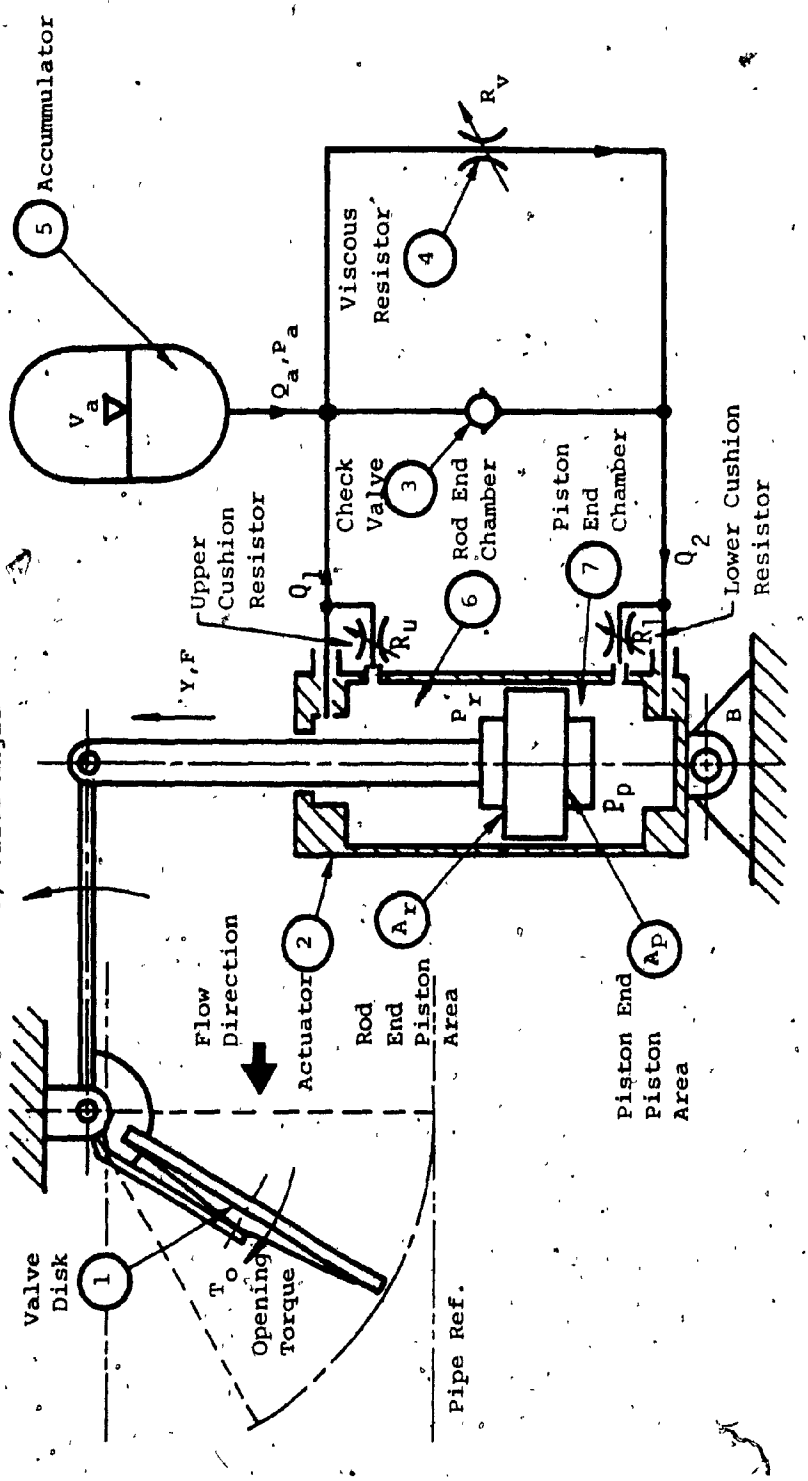

Figure 2-1 Schematic Diagram of Hydro-Pneumatic Spring Closing Valve

than that of (Q_1). The difference in flow is balanced by the delivery of fluid through check valve (3) into accumulator (5).

The opening operation produces a flow difference across the actuator (2) and results in increasing the energy stored in accumulator (5). When the opening torque is removed, the differential force across the piston of actuator (2) will cause the piston to extend and the disk valve to close. Stored oil is discharged from accumulator (5) via the adjustable needle valve (4). Thus variable viscous damping is obtained during closure.

2.3. System Description of the Counter Weight Closing Valve

Figure 2-2 shows the mechanical schematics of the counter weight closing check valve. The torque generated to close the clapper (B) results from the combined torsional moment due to the weight of the clapper (W_f) and the counter weight (W_b). ($\overline{OA}$) and ($\overline{OB}$) represent, respectively, the cantilever lengths from the weights (W_f) and (W_b) to the valve disk pivot (O). Torque generated at point (O) is transmitted through the pinion (5) to the rack (3), which in turn drives the plungers (1) and (2). In the closing operation, the

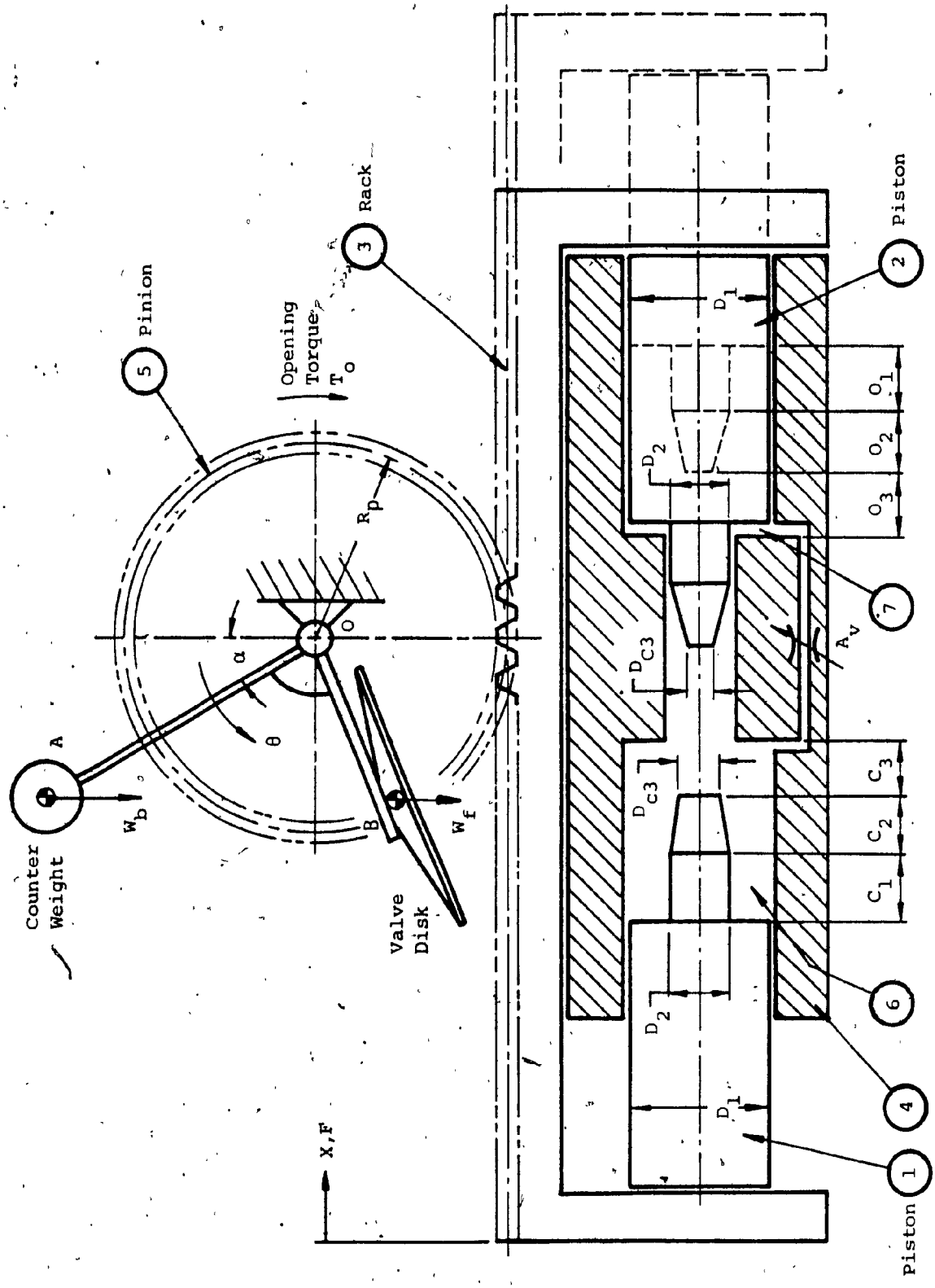

Figure 2-2 Schematic Diagram of Counter Weight Closing Valve

plungers move from left to right. During the initial portion of travel, when $(X<C_3)$, no fluid resistance is encountered and the valve closure is undamped. By further closing the valve, $((C_2<X<C_3+C_2))$, the conical portion of the plunger (1) enters the middle cylinder hole resulting in a damping effect of increasing intensity. Finally, plunger (1) seals-off the middle cylinder passage completely, $(X>(C_3+C_2))$, and oil is forced through the adjustable orifice (A_v) thus further restricting the oil flow for end cushioning.

The opening cycle of the valve is damped in a similar fashion by engaging of the plunger (2). During the opening operation, the valve disk is working against the closing torque created by the counter weight. During the portion of the travel when $(X>O_1)$, no fluid restrictance is encountered and the valve opening is undamped. By further opening the valve, the conical position of the plunger (2) enters the middle cylindrical hole, $(O_1<X<(O_1+O_2))$, and the fluid damping effect is increased. When the valve opens even more $(X<O_1)$ the plunger (2) seals off the middle cylindrical passage completely forcing fluid through the adjustable orifice (A_v) only. As a result, further and greater fluid damping is obtained.

CHAPTER 3

SYSTEM MODELLING

3.1. Introduction

This chapter is divided into two parts. The model development of hydro-pneumatic spring closing valve is discussed first, followed by the counter weight closing valve. Each of the system model is formed by modules of individual components in the system. This facilitates the changes and corrections required during later system development.

3.2. Valve Body and Valve Disk Design

The design of the valve body and the valve disk is the same for both valves. The valve body is made of cast iron and the valve disk is made of mild steel. As shown in figure 3-1, the valve inside diameter is 8", outside diameter is 11" and the internal flow diameter is 6.5". The valve disk pivot is located at 4.5" above the pipe center line. The disk shape is shown in the cross-section view of figure 3-1. The valve disk is bolted on to the linkage lever which is keyed on to the wafer shaft. The moment of inertia of the disk and its associated parts is calculated as 10.75 slug-in. The calculation is shown in appendix A.

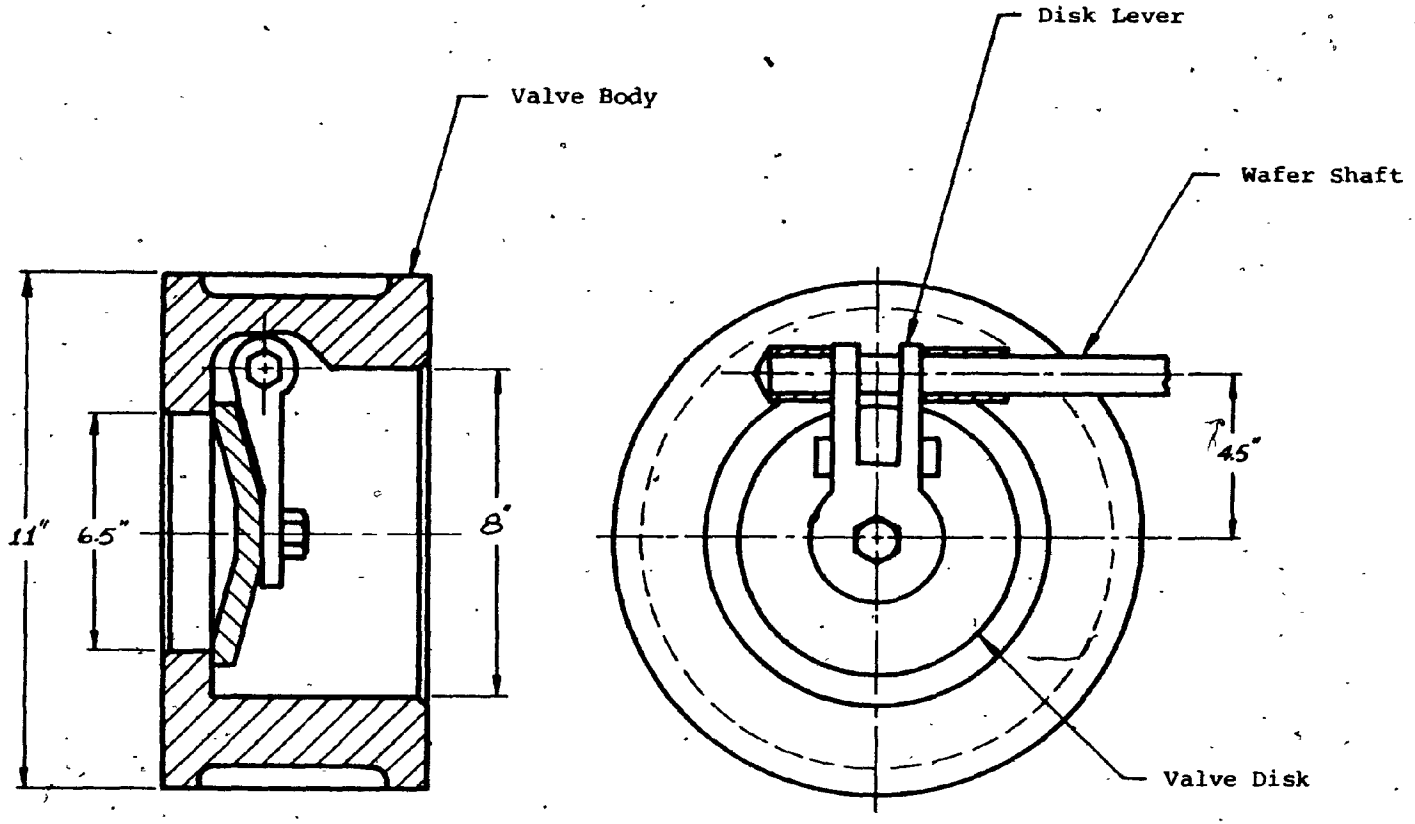

Figure 3-1 Valve Disk and Valve Body Configuration

3.3 Model Development of Hydro-Pneumatic Spring Closing Valve

Figure 3-2 shows the actual arrangement of the hydro-pneumatic spring closing valve. A simplified kinematic diagram of the actuator piston travel is shown in figure 3-3. The kinematic relationship of the arrangement can be found by using law of cosines, such that:

$$Y^2 = \overline{OA}^2 + \overline{OB}^2 - 2(\overline{OA}\cdot\overline{OB}\cdot\cos(\gamma+\theta)) \tag{3.1}$$

or $$Y = \left[\overline{OA}^2 + \overline{OB}^2 - 2(\overline{OA}\cdot\overline{OB}\cdot\cos(\gamma+\theta))\right]^{\frac{1}{2}} \tag{3.2}$$

and also

$$\alpha = \cos^{-1}\left[\frac{Y^2 + \overline{OA}^2 - \overline{OB}^2}{2(Y\cdot\overline{OA})}\right] \tag{3.3}$$

The hydraulic actuator (2) in figure 2-1 can be viewed as a dynamic component responding to the pressure difference (P_p-P_r) with the force (F) as output. In figure 3-4, assuming constant supply pressure (P_p) with fluid flow (Q_2), equation is

$$Q_2 - C_i(P_p - P_r) = \frac{d}{dt}V_p + \frac{V_p}{\beta_e}\cdot\frac{d}{dt}P_p \tag{3.4}$$

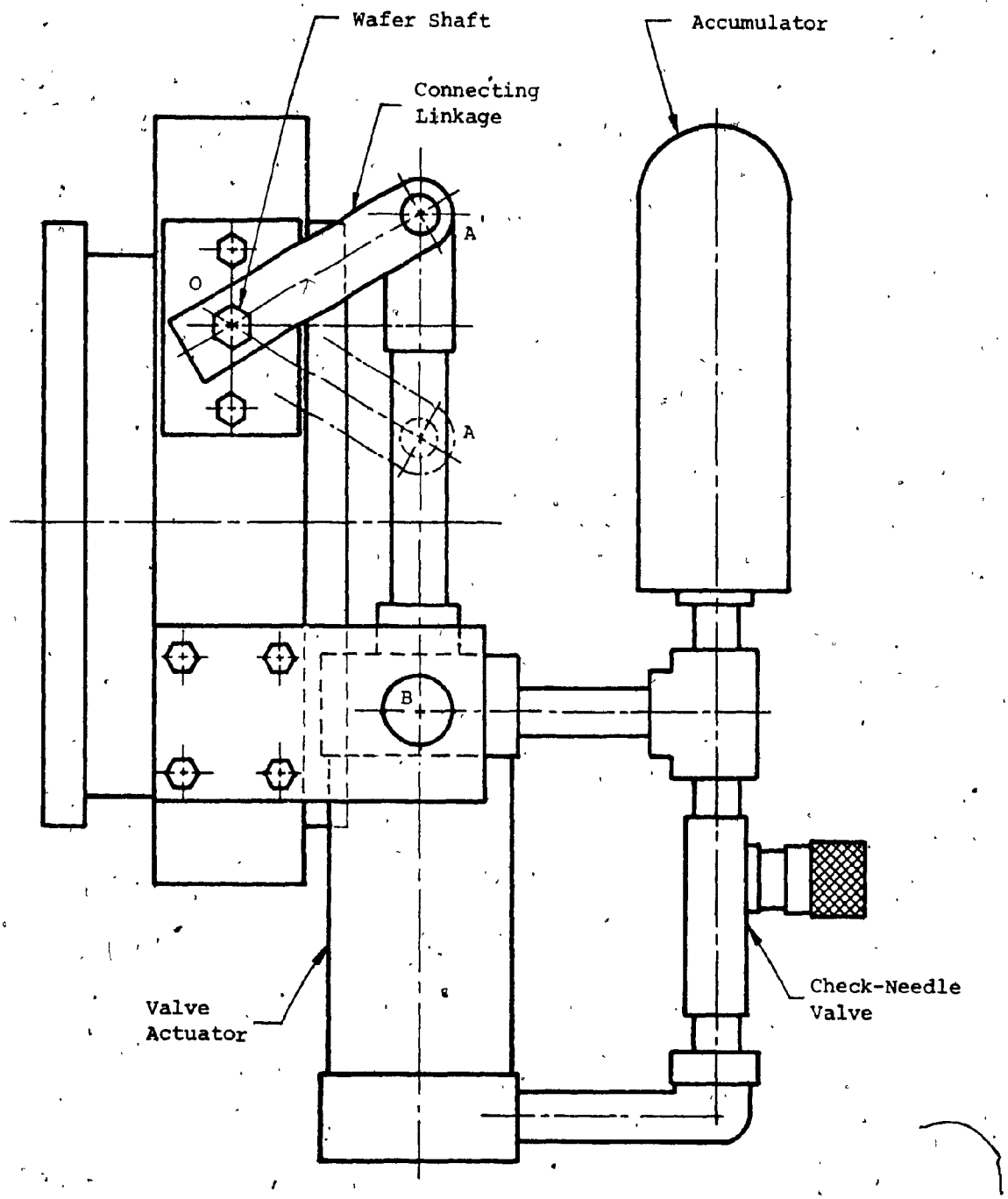

Figure 3-2 Hydro-Pneumatic Spring Closing Valve Actual Arrangement

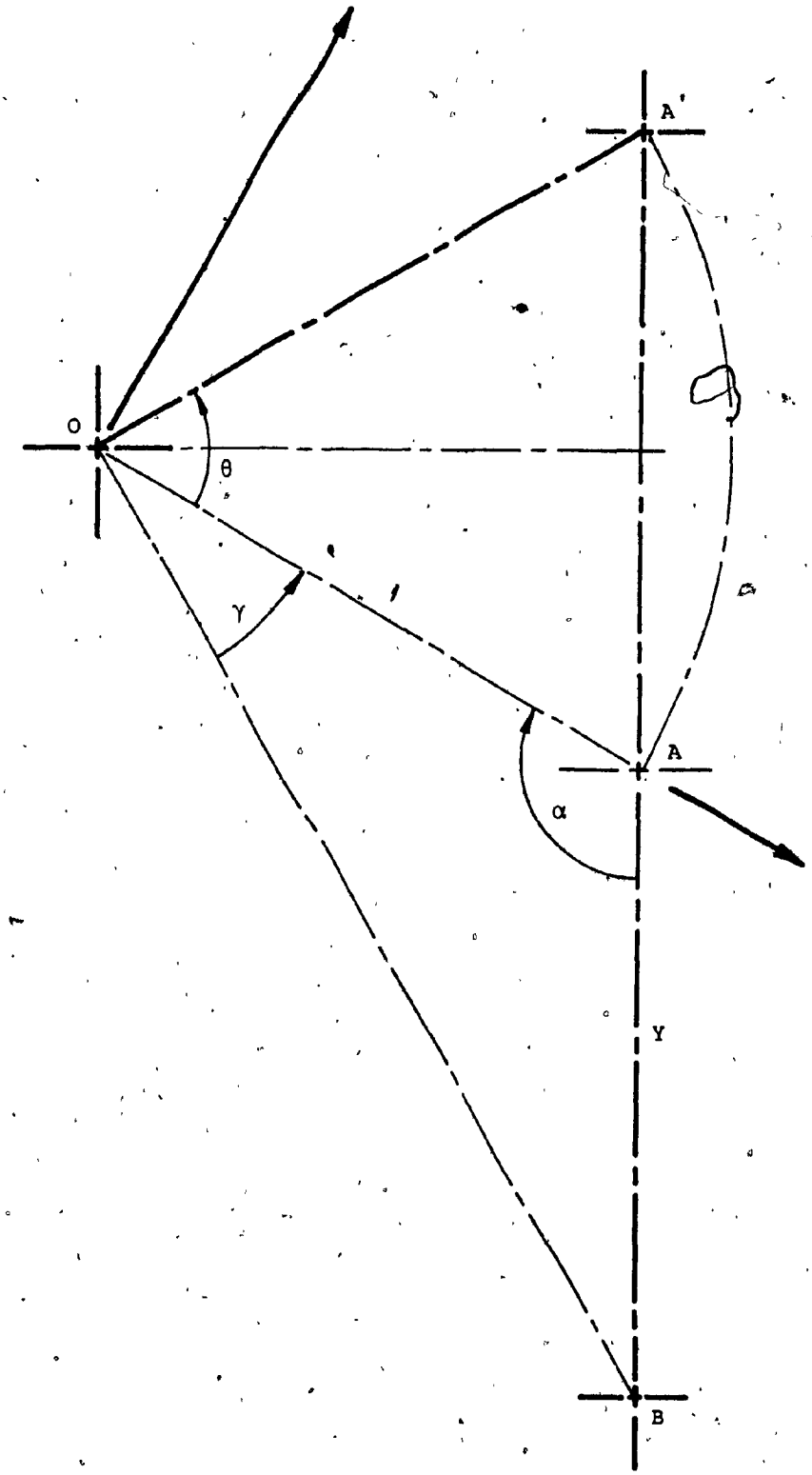

Figure 3-3 Simplified Kinematic Diagram of Hydro-Pneumatic Spring Closing Valve

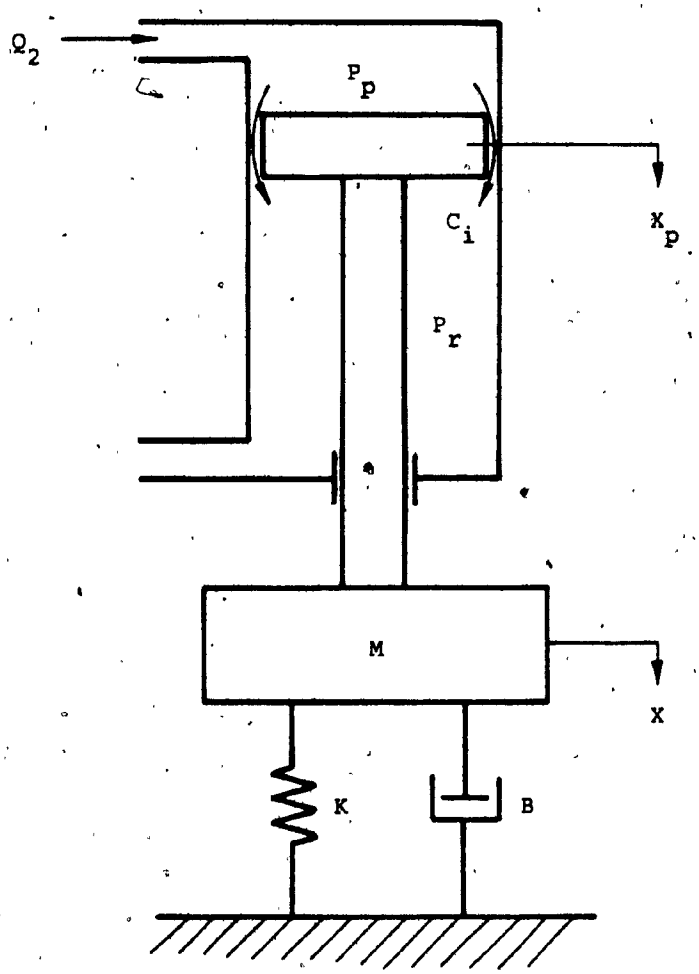

Figure 3-4 Flow Force on Cylinder Piston

where

C_i = internal leakage coefficient, $in^3/sec/psi$

V_p = piston side chamber volume, in^3

P_p = control pressure on the piston side, psi

β_e = effective bulk modulus, psi

The piston side chamber volume is given by

$$V_p = V_{po} + A_p X_p \tag{3.5}$$

where

V_{po} = initial piston side chamber volume, in^3

A_p = piston side piston area, in^2

If small piston motion is assumed such that $|A_p X_p| << V_{po}$ by substituting (3.5) into (3.3) then

$$Q_2 - C_i(P_p - P_r) = \frac{d}{dt}(V_{po} + A_p X_p) + \frac{V_{po} + A_p X_p}{\beta_e} \cdot \frac{d}{dt} P_p$$

$$= A_p \cdot \frac{d}{dt} X_p + \frac{V_{po}}{\beta_e} \cdot \frac{d}{dt} P_p \tag{3.6}$$

Since V_{po} is of a much smaller magnitude then $_e$ and $|A_p X_p| << V_{po}$, then the last term in equation (3.6) can be eliminated. To further simplify the equation, it is assumed that there is no internal and external leakages. Then the simplified continuity equation is

$$Q_2 = A_p \cdot \frac{d}{dt} X_p \tag{3.7}$$

The force equation for the piston is

$$F = P_p A_p - P_r A_r = M_t \cdot \frac{d^2}{dt^2} X_p + B \cdot \frac{d}{dt} X_p + K X_p \qquad (3.8)$$

where

F = force generated or developed by piston, lb_f

M_t = total mass of piston and load, $lb\text{-}sec^2/in$

B = viscous damping coefficient of piston and load, in-lb/sec

K = load spring gradient, lb/in

A_p = piston side piston area, in^2

A_r = rod side piston area, in^2

X_p = piston displacement, in

The specifications of the actuator used in the hydro-pneumatic spring closing valve are

manufacturer : Miller

cylinder bore : $2\frac{1}{2}$ in

rod dia : $1\frac{1}{4}$ in

stroke : 4 in

model : 81 B

The operation of the check-flow control valve is shown in figure 3-5. In forward flow, the fluid is restricted by the needle and body orifice. As the needle is with-

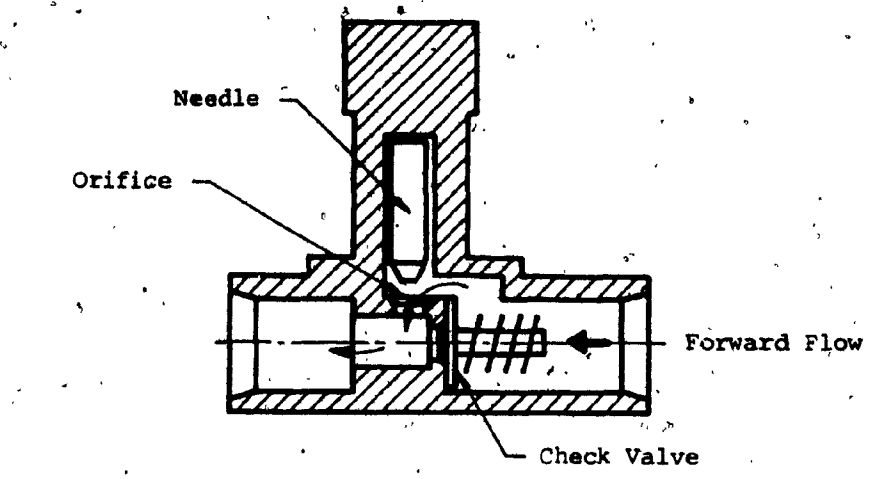

FORWARD FLOW OPERATION

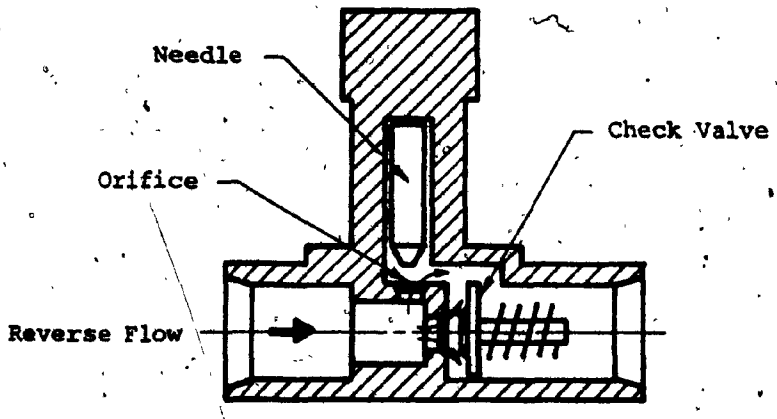

REVERSE FLOW OPERATION

Figure 3-5 Operation of the Check-Needle Valve

drawn from its seat, flow increases. In the reverse flow direction, pressure acts to unseat the integrated check valve and provides free flow. The fluid through the valving orific is described by

$$Q = C_d A_o \sqrt{\frac{2}{\rho}(P_1 - P_2)} \tag{3.9}$$

where

ρ = mass density, lb-sec^2/in^4

u_1 = upstream fluid velocity, in/sec

u_2 = downstream fluid velocity, in/sec

P_1 = upstream pressure, psi

P_2 = downstream presure, psi

Q = fluid flow, in^3/sec

C_d = discharge coefficient

A_o = effective orifice area, in^2

If P_1 and P_2 are constant, then the flow passing through is governed by the effective orifice area. For simplicity equation (3.9) can be written as

$$P_1 - P_2 = RQ^2 \tag{3.10}$$

where

$$R = \frac{1}{\frac{2}{\rho}(C_d A_o)^2} \quad \frac{\text{lb-sec}^2}{\text{in}^8} \tag{3.11}$$

assuming

C_d = 0.6, (for orifice)

ρ = 0.78×10^{-4}, lb-sec^2/in^4

(for petroluim base hydraulic oil)

The relationship between effective area A_o and equivalent fluid resistance R is shown in figure 3-6. The specifications of the check-flow control valve are

manufacturer	: Alkon Products
pipe size	: $\frac{1}{2}$ NPT
check valve orifice	: 0.515 in
needle valve	: 0.375 in
check valve C_v factor	: 4.96
needle valve C_v factor	: 1.25

Accumulator (5), in figure 2-1, has an initial volume of 30 in^3. The ideal-gas equation of state yields the relationship

$$\frac{P_{ao} V_{ao}}{T_{ao}} = \frac{P_{af} V_{af}}{T_{af}} \qquad (3.12)$$

where

P_{ao} = initial pressure, psi

V_{ao} = initial volume, in^3

T_{ao} = initial temperature, R

P_{af} = final pressure, psi

V_{af} = final volume, in^3

T_{af} = final temperature, R

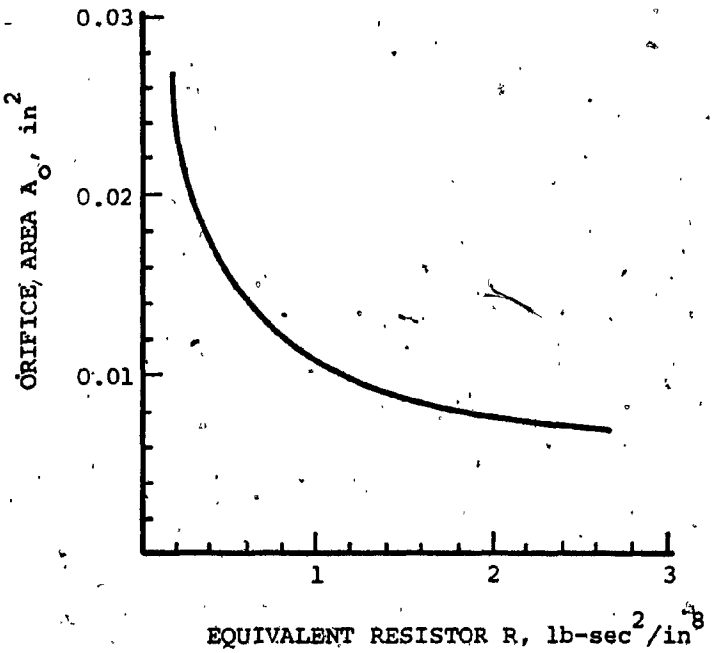

Figure 3-6 Plot of Effective Orifice Area A_o vs Equivalent Resistance R

If an isothermal process is assumed then equation (3.12) becomes

$$P_{ao} V_{ao} = P_{af} V_{af} \tag{3.13}$$

The accumulator specifications are

manufacturer	:	Miller
type	:	bladder
capacity	:	30 in^3
operating pressure	:	3000 psi
operating temperature	:	14 ^{o}F to 158 ^{o}F
model	:	05

To summarize, the hydro-pneumatic spring closing valve can be described by the following equations:

Cylinder hydraulic force:

$$F = P_p A_p - P_r A_r - F_f \text{ ; where } F_f = \text{friction} \tag{3.14}$$

Hydraulic torque:

$$T_{cy} = F \cdot \overline{OA} \cdot \sin \alpha \tag{3.15}$$

Torque angle:

$$\alpha = \cos^{-1}\left[\frac{Y^2 + \overline{OA}^2 - \overline{OB}^2}{2 \cdot Y \cdot \overline{OA}}\right] \tag{3.16}$$

Actuator displacement:

$$Y = \left[\overline{OA}^2 + \overline{OB}^2 - 2\,\overline{OA}\cdot\overline{OB}\cdot\cos(\gamma+\theta)\right]^{\frac{1}{2}} \qquad (3.17)$$

Actuator velocity:

$$\dot{Y} = \overline{OA}\cdot\overline{OB}\cdot\sin(\gamma+\theta)\cdot\dot{\theta} / Y \qquad (3.18)$$

Valve angular velocity:

$$\dot{\theta} = \frac{1}{I}\int_o^t (T_{cy} - T_o)\cdot dt + \dot{\theta}_o \qquad (3.19)$$

Valve angle:

$$\theta = \int_o^t \dot{\theta}_o \cdot dt + \theta_o \; ; \text{ where } \theta_{min} \leq \theta \leq \theta_{max} \qquad (3.20)$$

$$\theta_{max} = 1.0472 \text{ rad}$$

$$\theta_{min} = 0.0 \text{ rad}$$

Accumulator flow:

$$Q_a = Q_2 - Q_1 \qquad (3.21)$$

Cylinder flow:

$$Q_1 = \dot{Y}\cdot A_r \qquad (3.22)$$

$$Q_2 = \dot{Y}\cdot A_p \qquad (3.23)$$

Accumulator gas volume:

$$V_a = \int_0^t Q_a \cdot dt + V_{ao} \tag{3.24}$$

Accumulator pressure:

$$P_a = \frac{P_{ao} V_{ao}}{V_a} - P_{atm} \tag{3.25}$$

Cylinder pressures:

$$P_r = P_a \tag{3.26}$$

$$P_p = P_r - R_v \cdot Q_2^2 \; ; \text{ if } (\dot{Y} > 0) \text{ and } (Y < Y_{uc}) \tag{3.27}$$

$$P_p = P_r - R_u \cdot Q_2^2 \; ; \text{ if } (\dot{Y} > 0) \text{ and } (Y > Y_{uc}) \tag{3.28}$$

$$P_p = P_r + R_c \cdot Q_2^2 \; ; \text{ if } (\dot{Y} < 0) \text{ and } (Y > Y_{lc}) \tag{3.29}$$

$$P_p = P_r + R_l \cdot Q_2^2 \; ; \text{ if } (\dot{Y} < 0) \text{ and } (Y < Y_{lc}) \tag{3.30}$$

The system parameters are

A_R	= 3.68 in^2	A_p	= 4.9 in^2
R_c	= 0.15	R_v	= 0.5
I	= 10.75 slug-in^2	γ	= 0.588 rad.
θ_{max}	= 1.047 rad.	θ_{min}	= 0. rad.
$\overline{OA}$	= 4 in	$\overline{OB}$	= 8 in

R_u	= 1	R_l	= 0.8
Y_{uc}	= 8.25 in	Y_{lc}	= 5.75 in
V_{ao}	= 30 in^3	P_{ao}	= 150 psi
θ_o	= 1.047 rad.	$\dot{\theta}_o$	= 0. rad/sec

A listing of the computer MIMIC program solving the above equations is shown in appendix B. The particular algorithm employed for integrations is a Runge-Kutta Fourth Order method, which is described in appendix C.

3.4. Model Development of Counter Weight Closing Valve

The valve disk operating principle is governed by the orifice equation (3.9). The equations describing the counter weight closing valve are as follows:

The force balance equation:

$$T_o = W_b \cdot \overline{OA} \cdot \sin(\alpha+\theta) + W_f \cdot \overline{OB} \cdot \sin(\theta_{max}-\theta) + F \cdot R_p \quad (3.31)$$

Rack (piston) displacement:

$$X = R_p \cdot \theta \quad (3.32)$$

Rack (piston) velocity

$$\dot{X} = R_p \cdot \dot{\theta} \tag{3.33}$$

Oil flow rate:

$$Q = \frac{\pi}{4}(D_1^2 - D_2^2) \cdot \dot{X} \tag{3.34}$$

Valve angular velocity:

$$\dot{\theta} = \frac{1}{I}\int_o^t [W_b \cdot \overline{OA} \cdot \sin(\alpha+\theta) + W_f \cdot \overline{OB} \cdot \sin(\theta_{max}-\theta) + F \cdot R_p - T_o]dt + \dot{\theta}_o \tag{3.35}$$

Valve angle:

$$\theta = \int_o^t \dot{\theta} \cdot dt + \theta_o \; ; \text{ where } \theta_{min} \leq \theta \leq \theta_{max} \tag{3.36}$$

Hydraulic force:

$$F = -\frac{\pi}{4} \cdot D_1^2 \cdot P \quad ; \text{ if CFRTP} \tag{3.37}$$

$$F = -\frac{\pi}{4} \cdot (D_1^2 - D_2^2) \cdot P \; ; \text{ if CRES} \tag{3.38}$$

$$F = \frac{\pi}{4} \cdot D_1^2 \cdot P \quad ; \text{ if OFRTP} \tag{3.39}$$

$$F = \frac{\pi}{4} \cdot (D_1^2 - D_2^2) \cdot P \quad ; \text{ if ORES} \tag{3.40}$$

Cylinder pressure:

$$P = 0 \quad ; \text{if FREE} \tag{3.41}$$

$$P = \frac{\rho}{2 \cdot C_d^2 \cdot A_v^2} \cdot Q^2 \quad ; \text{if RES} \tag{3.42}$$

$$P = \frac{\rho}{2 \cdot C_d^2 (A_v + A_{cx})^2} \cdot Q^2 \quad ; \text{if CTAPP, } A_{cx} = f_1(X) \tag{3.43}$$

$$P = \frac{\rho}{2 \cdot C_d^2 (A_v + A_{ox})^2} \cdot Q^2 \quad ; \text{if OTAPP, } A_{ox} = f_2(X) \tag{3.44}$$

Logic functions:

$$\text{CFRTP} = (\dot{\theta} \leq 0) \text{ and } (X < C_2 + C_3) \tag{3.45}$$

$$\text{CRES} = (\dot{\theta} \geq 0) \text{ and } (X \geq C_2 + C_3) \tag{3.46}$$

$$\text{OFRTP} = (\dot{\theta} < 0) \text{ and } (X \geq O_1) \tag{3.47}$$

$$\text{ORES} = (\dot{\theta} < 0) \text{ and } (X < O_1) \tag{3.48}$$

$$\text{FREE} = [(\dot{\theta} \geq 0) \text{ and } (X < C_3)] \text{ or } [(\dot{\theta} < 0) \text{ and } (X > O_1 + O_2)] \tag{3.49}$$

$$\text{RES} = [(\dot{\theta} \geq 0) \text{ and } (X \geq C_2 + C_3)] \text{ or } [(\dot{\theta} < 0) \text{ and } (X < O_1)] \tag{3.50}$$

$$\text{CTAP} = (\dot{\theta} \geq 0) \text{ and } (C_3 \leq X < C_2 + C_3) \tag{3.51}$$

$$\text{OTAP} = (\dot{\theta} < 0) \text{ and } (O_1 \leq X \leq O_1 + O_2) \tag{3.52}$$

The system parameters are

D_1 = 1.75 in		D_2 = 0.625 in	
DC_3 = 0.3125 in		DO_3 = 0.437 in	
R_p = 2.25 in		I = 4 slug-ft-in	
C_1 = 0.875 in		O_1 = 0.875 in	
C_2 = 0.875 in		O_2 = 0.875 in	
C_3 = 0.875 in		O_3 = 0.875 in	
W_b = 10 lb_f		W_f = 1 lb_f	
$\overline{OA}$ = 12 in		$\overline{OB}$ = 4.5 in	
α = 0.523 rad.		ρ = 0.78×10^{-4} lb-sec^2/in^4	
C_d = 0.6		A_v = 0.0123 in^2	
θ_{max} = 1.0471 rad.		θ_{min} = 0. rad.	
$\dot{\theta}_o$ = 0 rad/sec		θ_o = 1.0471 rad.	

A computer MIMIC program solving the above equations is listed in appendix D.

CHAPTER 4

DEVELOPMENT OF EXPERIMENTAL TEST STAND

4.1. Introduction

The experimental tests have been performed in order to tune-up the computer models and to acquire a better insight into the actual system dynamics. The design of the test stand is based on a force feedback system which has the capability of controlling force or torque input applied to the wafer shaft. Some design problems such as safety, stability and accuracy which occured during the test stand development are considered and discussed.

4.2. Test Stand Description

A block diagram of the force feedback test stand system is shown in figure 4-1. The closed-loop control system derives the output until it equals the input and the error is zero. Any differences between the actual and desired output will be automatically corrected in the closed-loop system. The fluid force on the valve disk is simulated and controlled by the force feed back loop.

A slightly modified hydro-pneumatic spring closing

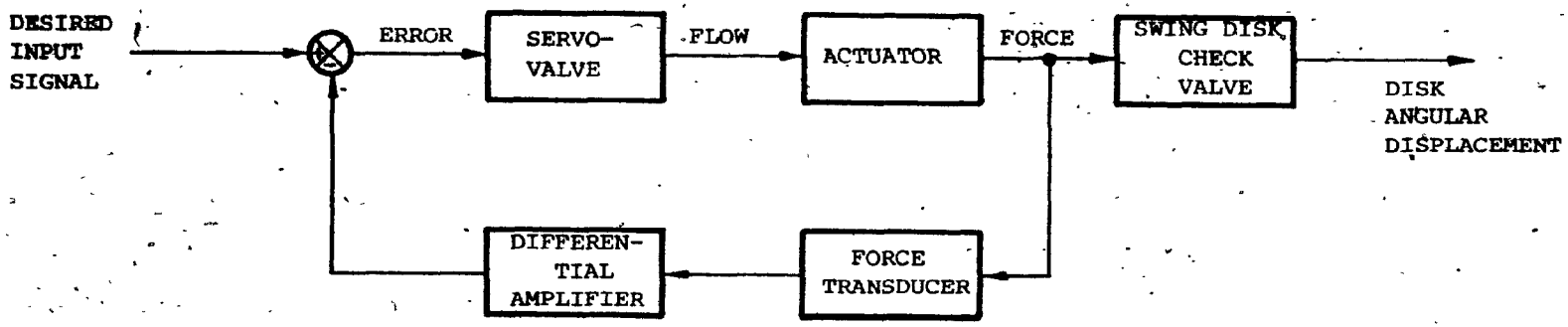

Figure 4-1 Block Diagram of the Test Rig

valve is used in the experiment. Figure 4-2 and figure 4-3 show the assembly drawing of the test rig and the detailed drawings are shown in appendix E. The arrangement of the test rig can also be seen in the pictorial view in figure 4-4. The complete schematic of the experimental test stand is shown in figure 4-5 followed by the pictorial view of the entire experimental set-up in figure 4-6. Calibrations and descriptions of the equipments used in the experiment are described in appendix F.

4.3. Test Stand Design Problems

Safety is one of the important considerations in the test stand design. Thus it is necessary to control the peak pressure value in the hydraulic driving system. It would be possible to control the movement of the actuator in order to eliminate shocks. However, this would require a fairly elaborate and costly control. A far simpler solution is to insert a relief valve on the supply line. The relief valve permits pressure to rise to a set value and to maintain that pressure.

Stability is another important consideration in the test stand design. In order to obtain stabilty in the system, certain damping should be maintained. A needle

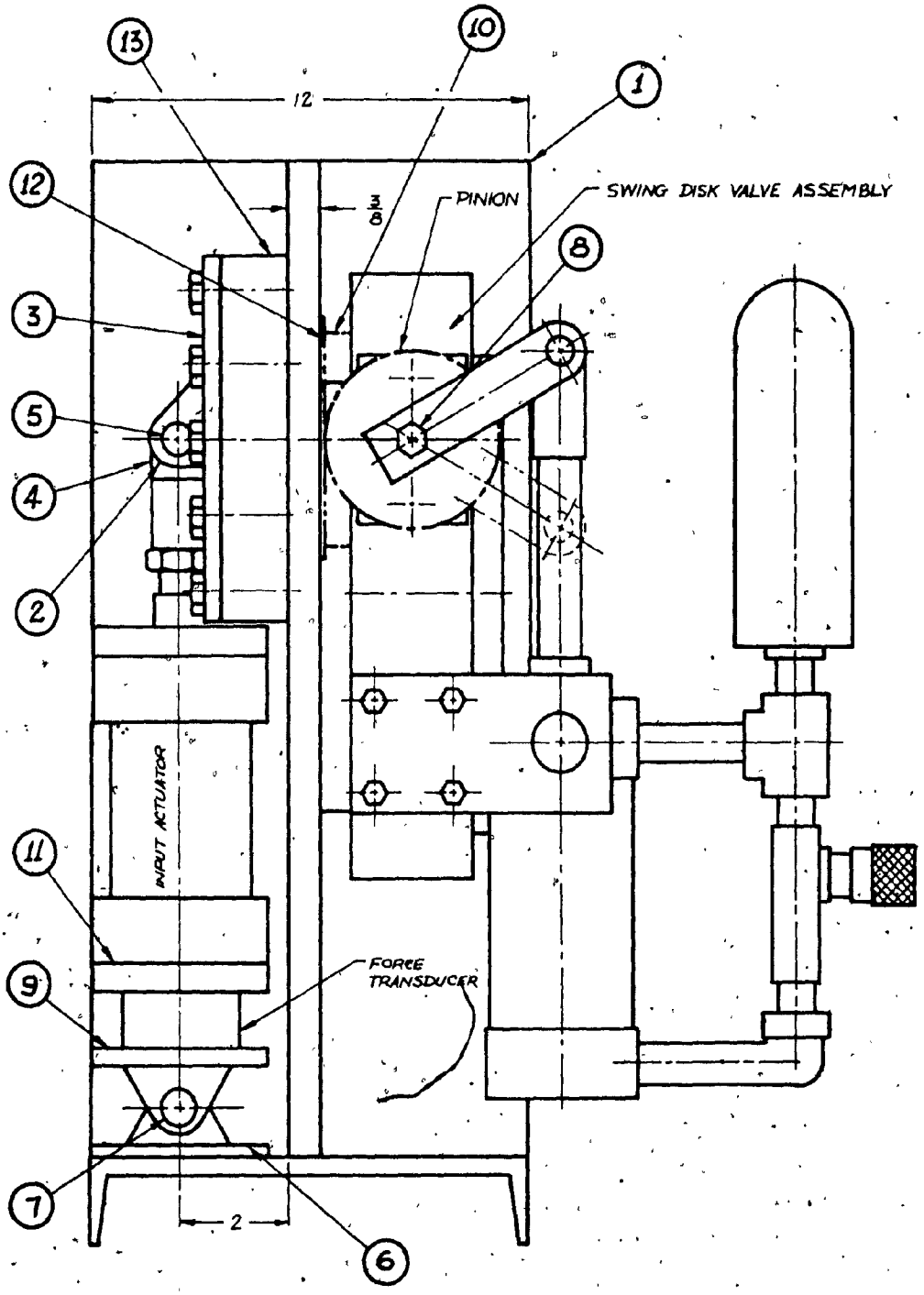

Figure 4-2 Side View of the Test Rig

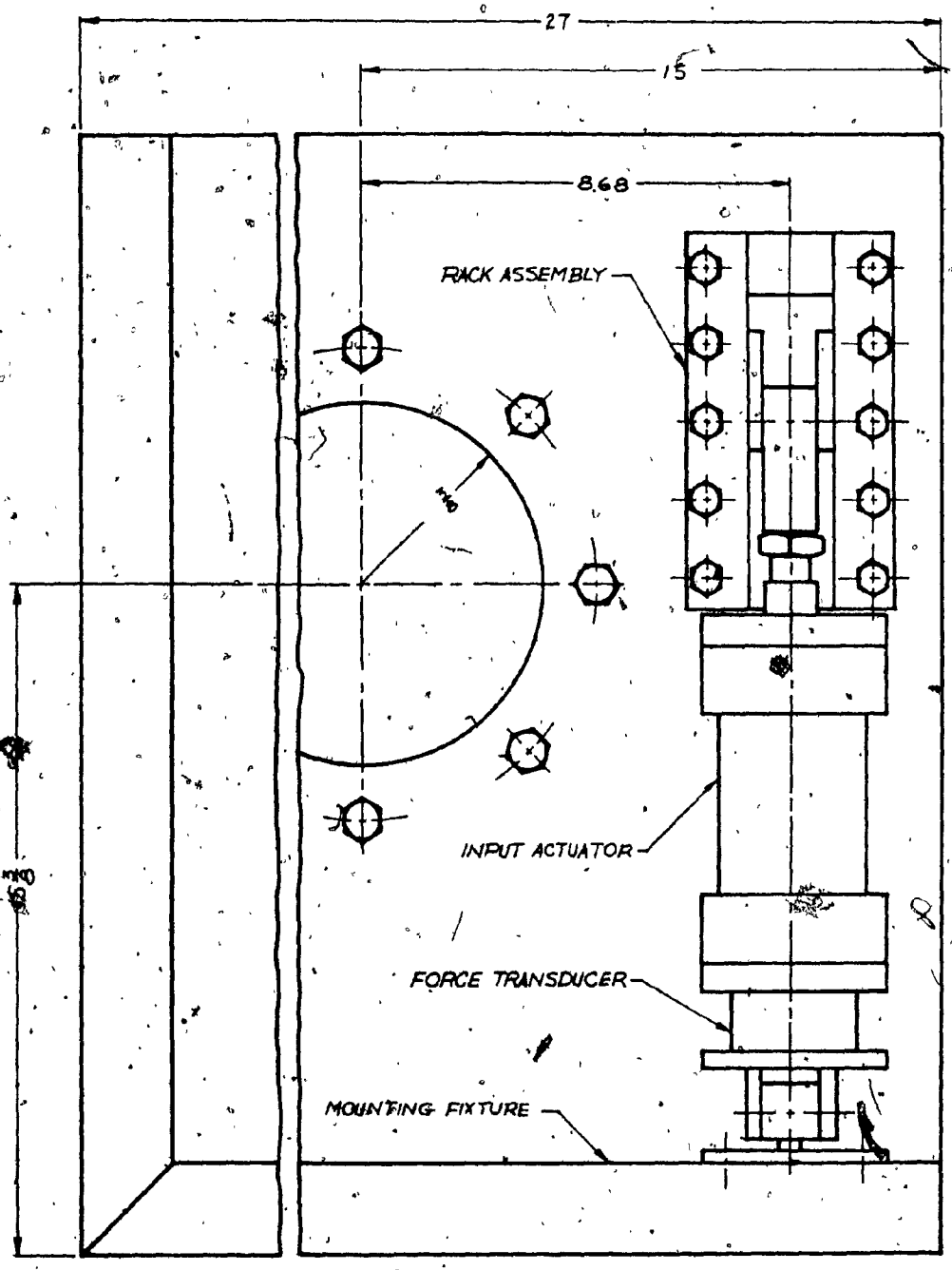

Figure 4-3 Front View of the Test Rig

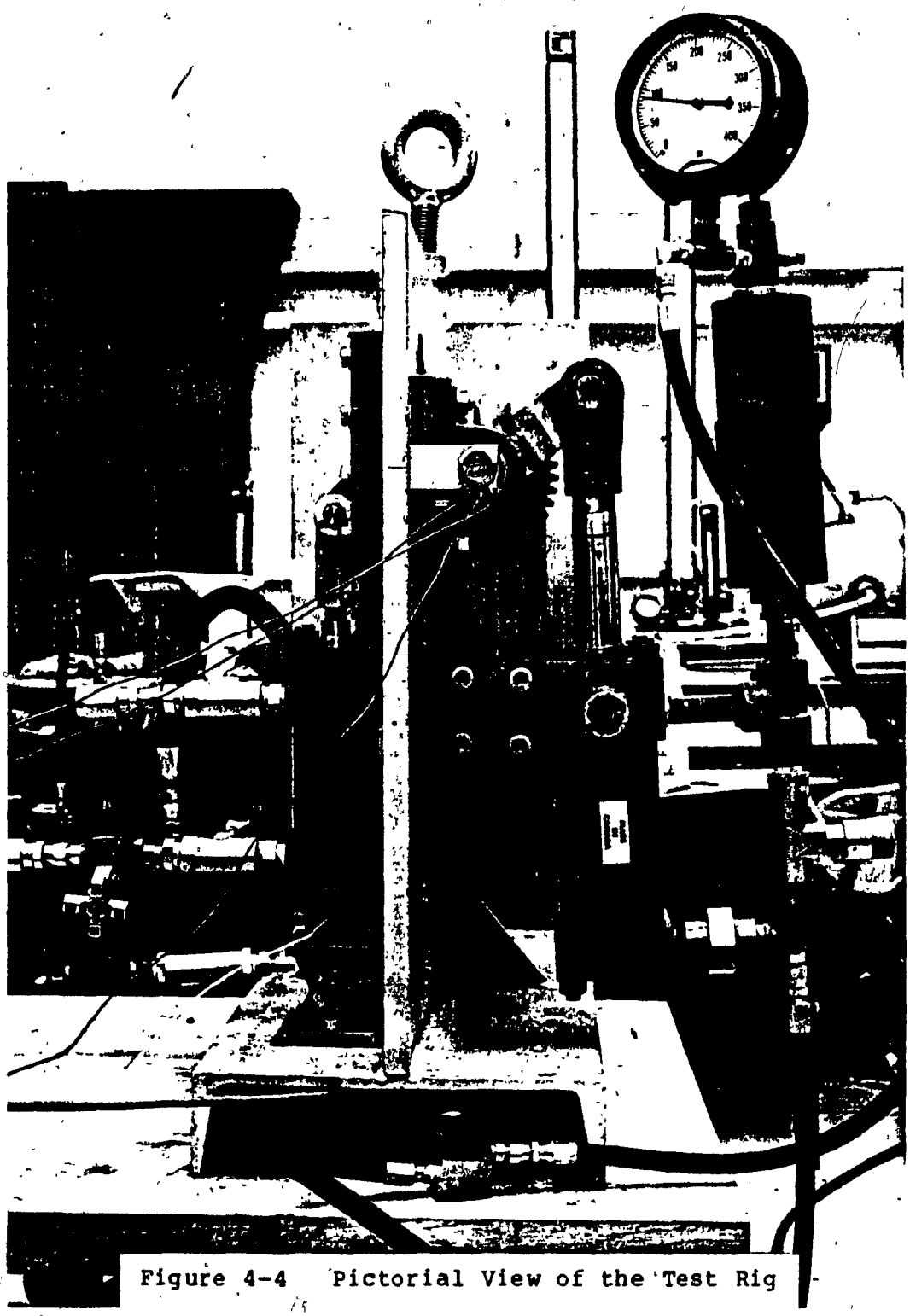

Figure 4-4 Pictorial View of the Test Rig

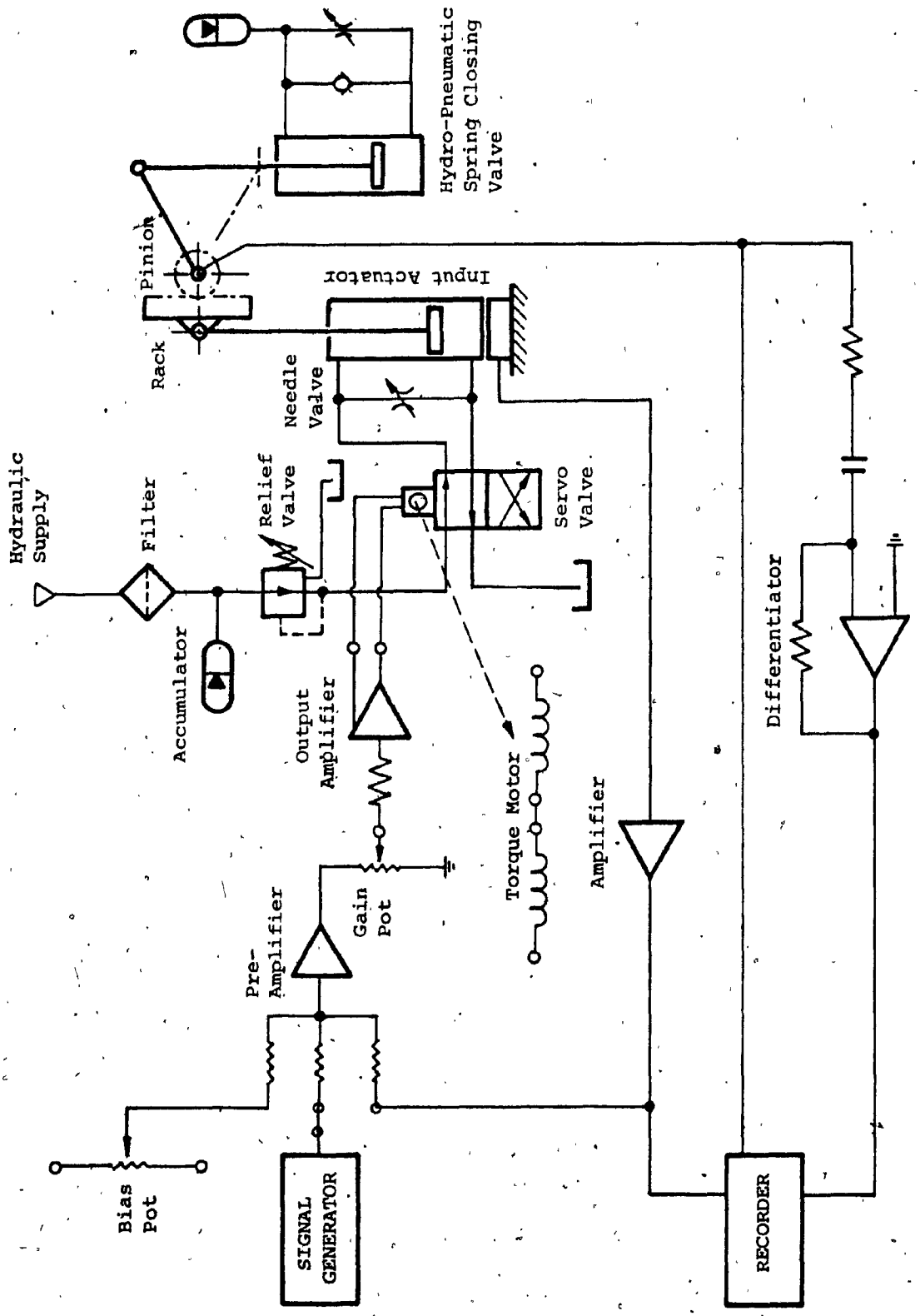

Figure 4-5 Experimental Test Stand Schematics

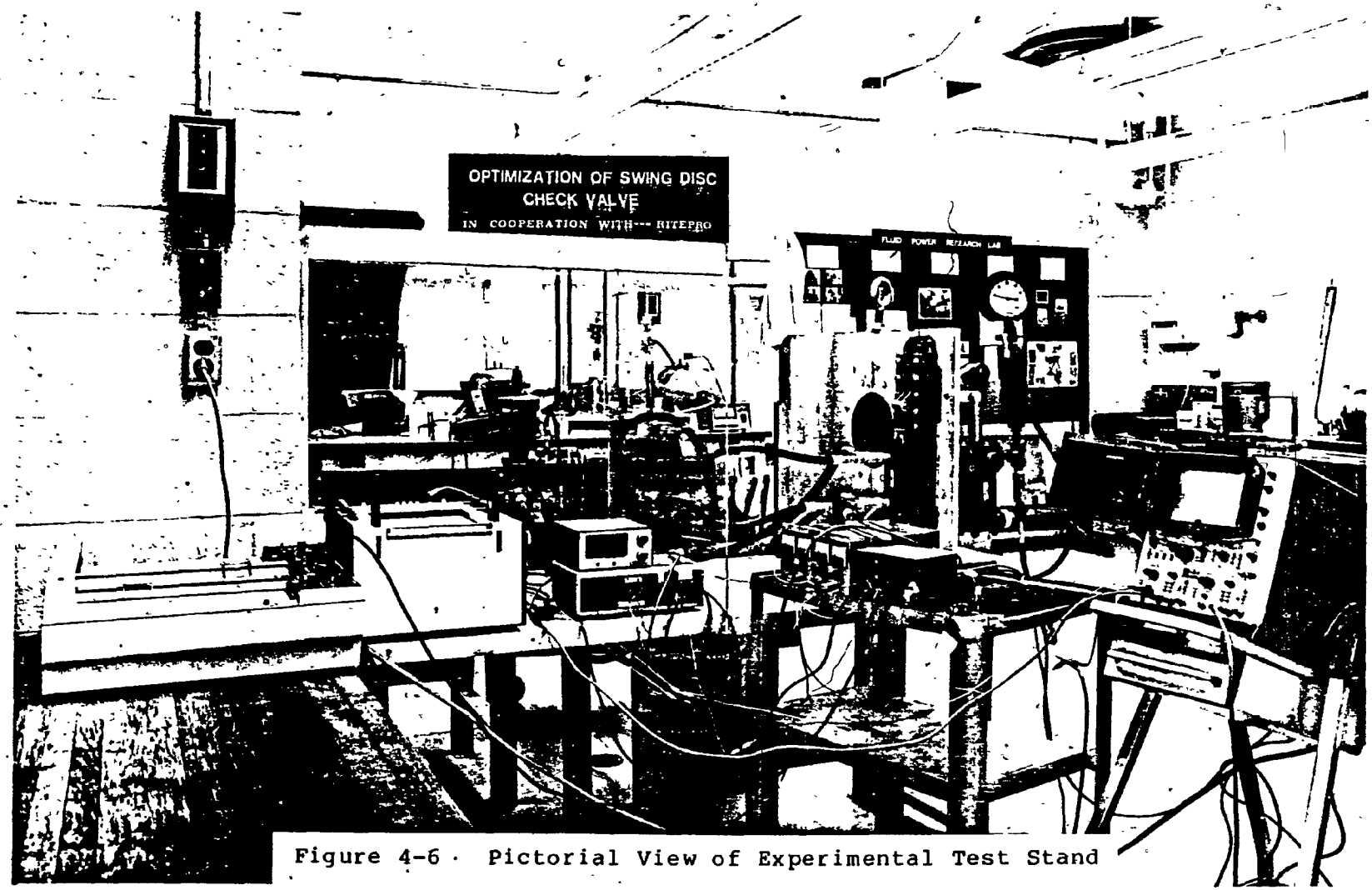

Figure 4-6 · Pictorial View of Experimental Test Stand

valve as cross-port leakage, is inserted across the cylinder lines to adjust the test stand damping ratio. The drawbacks of this are the increased power loss and the decreased pressure sensitivity.

Besides the above mentioned considerations, an accumulator is added to the test stand hydraulic power supply. It is a device which holds reserve fluid at the system pressure. It functions to filter pressure pulsations from the pump and to provide additional fluid under pressure to accomodate peak flow demands and thus improving system response. Figure 4-7 shows a test stand force-servo performance without the accumulator. Figure 4.8 shows the force-servo performances when accumulator was added. The performance of the system with accumulator is clearly superior.

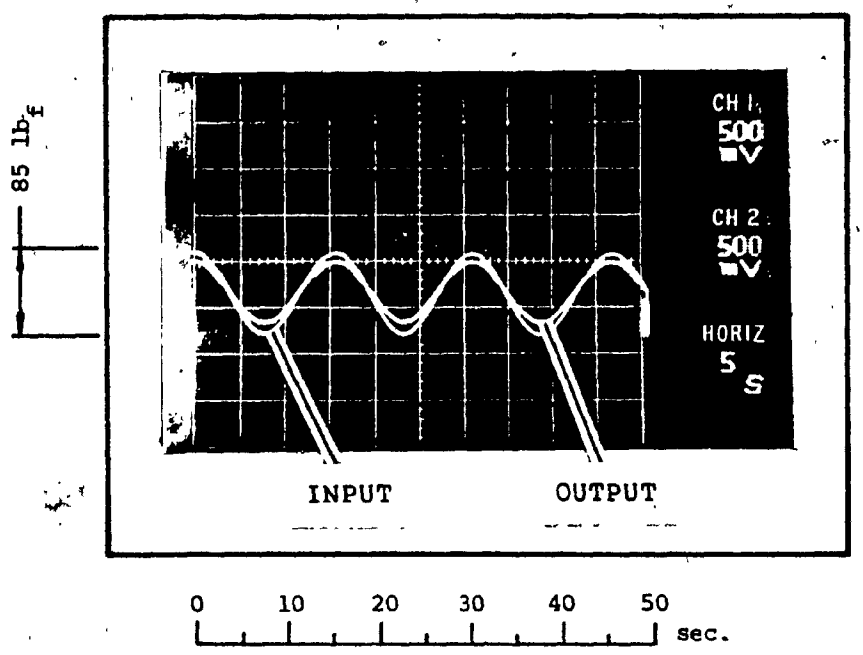

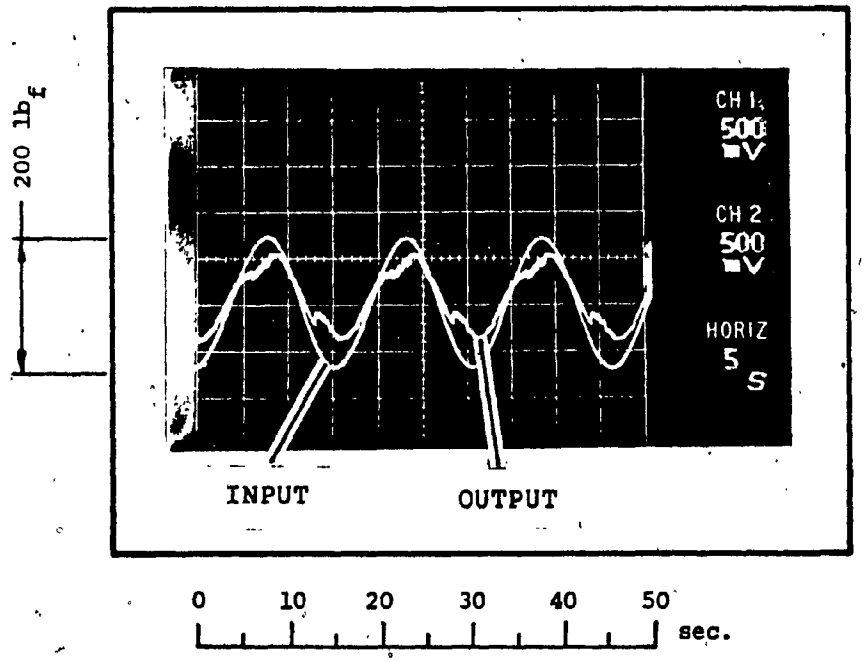

Figure 4-7 Test Stand Force-Servo Performance without Accumulator

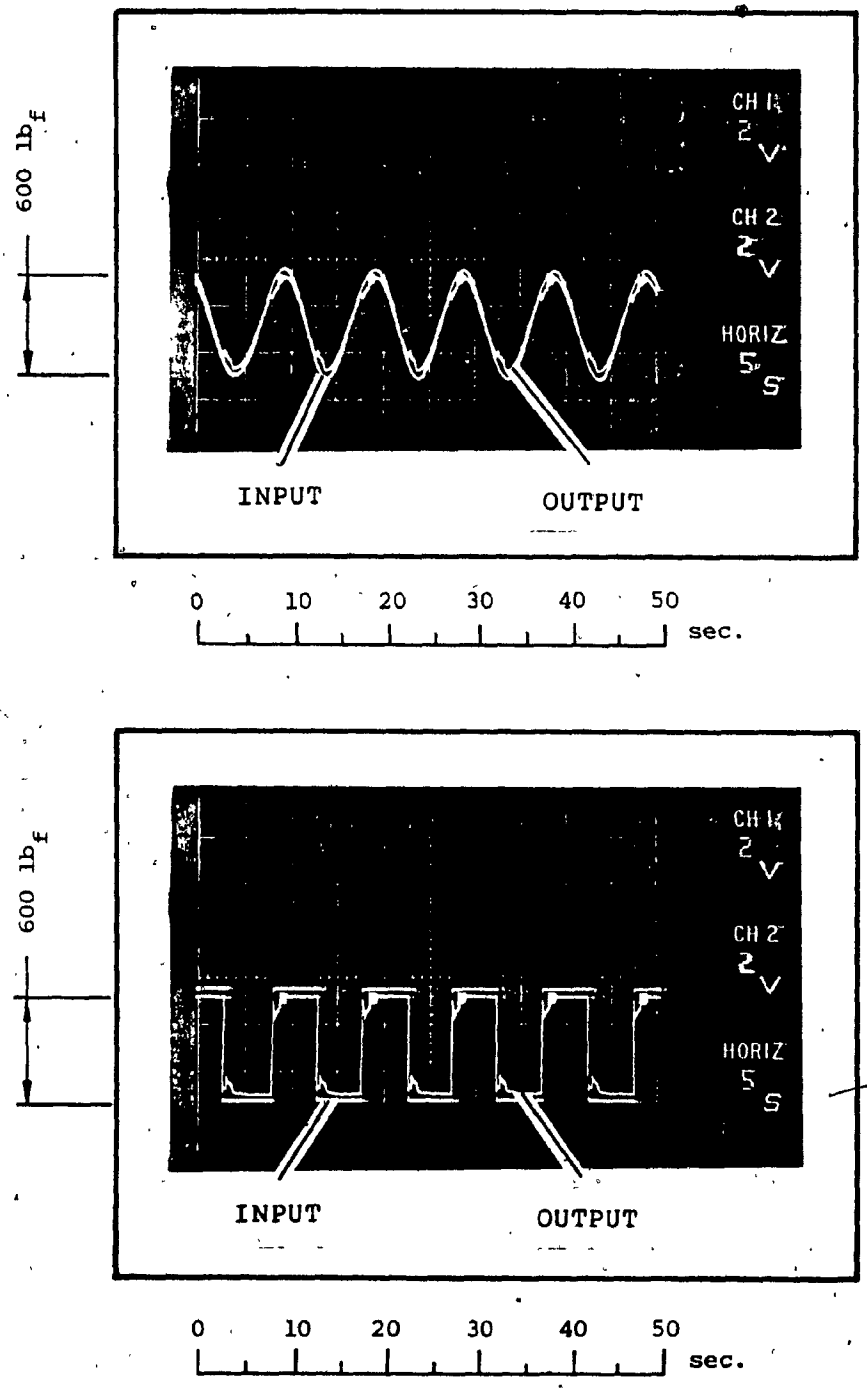

Figure 4-8 Test Stand Force-Servo Performance with Accumulator

CHAPTER 5

SYSTEM PERFORMANCE

5.1. Introduction

In order to investigate the relative effects of various system parameters on valve dynamics, model performance and experimental performance are discussed and compared. It shows how the governing equations describe the system adequately. It is seen that systems dynamics are generally governed by two of the major parameters such as valve closing force and fluid resistor.

5.2. Model Performance of Hydro-Pneumatic Spring Closing Valve

The theoretical investigation of the hydro-pneumatic spring closing valve using the model mentioned in section 3-3 is carried out. Figure 5-1 shows the model response with an input torque of 1000 lb_f-in applied to the wafer shaft. It shows the valve has a maximum opening velocity of 0.64 rad/sec and a maximum closing velocity of 0.5 rad/sec. The valve disk closing and opening impact velocity are 0.36 rad/sec and 0.24 rad/sec respectively. In the opening process, the accumulator is charged to a higher pressure.

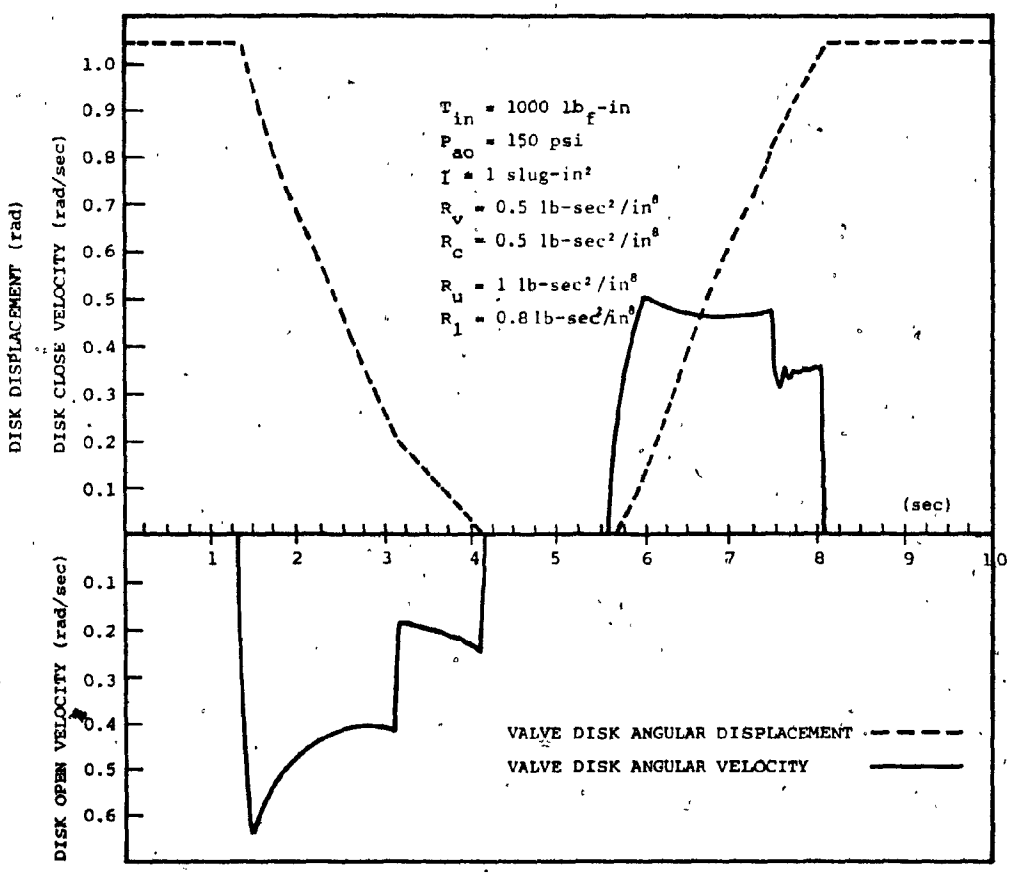

Figure 5-1 Typical Model Response of Hydro-Pneumatic Valve

It acts as a spring to work against the valve opening. The valve disk velocity decreases from 0.42 rad/sec to 0.18 rad/sec when the cylinder piston reaches the lower cushion. This is because the pressure difference across the cylinder chambers increases. During the closing process, the closing velocity is governed by the check-needle control valve. The upper cushion has the same effects as the lower cushion in the opening process. It increases the cylinder chamber pressure difference. As a result it slows down the closing velocity.

5.3. Experimental Performance of Hydro-Pneumatic Spring Closing Valve

The settings of the check-needle control valve and the cushions used in the test are shown in table 5-1. The input torque on the wafer shaft is adjusted to 1500 lb_f-in. The torque is generated by a force acting on the piston of the wafer shaft, as shown in the plot in figure 5-2. Figures 5-3, 5-4 and 5-5 depict the typical results of test runs no. 4, 5, and 6, respectively (see table 5-1). In test run no. 4, for example, the maximum opening and closing velocities are 0.68 and 0.60 rad/sec respectively. The valve disk opening and closing impact velocities are 0.45 and 0.23 rad/sec respectively. The fluid resistor effect of the

TEST RUN NO.	NUMBER OF TURNS FROM SHUT OFF		
	ONE-WAY FLOW CONTROL	ROD END CUSHION	PISTON END CUSHION
1	5	2.5	2.5
2	3	2,5	2.5
3	2.5	2.5	2.5
4	5	2.0	2.0
5	3	2.0	2.0
6	2.5	2.0	2.0
7	5	1.0	1.0
8	3	1.0	1.0
9	2.5	1.0	1.0

Table 5-1 Experimental Fluid Resistor Settings

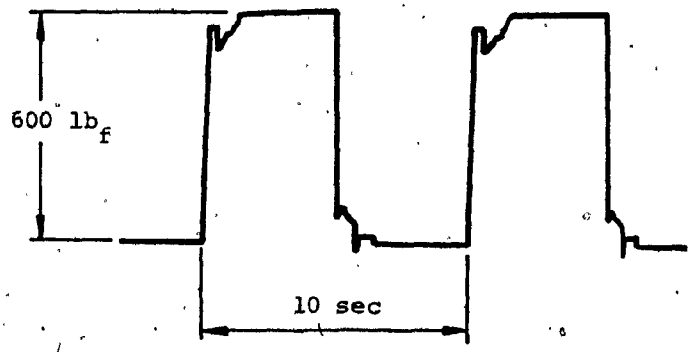

Figure 5-2 Experimental Force Input

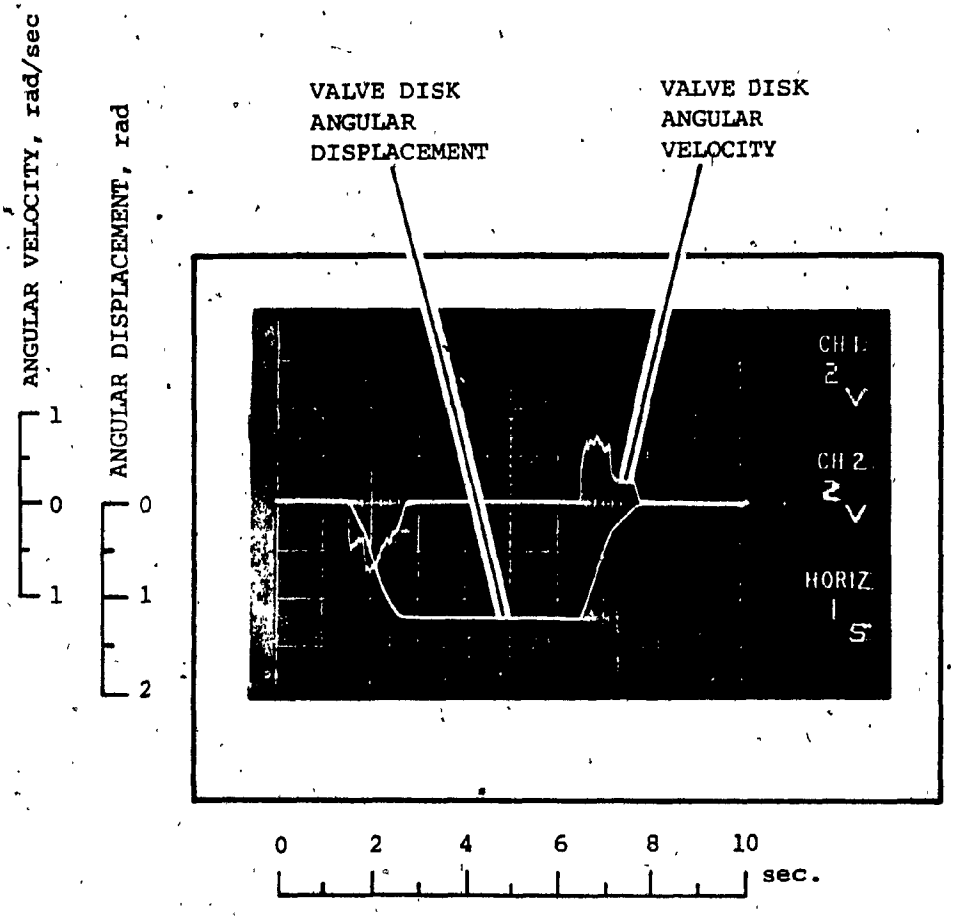

Figure 5-3 Typical Experimental Results of Test Run No. 4

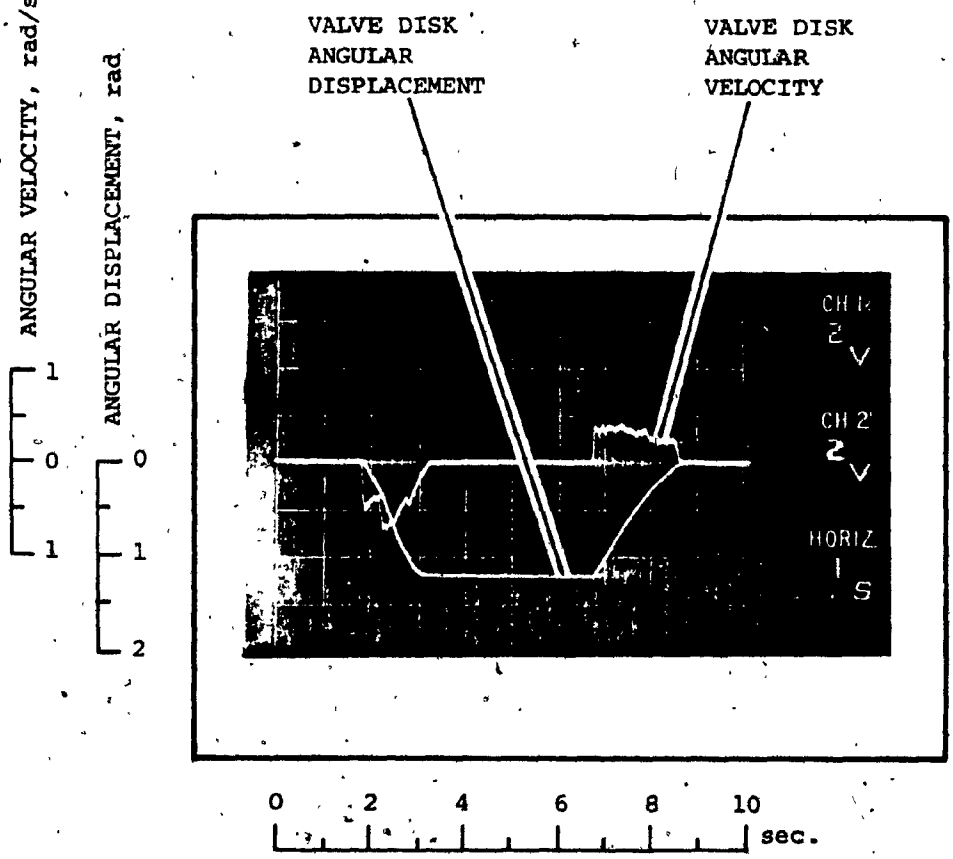

Figure 5-4 Typical Experimental Results of Test Run No. 5

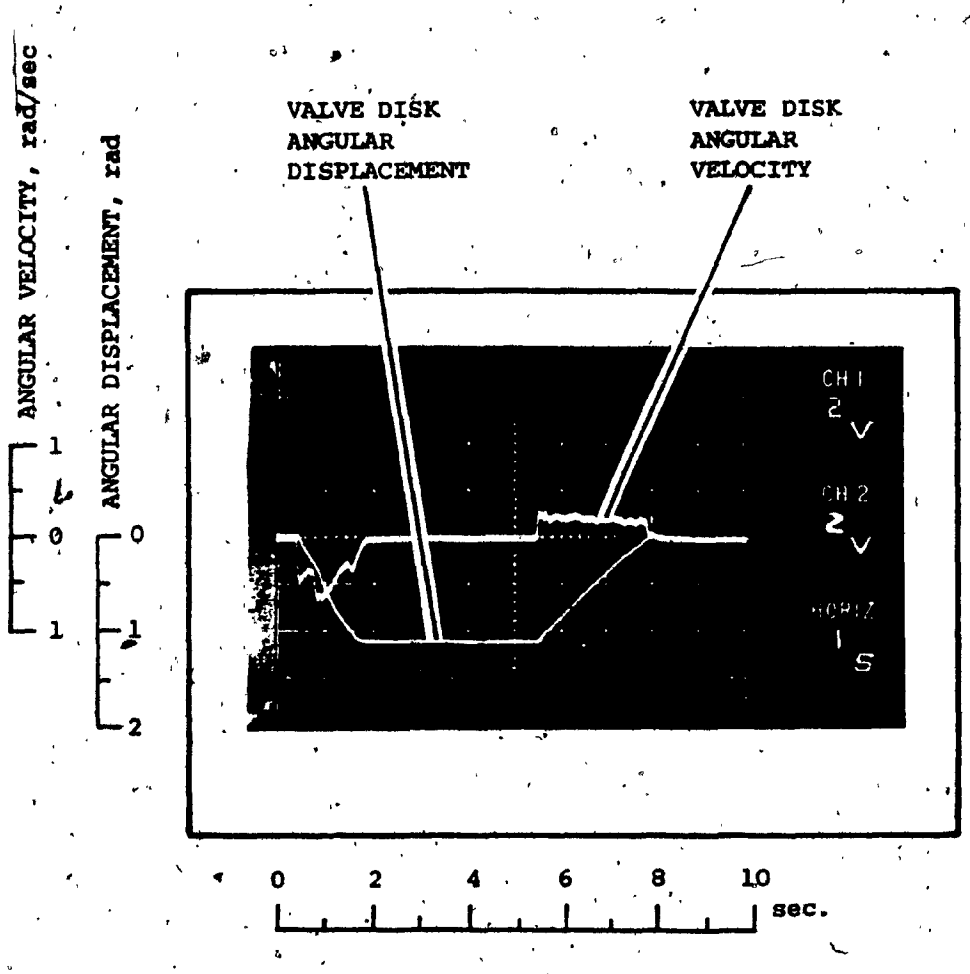

Figure 5-5 Typical Experimental Results of Test Run No. 6

check-needle control valve is clearly shown. It reduces the maximum closing velocity from 0.6 to 0.23 rad/sec. However, the adjustment on both cushions does not work properly. Even with different cushion settings, the results of test run no. 7, shown in figure 5-6, do not differ from those of test run no. 4. It is also learned that the checking function of the cushion mechanism does not function properly.

5.4. Correlation and Effects of Various Parameters on Hydro-Pneumatic Spring Closing Valve

The experimentally found cushioning conditions are inserted into the model by omitting the cushion checking mechanism. The computer listing of the modified model is shown in appendix G. The model output is shown in figure 5-7, indicating the maximum opening and closing velocity, 0.64 and 0.48 rad/sec respectively.

By carefully replotting and superimposing the experimental result of test run no. 4 in figure 5-3, and the model response in figure 5-7, a good correlation is found. This is shown clearly in figure 5-8.

Some deviations are observed from figure 5-8. The experimental response is somewhat slower than the model response. The deviation is due to the friction between

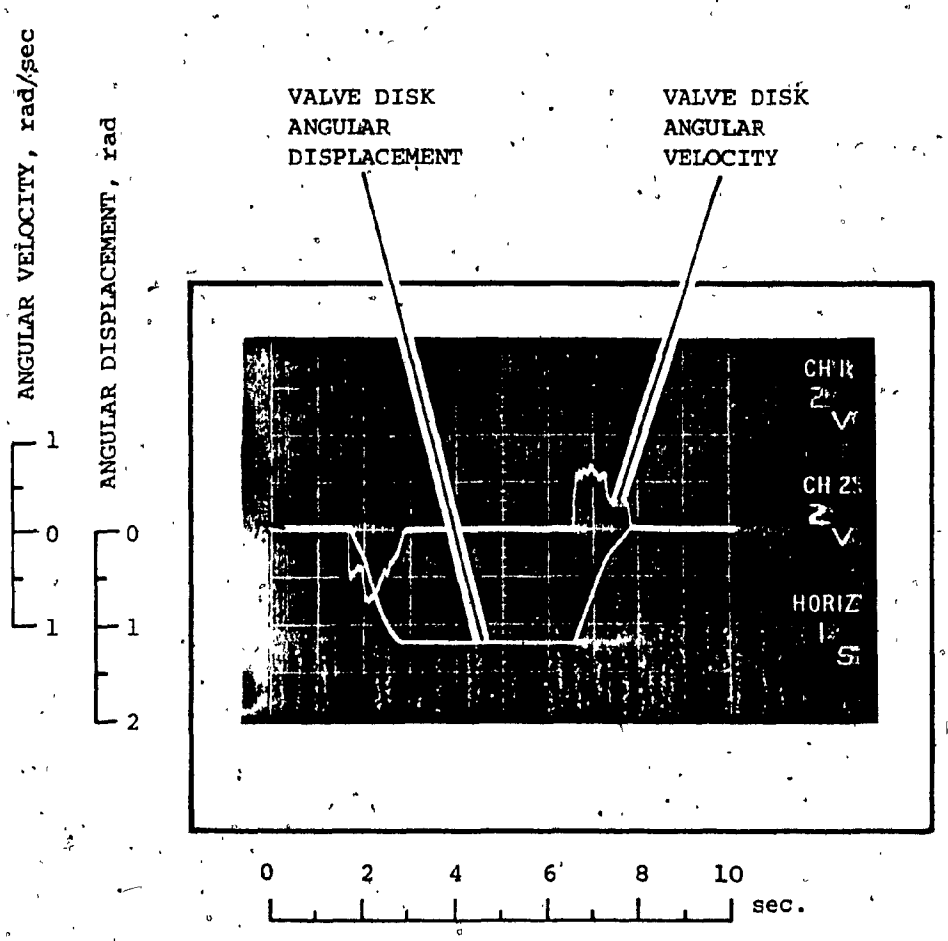

Figure 5-6 Experimental Result of Test Run No. 7 with Different Cushion Settings

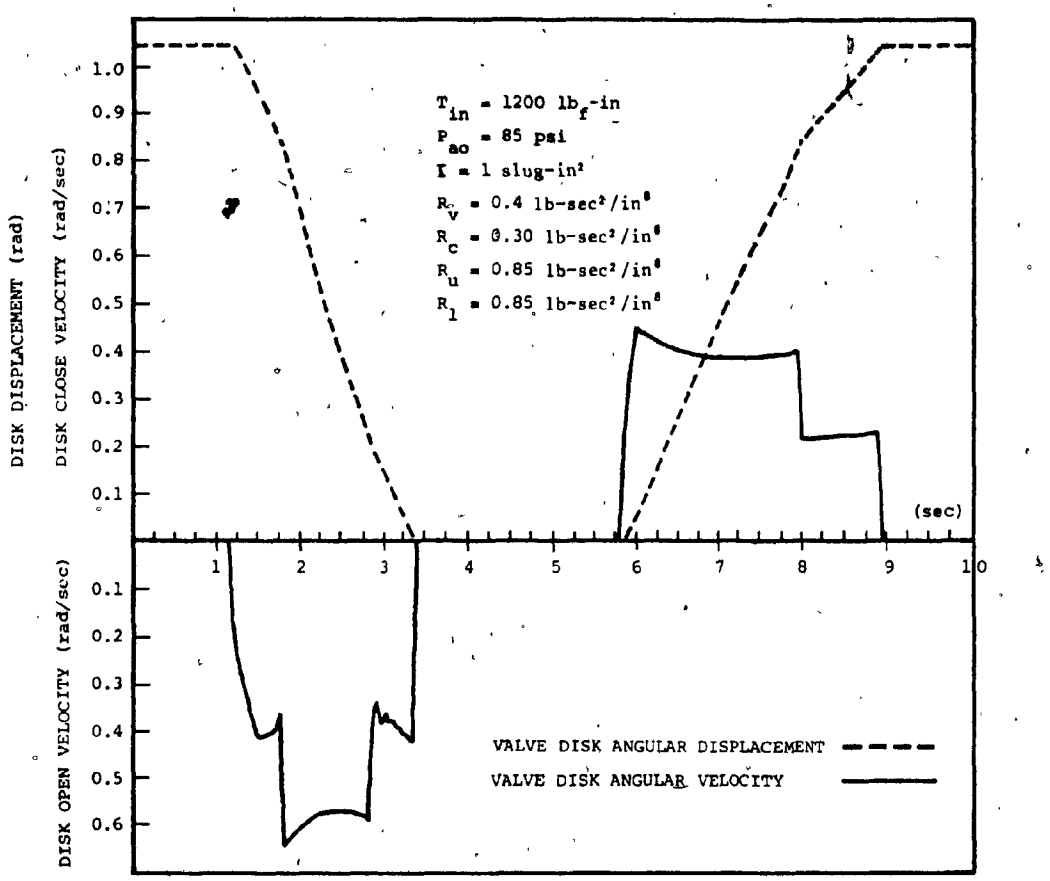

Figure 5-7 Model Response of Hydro-Pneumatic Valve without Cushion Checking

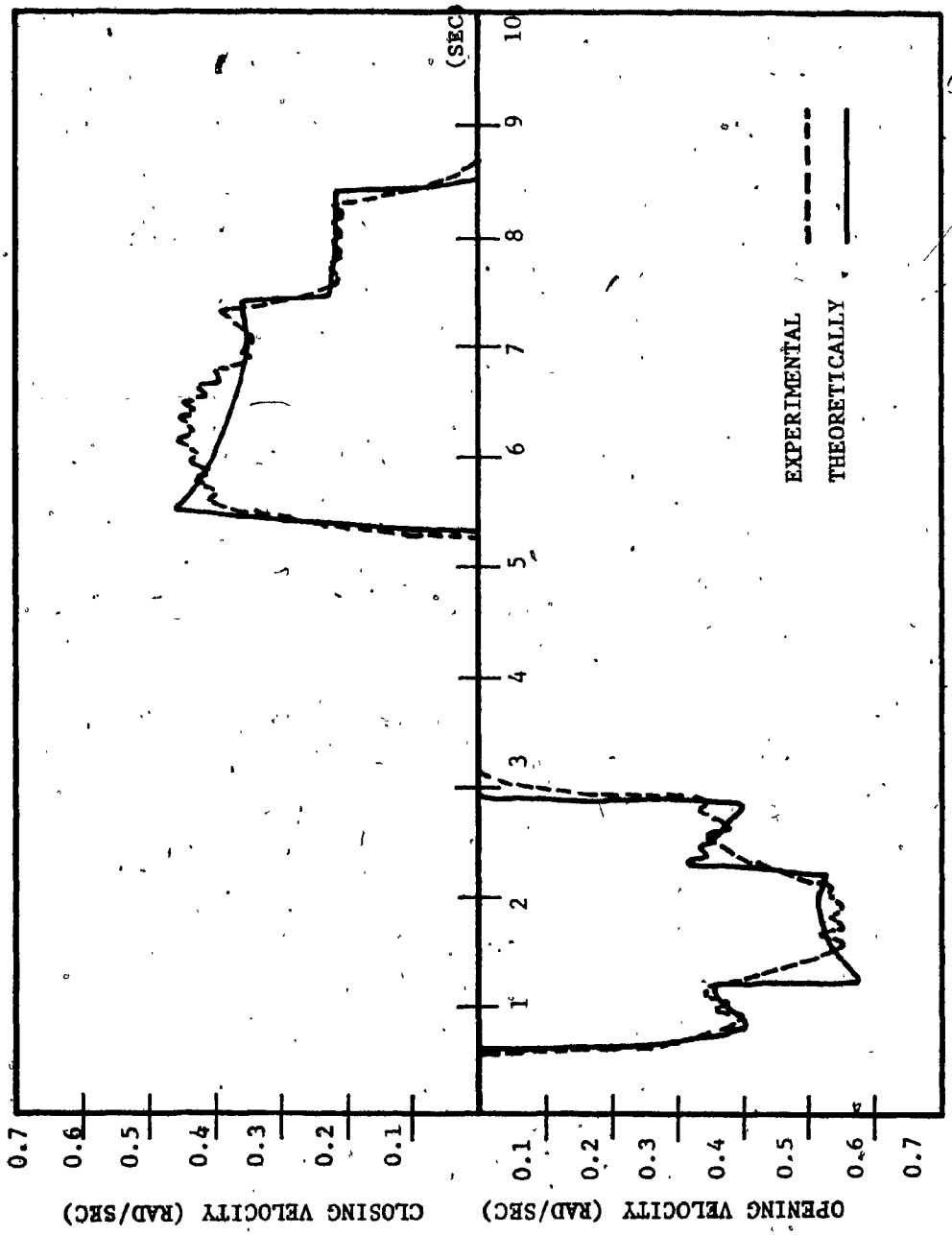

Figure 5-8 Correlation of Experimental Test Run No. 4 and the Model Response

mechanical moving parts is not implemented in the model. However, the overall response of both model and experimental agree with each other. The deviations are well within acceptable limits. It leads to the conclusion that the equations describing the hydro-pneumatic spring closing valve are adequate. Also confidence is gained for the counter weight closing valve model which is based on the similar principle. As a result, the experimental investigation for the counter weight closing valve is not necessary.

The effects of various parameters on the hydro-pneumatic spring closing valve are studied by using the model listed in appendix B.

Considering a system as shown in figure 5-9. The flow equation is

$$Q = C_d A_o \sqrt{\frac{2}{\rho}(P_p - P_r)} \qquad (5.1)$$

where

Q = fluid flow, in^3/sec

C_d = discharge coefficient

A_o = effective orifice area, in^2

P_p = piston head end pressure, psi

P_r = piston rod end pressure, psi

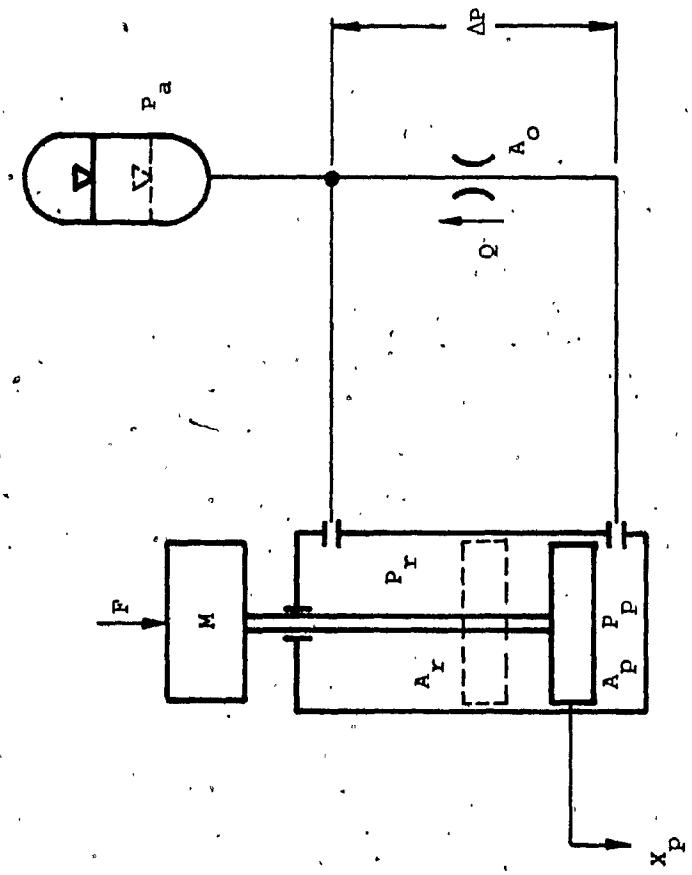

Figure 5-9 Piston-Accumulator Arrangement

The continuity eguation is

$$Q = A_p \frac{d}{dt} X_p + \frac{V_p}{\beta_e} \frac{d}{dt} P_p \qquad (5.2)$$

where

A_p = head side piston area, in^2

X_p = piston displacement, in

V_p = head side chamber volume, in^3

β_e = effective bulk modulus, psi

The relationship between the accumulator pressure, P_a, and the piston displacement can be expressed as

$$P_a = P_r = \frac{P_{ao} V_{ao}}{V_{ao} - (A_p - A_r) X_p} \qquad (5.3)$$

assuming $P_a = P_r$

and

P_{ao} = initial accumulator pressure

V_{ao} = initial accumulator volume

By neglecting friction and leakages, the system equation is

$$F - (P_p A_p - P_r A_r) = M \ddot{X}_p \qquad (5.4)$$

where

F = force, lb_f

M = system mass, $lb_f\text{-sec}^2/in$

From (5.1) and (5.2) it yields

$$A_p \dot{X}_p + \frac{V_p}{\beta_e}\frac{d}{dt}P_p = C_d A_o \sqrt{\frac{2}{\rho}(P_p - P_r)} \qquad (5.5)$$

And by arranging terms, equation (5.5) becomes

$$P_p = P_r + \frac{\rho}{2}\left[\frac{1}{C_d A_o}\left(A_p \dot{X}_p + \frac{V_p}{\beta_e}\frac{d}{dt}P_p\right)\right]^2 \qquad (5.6)$$

Substituting (5.6) into (5.4) it gives

$$F - \left\{A_p\left[P_r + \frac{\rho}{2}\left[\frac{1}{C_d A_o}\left(A_p \dot{X}_p + \frac{V_p}{\beta_e}\frac{d}{dt}P_p\right)\right]^2\right] - P_r A_r\right\} = M\ddot{X}_p \qquad (5.7)$$

Substituting (5.3) into (5.7) and rearranging terms will yield

$$F = M\ddot{X}_p + \frac{A_p\rho}{2}\left(\frac{A_p \dot{X}_p}{C_d A_o}\right)^2 + \frac{A_p\rho}{2}\left(\frac{V_p}{C_d A_o \beta}\frac{d}{dt}P_p\right)^2 + (A_p - A_r)\frac{P_{ao} V_{ao}}{V_{ao} - (A_p - A_r)X_p} \qquad (5.8)$$

By neglecting the hydraulic compressibility term, which is usually small, equation (5.8) becomes

$$F = M\ddot{X}_p + \frac{A_p\rho}{2}\left(\frac{A_p \dot{X}_p}{C_d A_o}\right)^2 + (A_p - A_r)\frac{P_{ao} V_{ao}}{V_{ao} - (A_p - A_r)X_p} \qquad (5.9)$$

describing the system when the piston is moving towards the valve opening.

Similarly, if the force, F, in figure 5-9 is removed, the equation describing the piston moving upwards thus closing valve is

$$(A_p - A_r)\frac{P_{ao} V_{ao}}{V_{ao} - (A_p - A_r)X_p} = M\ddot{X}_p + \frac{A_p \rho}{2}\left(\frac{A_p \dot{X}_p}{C_d A_o}\right)^2 \qquad (5.10)$$

$$\text{Let} \quad f(X_p) = (A_p - A_r)\frac{P_{ao} V_{ao}}{V_{ao} - (A_p - A_r)X_p} \qquad (5.11)$$

Which is the hydro-pneumatic spring force of the system. The relationship between $f(X_p)$, and the piston displacement, X_p, is shown in figure 5-10.

From equations (5.9) and (5.10), it is shown that by decreasing the accumulator precharge pressure, the valve opens faster and closes slower. The model response shown in figure 5-11 confirms the above analysis. With a lower accumulator precharge pressure at 85 psi, the valve opens faster with a maximum opening velocity of 0.81 rad/sec. It closes slower with a maximum velocity of 0.4 rad/sec. The opening and closing impact velocities are 0.37 rad/sec and 0.27 rad/sec respectively.

From equation (5.5), if the orifice area A_o decreases, the velocity also decreases. However, the damping term,

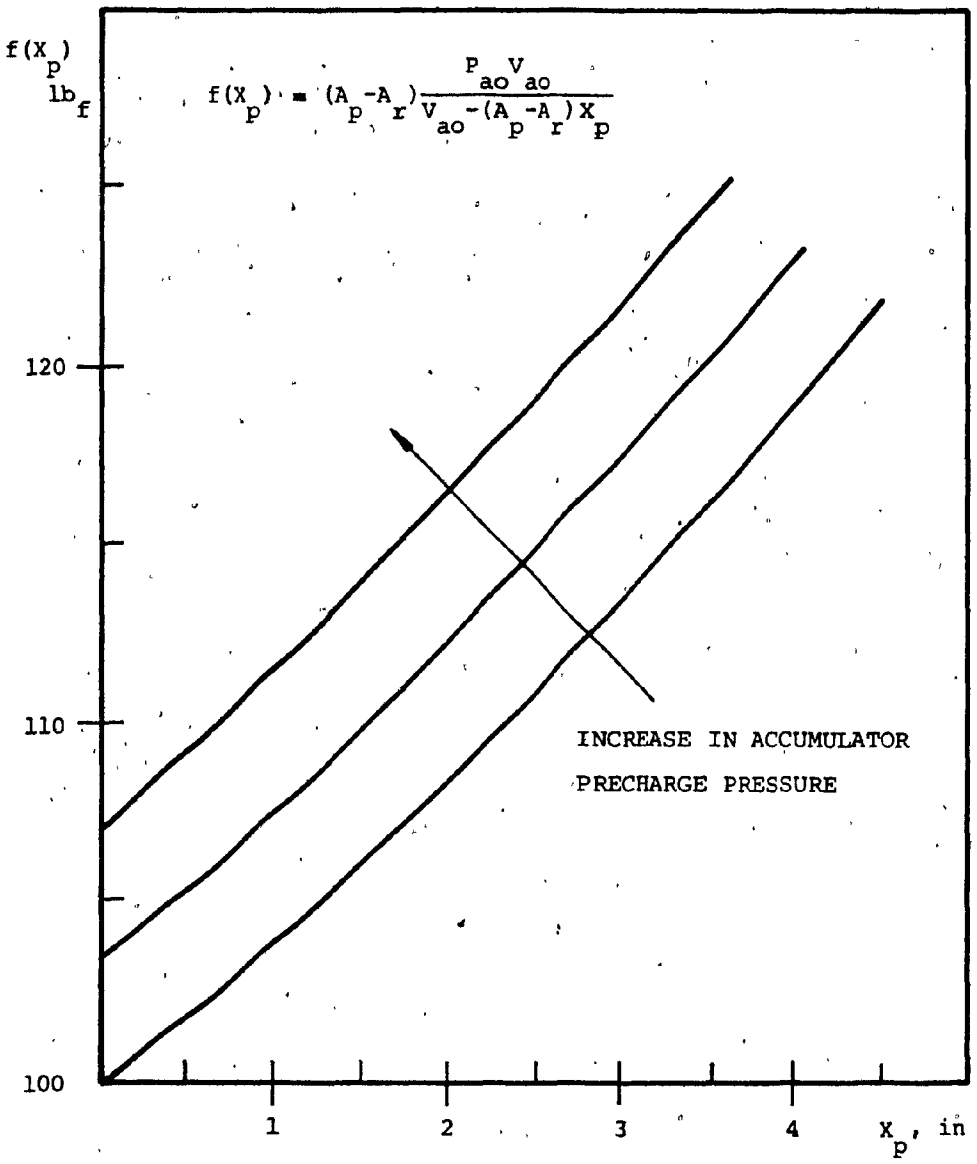

Figure 5-10 The Hydro-Pneumatic Spring Force and Piston Displacement Relationship

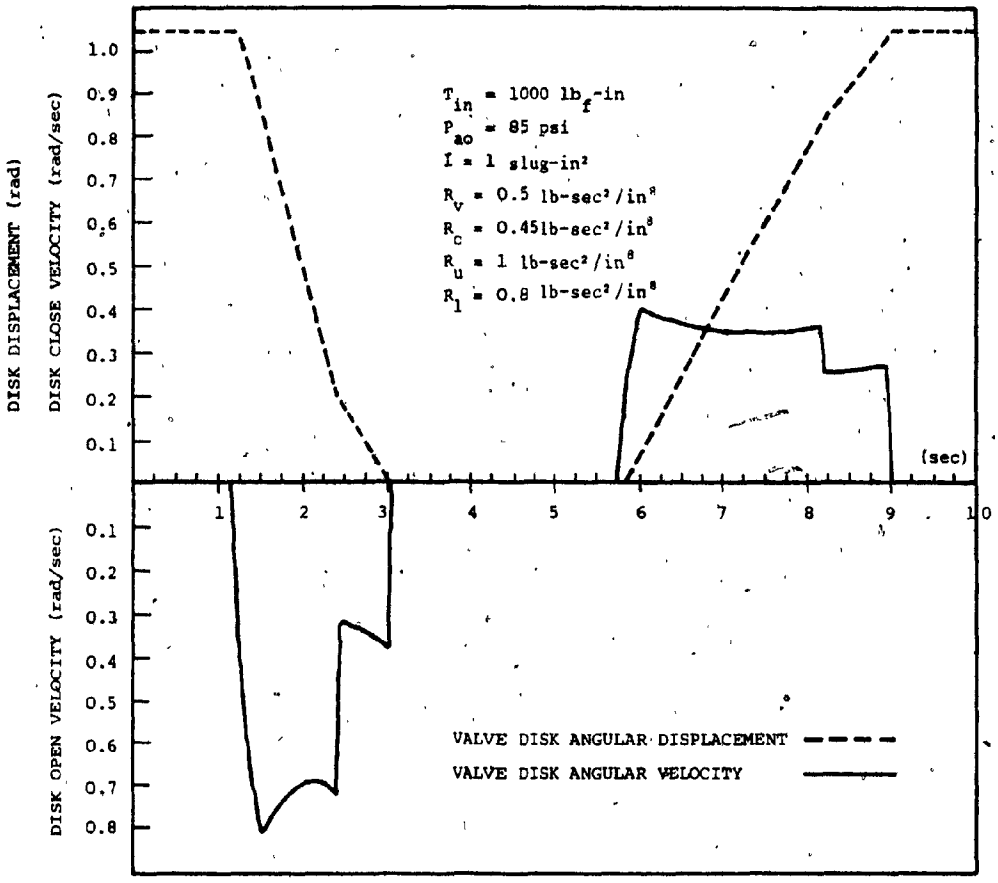

Figure 5-11 Model Response of Hydro-Pneumatic Valve with Decrease in Accumulator Precharge Pressure

$\frac{A_p \rho}{2}\left(\frac{A_p \dot{X}_p}{C_d A_o}\right)^2$, in equation (5.10) decreases much faster. As a matter of fact, the damping force becomes comparitively small and can be neglected. Then equation (5.10) can be written as

$$(A_p - A_r)\frac{P_{ao}V_{ao}}{V_{ao} - (A_p - A_r)X_p} = M\ddot{X}_p \qquad (5.12)$$

indicating a spring-mass oscillating system. The analysis is again confirmed with the model response shown in figure 5-12. It shows that a decrease in orifice area, results in a decrease of the input velocity. The opening and closing impact velocities are found to be 0.17 rad/sec and 0.24 rad/sec respectively. However, the decrease of damping results in oscillation during closing.

Equations (5.9) and (5.10) indicate that the valve inertia will affect the valve response. However, if the damping and the hydro-pneumatic spring force in the system are comparatively large, the effect of variation in valve inertia becomes negligible. Figure 5-13 shows, even with valve inertia increased, that the model response displays a negligible change.

It is also observed from the above equations that the differential piston area, $A_p - A_r$, has the similar effect as the accumulator precharge pressure. The increase in the

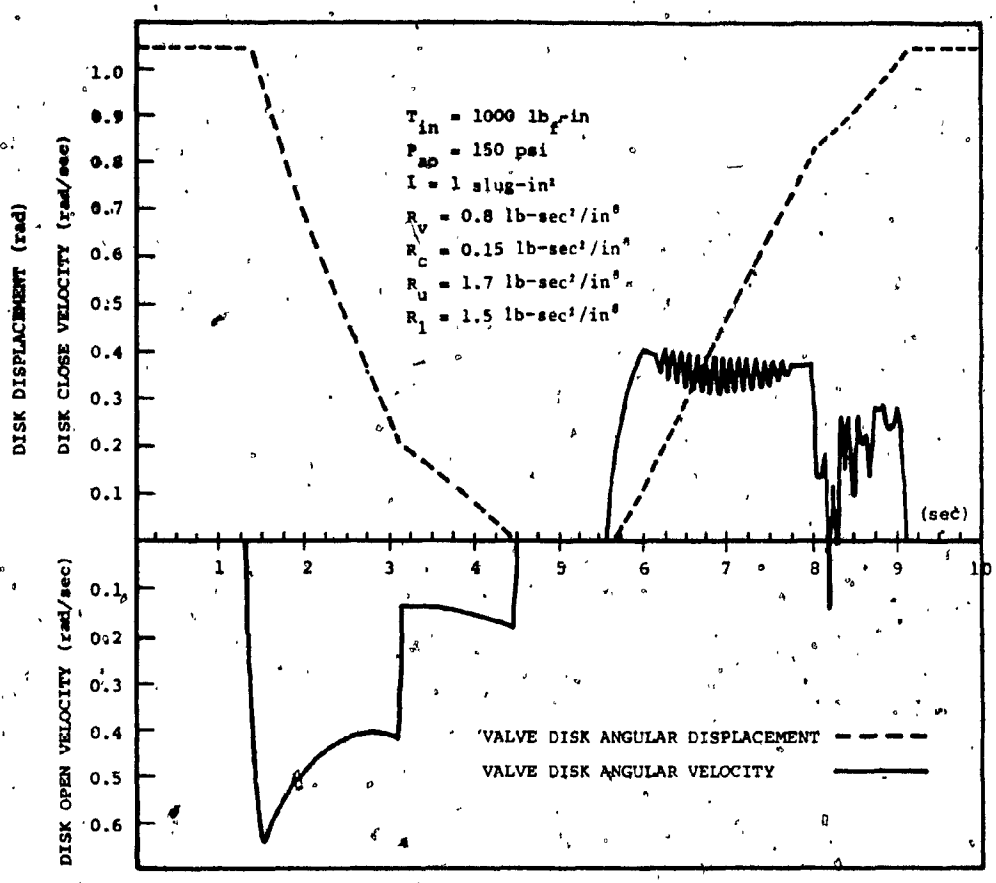

Figure 5-12 Model Response of Hydro-Pneumatic Valve with Decrease in Orifice Area, A_o

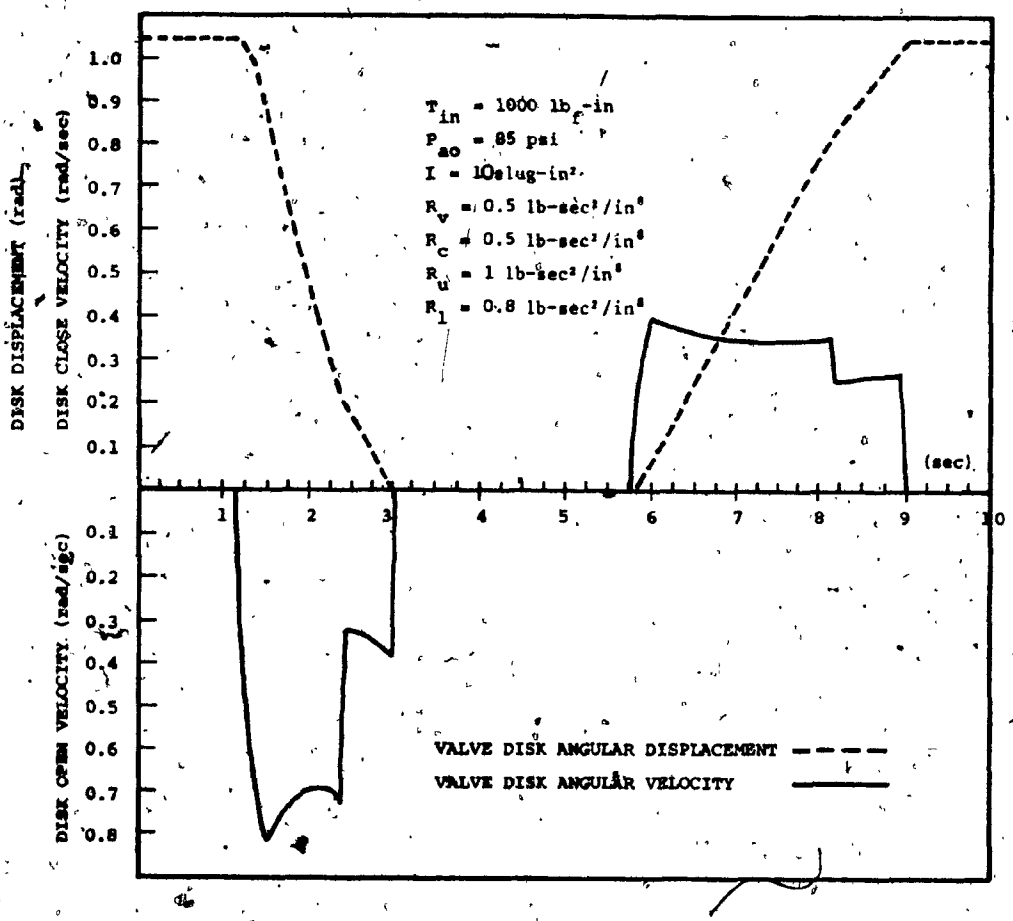

Figure 5-13 Model Response of Hydro-Pneumatic Valve with Increase in Inertia

differential piston area increases the hydro-pneumatic spring force of the system.

5.5 Model Performance of Counter Weight Closing Valve

Figure 5-14 depicts the response of the model described in section 3-3. With an input torque of 500 lb_f-in on the wafer shaft, the maximum opening and closing velocities are 4.97 rad/sec and 4.1 rad/sec respectively. It is found that the opening impact velocity is 0.64 rad/sec and the closing impact velocity is 0.34 rad/sec. The performance shows, the fluid resistor is one of the major system parameters. It controls the valve disk velocity.

During the valve opening, the input torque works against the closing torque created by the counter weight. If the input torque is removed, the valve is closed by the closing torque.

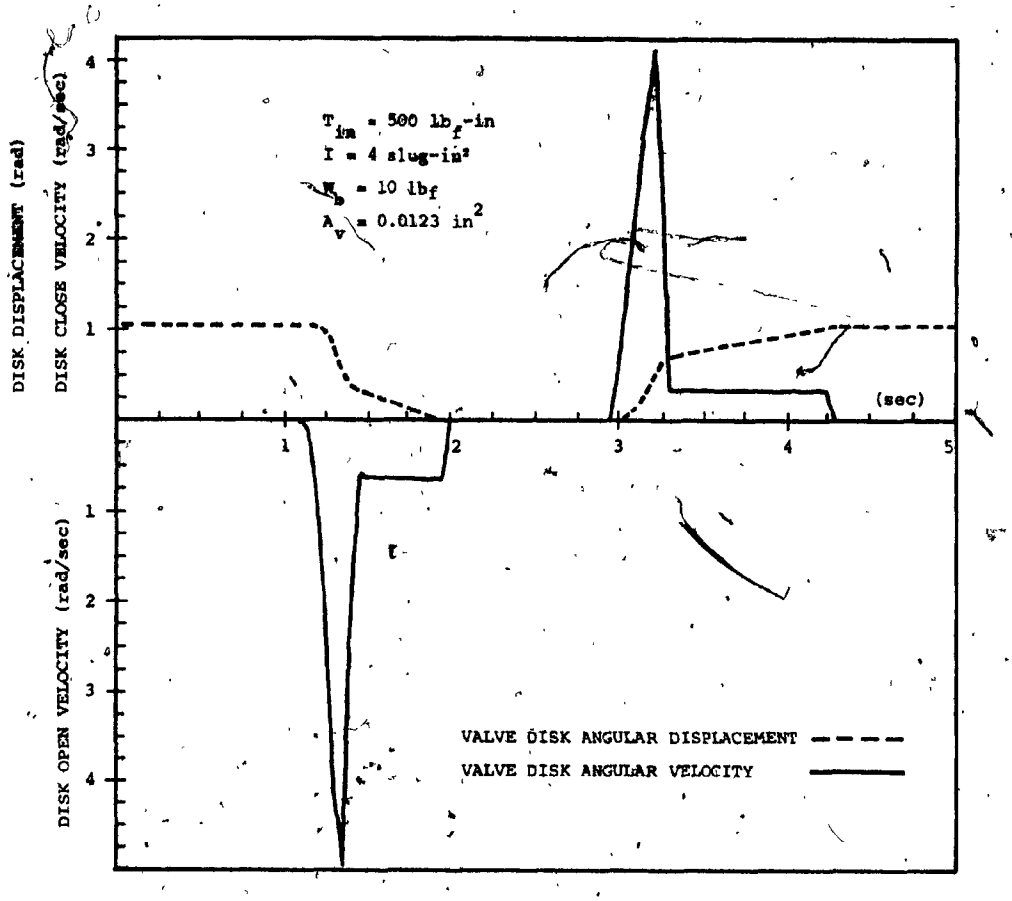

Figure 5-14 Typical Model Response of Counter-Weight Valve

5.6. Effects of Various Parameters on Counter Weight Closing Valve

Considering a system as shown in figure 5-15, the flow equation is

$$Q = C_d A_o \sqrt{\frac{2}{\rho} \Delta P} \tag{5.13}$$

where $\Delta P = P_p - P_r$

The continuity equation is

$$Q = A_p \frac{d}{dt} X_p + \frac{V_p}{\beta_e} \frac{d}{dt} P_p \tag{5.14}$$

and the system equation is

$$F - (P_p A_p - P_r A_r) = M \ddot{X}_p \tag{5.15}$$

For $A_p = A_r$, equation (5.15) becomes

$$F - A_p (P_p - P_r) = M \ddot{X}_p \tag{5.16}$$

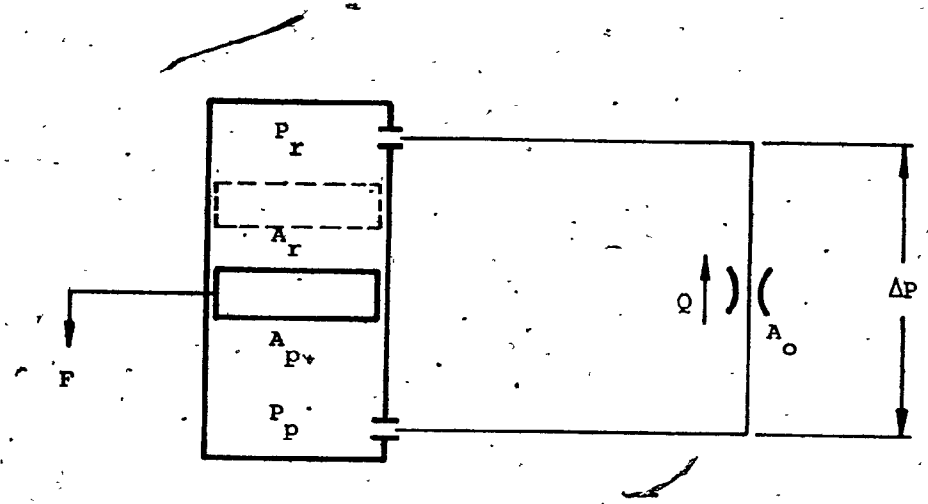

Figure 5-15 Piston-Orifice Arrangement

Combining equation (5.13) and (5.14) becomes

$$A_p \frac{d}{dt} X_p + \frac{V_p}{\beta_e} \frac{d}{dt} P_p = C_d A_o \sqrt{\frac{2}{\rho} \Delta P} \qquad (5.17)$$

or $$\frac{\rho}{2} \left\{ \frac{1}{C_d A_o} \left[A_p \frac{d}{dt} X_p + \frac{V_p}{\beta_e} \frac{d}{dt} P_p \right] \right\}^2 = \Delta P$$

Substituting (5.17) into (5.16) yields

$$F - \frac{A_p \rho}{2} \left\{ \frac{1}{C_d A_o} \left[A_p \frac{d}{dt} X_p + \frac{V_p}{\beta_e} \frac{d}{dt} P_p \right] \right\}^2 = M \ddot{X}_p \qquad (5.18)$$

By neglecting the hydraulic compressibility, (5.18) becomes

$$F = M \ddot{X}_p + \frac{A_p \rho}{2} \left[\frac{A_p \dot{X}_p}{C_d A_o} \right]^2 \qquad (5.19)$$

For valve opening, the net force equation is

$$F = F_o - F_c \qquad (5.20)$$

where

F_o = opening force, lb_f

F_c = closing force, lb_f

and equation (5.19) becomes

$$F_o - F_c = M \ddot{X}_p + \frac{A_p \rho}{2} \left[\frac{A_p \dot{X}_p}{C_d A_o} \right]^2 \qquad (5.21)$$

Similarly, for valve closing, equation (5.19) becomes

$$F_c = M\ddot{X}_p + \frac{A_p \rho}{2}\left[\frac{A_p \dot{X}_p}{C_d A_o}\right]^2 \qquad (5.22)$$

From equations (5.21) and (5.22), with increase in closing force, F_c, the valve opens slower and closes faster.

The model result in figure 5-16 confirms the above analysis. By increasing the closing torque which is created by increasing the counter weight, the valve opens slower with maximum opening velocity of 4.2 rad/sec and closes faster with maximum closing velocity of 4.3 rad/sec. The opening and closing impact velocities are 0.6 and 0.48 rad/sec respectively.

The equation (5.17) shows that the velocity, $\dot{X}_p$, decreases with decreases in orifice area, A_o. This is also confirmed by the model response in figure 5-17. The opening and closing impact velocities are decreased to 0.36 and 0.19 rad/sec respectively.

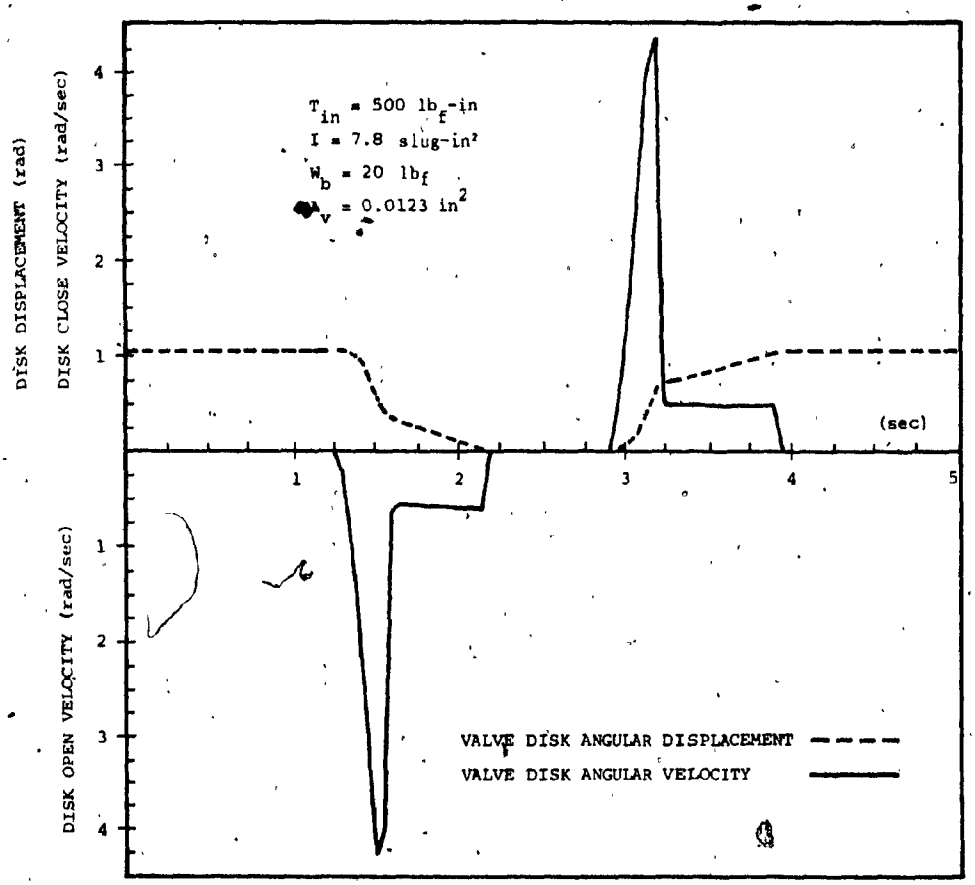

Figure 5-16 Model Response of Counter-Weight Valve with Increases in Counter Weight

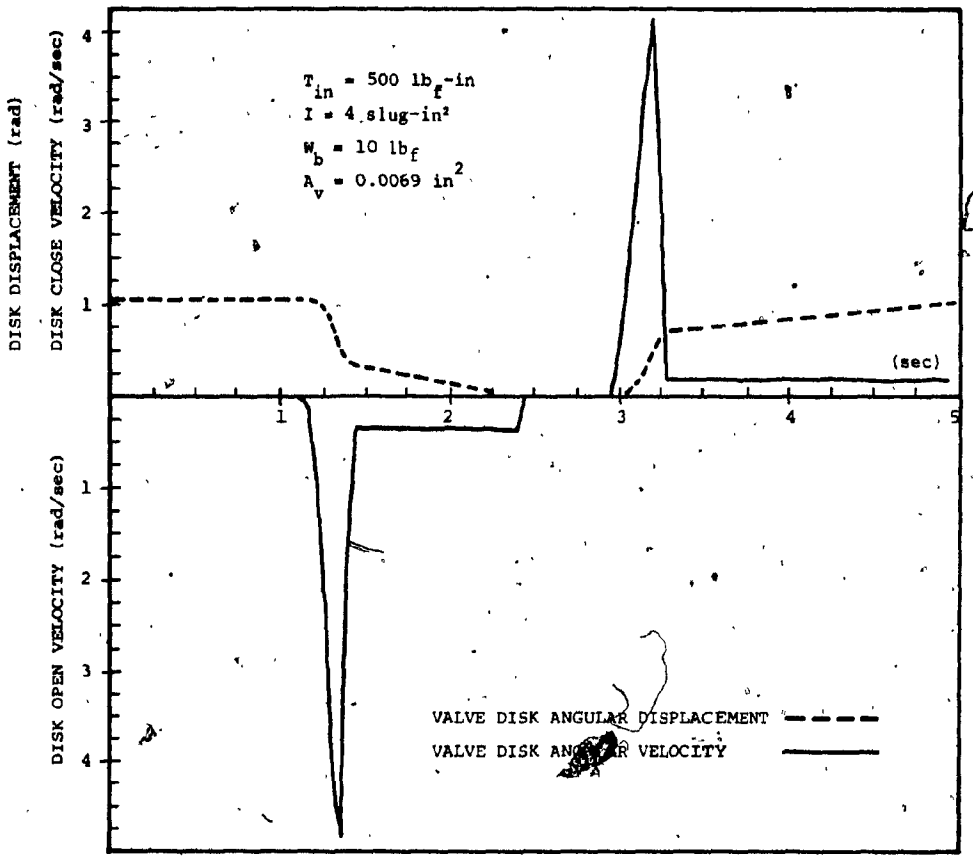

Figure 5 -17 Model Response of Counter-Weight Valve with Decreases in Orifice Area

CHAPTER 6

CONCLUSIONS AND RECOMMENDATIONS FOR FUTURE WORK

The dynamic performance of the hydro-pneumatic spring closing and the counter weight closing valves are investigated in this thesis. It is performed by studying the dynamic response of both digital simulation models. The models are made accurate and realistic by utilizing manufacturer's data of individual component whenever possible.

Experimental investigation of the hydro-pneumatic spring closing valve shows good correlation with the simulation model. It can be concluded that the model equations describing the valve are quite adequate. Confidence is also gained in the fidelity of the counter weight closing valve simulation model.

The development of simulation models is an essential and initial step in the valve dynamic study. The models will be used to study the valves dynamics as related to the valve flow forces and the fluid transients.

Based on the results of the valve dynamic study, the following conclusions can be drawn.

(A) Hydro-pneumatic spring closing check valve

1. The valve dynamics depends to a great extent, on the accumulator precharge pressure and the adjustment of the fluid resistor.
2. The increase in the accumulator precharge pressure increases the system spring constant.
3. With lower accumulator precharge pressure, the valve opens faster and closes slower.
4. The system damping is provided by the fluid resistor which is governed by the orifice area of the fluid resistor. Decreasing the orifice area until a certain critical value increases the damping. Further decreasing of the orifice area beyond the critical value results in the decrease of damping and oscillations may occur.
5. The valve disk velocity is governed by the orifice area of the fluid resistor. The disk velocity decreases with decrease in fluid resistor orifice area.
6. The system spring constant increases with increases in piston differential area.

(B) Counter weight closing check valve

1. The valve dynamics depends mainly on the value of the counter weight and the adjustment of the resistor.
2. The increase in the counter weight increases the closing torque. The valve closes faster and opens slower with increase in counter weight.
3. The system damping is governed by the fluid resistor. System damping increases with decrease in orifice area of the fluid resistor.
4. The valve disk velocity is governed by the fluid resistor orifice area. The disk velocity decreases with decrease in orifice area.

For future investigation in the area of hydraulically damped swing-disk check valve, the following suggestions are made.

1. For the hydro-pneumatic spring closing valve, the accumulator precharge pressure should be optimized by the application objectives.
2. Experimental investigation should be carried out to study dynamics under the influence of water hammer.
3. Investigation should be carried on to study the cylinder chamber leakage effect on the valve dynamics.
4. For the counter weight closing valve, investigation of valve dynamics should be carried out with various

where R_P = radius of pinion, 2.25 in

R_{PH} = radius of pinion hole, 0.4375 in

m_P = mass of pinion, 0.21 slug

m_{PH} = mass of pinion hole, 0.002 slug

3. Moment of Inertia of Disk Lever about Z-axis

is calculated as

$$I_L = \left[\frac{1}{2} m_{LC} R_C^2 - \frac{1}{2} m_{LH} R_{LH}^2\right] + \left[\frac{m_{LR}(b_{LR}^2 + C_{LR}^2)}{12} + m_{LR} l_{LR}^2\right]$$

$$= \left[\frac{1}{2}(0.0258)(0.68)^2 - \frac{1}{2}(0.010)(0.4375)^2\right]$$

$$+ \left[\frac{0.021(0.25^2 + 4.812^2)}{12} + 0.021(3.0)^2\right]$$

$$= 0.234 \text{ slug-in}^2$$

where m_{LC} = mass of lever circular portion, 0.0255 slug

m_{LH} = mass of lever hole, 0.0107 slug

m_{LR} = mass of lever rectangular portion, 0.021 slug

R_C = radius of lever circular portion, 0.68 in

R_{LH} = radius of lever hole, 0.4375 in

l_{LR} = distance from mass center of lever rectangular portion to Z-axis, 3 in

b_{LR} = width of lever rectangular portion, 0.25 in

C_{LR} = height of lever rectangular portion, 4.812 in

4. Moment of Inertia of Valve Disk about Z-axis

is calculated as

$$I_D = \frac{m_D(b_D^2 + C_D^2)}{12} + m_D l_D^2$$

$$= \frac{0.133(0.375^2 + 7.125^2)}{12} + 0.133(4.437)^2$$

$$= 3.18 \text{ slug-in}^2$$

where m_D = mass of valve disk, 0.133 slug

C_D = height of valve disk, 7.125 in

b_D = width of valve disk, 0.375 in

l_D = distance from valve disk mass center to Z-axis, .437 in

5. Moment of Inertia of Connecting Linkage about Z-axis

is calculated as

$$I_C = \left[\frac{m_C(b_C^2 + C_C^2)}{12} + m_C l_C\right] - \frac{1}{2} m_{CH} R_{CH}^2$$

$$= \left[\frac{0.112(1.75^2 + 5.75^2)}{12} + 0.112(2.0)^2\right]$$

$$- \left[\frac{1}{2}(0.007)(4.375)^2\right]$$

$$= 0.78 \text{ slug-in}^2$$

where m_C = mass of connecting linkage, 0.112 slug

m_{CH} = mass of linkage hole, 0.007 slug

C_C = height of linkage, 0.57 in

b_C = width of linkage, 1.75 in

l_C = distance from linkage mass center to Z-axis, 2 in

R_{CH} = radius of linkage hole, 0.4375 in

6. Moment of Inertia of Valve Actuator Piston about Z-axis

is calculated as

$$I_a = m_a l_a^2$$

$$= 1.88 \text{ slug-in}^2$$

where m_a = mass of actuator piston, 0.1179 slug

l_a = distance from actuator mass center to Z-axis, 4 in

7. Moment of Inertia of Rack about Z-axis

is calculated as

$$I_R = m_R l_R^2$$

$$= 2.33 \text{ slug-in}^2$$

where m_R = mass of rack, 0.23 slug

l_R = distance from rack center to Z-axis, 3.187 in

8. Moment of Inertia of Input Actuator about Z-axis

is calculated as

$$I_I = m_I l_I^2$$

$$= 1.812 \text{ slug-in}^2$$

where m_I = mass of input actuator piton, 0.069 slug

l_I = distance from acuator mass center to Z-axis, 5.125 in

The total moment of inertia of valve disk and the associated parts about the Z-axis is found to be

$$10.75 \text{ slug-in}^2$$

APPENDIX B

MIMIC Model of the Hydro-Pneumatic Spring Closing Valve

```
*
*               DYNAMICS SIMULATION OF HYDRO-PNEUMATIC CLOSING
*               VALVE
*
*
*               INPUT FUNCTION GENERATOR
*
        FN1     CFN(6.)
*
*               INITIAL CONDITIONS
*
*               PAR(DTETA,TETA,ALFA,DY)
*
*               SYSTEM PARAMETERS
*
        VA0     30.
        PA0     150.
        A1      3.68
        A2      4.9
        J       1.
        RV      0.5
        RC      0.15
        RU      1.
        RL      0.8
*
*               INPUT TORQUE FUNCTION
*
        TIN     FUN(FN1,T)
*
*               HYDRAULIC CYLINDER TORQUE AT ANGLE ALFA
*
        TCY     (P2*A2-P1*A1)*SIN(ALFA)*4.0
*
*               DISK ANGULAR ACCELERATION IS OBTAINED
*               FROM DIVIDING TORQUE DIFFERENCE BY INERTIA
*
        TDIFF   (TCY-TIN)/J
*
*               MAXIMUM ANGULAR DISPLACEMENT WHICH IS 1.0472 RAD.
*
        TEMAX   FSW(TETA-1.0472,FALSE,TRUE,TRUE)
*
*               MINIMUM ANGULAR DISPLACEMENT WHICH IS 0. RAD.
*
        TEMIN   FSW(TETA,TRUE,TRUE,FALSE)
*
*               POSITIVE ANGULAR VELOCITY
*
        PDTETA  FSW(DTETA,FALSE,FALSE,TRUE)
*
*               NEGATIVE ANGULAR VELOCITY
*
        NDTETA  FSW(DTETA,TRUE,FALSE,FALSE)
*
*               PHYSICAL LIMITATIONS
*               FIRST LIMITATION IS MAX. DISPLACEMENT
*               AND POSITIVE ANGULAR VELOCITY
```

```
*                    SECOND LIMITATION IS MIN. DISPLACEMENT
*                    AND NEGATIVE ANGULAR VELOCITY
*
          LIMIT      IOR(AND(TEMAX,PDTETA),AND(TEMIN,NDTETA))
          RANGE      NOT(LIMIT)
*
*                    WHEN LIMIT CONDITION IS SATISFIED
*                    THE ACCELERATION IS SET TO ZERO
 LIMIT    TDIFF1     0.
 RANGE    TDIFF1     TDIFF
*
*                    TO FIND ANGULAR VELOCITY BY INTEGRATING
*                    ACCELERATION
*
 LIMIT    DTETA      0.
 RANGE    DTETA      INT(TDIFF1,0.,LIMIT,FALSE)
*
*                    TO FIND ANGULAR DISPLACEMENT BY INTEGRATING
*                    ANGULAR VELOCITY
*
          TETA1      INT(DTETA,TETA)
*
*                    THE ACCEPTABLE ANGULAR DISPLACEMENT VALUE
*                    IS FROM 0. TO 1.0472 RAD.
*
          SET1       FSW(TETA1,TRUE,TRUE,FALSE)
          SET2       FSW(TETA1-1.0472,FALSE,TRUE,TRUE)
          SET3       NOT(IOR(SET1,SET2))
 SET1     TETA       0.
 SET2     TETA       1.0472
 SET3     TETA       TETA1
*
*                    HYDRAULIC ACTUATOR DISPLACEMENT
*
          Y          SQR(76.999-62.482*(COS(.5877+TETA)))
*
*                    TO FIND ANGLE ALFA
*
          FN         (Y*Y-45.)/(8.*Y)
          ALFA       ACS(FN)
*
*                    HYDRAULIC ACTUATOR VELOCITY
*                    WITH PHYSICAL LIMITATIONS IN CONSIDERATION
*
 LIMIT    DY         0.
 RANGE    DY         62.482*SIN(0.5877+TETA)*DTETA/(2.*Y)
*
*                    ROD END FLUID FLOW RATE
*
          Q1         A1*DY
*
*                    PISTON END FLUID FLOW RATE
*
          Q2         A2*DY
*
*                    ACCUMULATOR FLUID FLOW RATE
          QA         Q2-Q1
```

```
*
*                   THE COMPRESSED GAS VOLUME IS OBTAINED
*                   BY INTEGRATING THE ACCUMULATOR FLUID FLOW RATE
*
          VA        INT(QA,30.)
*
*                   INSTANTANEOUS ACCUMULATOR PRESSURE
*
          PA        PA0*VA0/VA
          P1        PA
*
*                   POSITIVE ACTUATOR VELOCITY
*
          PDY       FSW(DY,FALSE,FALSE,TRUE)
*
*                   UPPER CUSHION REGION IS .75 IN. FROM THE END OF
*                   STROKE
*
          UPCU      FSW(Y-8.25,FALSE,FALSE,TRUE)
*
*                   THE P2 VALUE DEPENDS ON THE FLUID RESTRICTION
*
 PDY      P2        LSW(UPCU,P1-RU*Q2*Q2,P1-RV*Q2*Q2)
*
*                   NEGATIVE ACTUATOR VELOCITY
*
          NDY       FSW(DY,TRUE,FALSE,FALSE)
*
*                   LOWER CUSHION REGION IS .75 IN. FROM THE END OF
*                   STROKE
*
          LOCU      FSW(Y-5.75,TRUE,FALSE,FALSE)
*
*                   THE P2 VALUE DEPENDS ON THE FLUID RESTRICTION
*
 NDY      P2        LSW(LOCU,P1+RL*Q2*Q2,P1+RC*Q2*Q2)
*
*                   FOR ZERO ACTUATOR VELOCITY P2=P1
*
          ODY       FSW(DY,FALSE,TRUE,FALSE)
 ODY      P2        P1
*
*                   OUTPUT TIME INTERVAL AND INTEGRATING TIME
*                   INTERVAL
*
          DT        0.05
          DTMAX     0.0005
          DTMIN     0.0005
*
*                   OUTPUT FORMAT
*
                    OUT(T,DTETA,TETA)
                    OUT(DY,Y,PA)
                    OUT(VA,TCY,TIN,IDIFF,P1,P2)
                    OUT(,Q2,Q1,QA,TETA1,DTETA1)
                    PLO(T,DTETA,TIN,TETA)
                    FIN(T,9.9)
                    END
```

0.	0.		
1.	0.		
1.5	1200.		
5.5	1200.		
6.0	0.		
10.	0.		
0.	1.0472	1.0472	0.

APPENDIX C

Fourth-Order Runge-Kutta Method

APPENDIX C

Fourth-Order Runge-Kutta Method

Ordinary differential equations can be solved using a Runge-Kutta integration method. The procedure for the Fourth-Order Runge-Kutta method started by evaluating the dependent variable at the beginning, halfway, and end of the integration interval. The final step is then made across the interval using a weighted average of all three derivations. The general procedure involved is outlined as follows.

Let $\frac{dy}{dx} = F(x,y)$

then using the Fourth-Order Runge-Kutta method [27], the discrete solution is given as

$$y(n+1) = y(n) + \frac{1}{6}(k_1+2k_2+2k_3+k_4)$$

where

$$k_1 = h \cdot F(x,y)$$

$$k_2 = h \cdot F(x+\frac{h}{2}, y+\frac{k_1}{2})$$

$$k_3 = h \cdot F(x+\frac{h}{2}, y+\frac{k_2}{2})$$

$$k_4 = h \cdot F(x+h, y+k_3)$$

h is the step size equal to [x(n+1) - x(n)]

APPENDIX D

MIMIC Model of Counter Weight Closing Valve

```
*
*               DYNAMICS SIMULATION OF COUNTER WEIGHT CLOSING
*               VALVE
*
*
*               SYSTEM CONSTANTS
*
                CON(D1,D2,DC3,DO3,R)
                CON(C1,C2,C3,O1,O2,O3)
                CON(IM,WB,WF,OA,OB,ALFA)
                CON(RO,CD,AV)
                CON(TEMAXO,TEMINO)
*
*               FUNCTION GENERATOR
*
F1              CFN(6.)
F2              CFN(2.)
F3              CFN(2.)
*
*               SYSTEM INITIAL PARAMETERS
*
                PAR(DTETAO,TETAO)
*
*               INPUT VALVE OPENING TORQUE
*
TO              FUN(F1,T)
*
*               PLUNGER TAPER FUNCTION
*
ACX             FUN(F2,X)
AOX             FUN(F3,X)
*
*               TORQUE BALANCE EQUATION
*
DELTA           WB*OA*SIN(ALFA+TETA)+WF*OB*SIN(TEMAXO-TETA)+F*R-TO
*
*               VALVE DISK ACCELERATION
*
TDIFF           DELTA/IM
*
*               MAXIMUMANGULAR DISPLACEMENT WHICH IS TEMAXO
*
TEMAX           FSW(TETA-TEMAXO,FALSE,TRUE,TRUE)
*
*               MINIMUM ANGULAR DISPLACEMENT WHICH IS TEMINO
*
TEMIN           FSW(TETA-TEMINO,TRUE,TRUE,FALSE)
*
*               POSITIVE ANGULAR VELOCITY
*
PDTETA          FSW(DTETA,FALSE,FALSE,TRUE)
*
*               NEGATIVE ANGULAR VELOCITY
*
NDTETA          FSW(DTETA,TRUE,FALSE,FALSE)
*
*               PHYSICAL LIMITATIONS
```

```
*                   FIRST LIMITATION IS MAX. DISPLACEMENT
*                   AND POSITIVE ANGULAR VELOCITY.
*                   SECOND LIMITATION IS MIN. DISPLACEMENT
*                   AND NEGATIVE ANGULAR VELOCITY.
*
          LIMIT     IOR(AND(TEMAX,PDTETA),AND(TEMIN,NDTETA))
          RANGE     NOT(LIMIT)
*
*                   WHEN LIMIT CONDITION IS SATISFIED
*                   THE ACCELERATION IS SET TO ZERO.
*
 LIMIT    TDIFF1    0.
 RANGE    TDIFF1    TDIFF
*
*                   TO FIND ANGULAR VELOCITY BY
*                   INTEGRATING THE ANGULAR ACCELERATION.
*
          DTETA     INT(TDIFF1,DTETAO,LIMIT,FALSE)
*
*                   PHYSICAL LIMITAIONS SAME AS BEFORE
*                   ANGULAR VELOCITY IS SET TO ZERO
*                   WHEN LIMIT CONDITION IS SATISFIED.
*
 LIMIT    DTETA1    0.
 RANGE    DTETA1    DTETA
*
*                   TO FIND ANGULAR DISPLACEMENT BY
*                   INTEGRATING ANGULAR VELOCITY.
*
          TETA1     INT(DTETA,TETAO)
*
*                   THE ACCEPTABLE ANGULAR DISPLACEMENT VALUE
*                   IS FROM TEMINO TO TEMAXO RAD.
*
          SET1      FSW(TETA1,TRUE,TRUE,FALSE)
          SET2      FSW(TETA1-TEMAXO,FALSE,TRUE,TRUE)
          SET3      NOT(IOR(SET1,SET2))
 SET1     TETA      TEMINO
 SET2     TETA      TEMAXO
 SET3     TETA      TETA1
*
*                   RACK DISPLACEMENT AND VELOCITY
*
          X         R*TETA
          DX        R*DTETA1
*
*                   FLUID FLOW RATE
*
          Q         0.785*(D1*D1-D2*D2)*DX
*
*                   THE PRESSURE DROP ACROSS THE CHAMBERS
*                   AND THE HYDRAULIC FORCE ON THE PLUNGERS
*                   DEPENDS ON THE ORIFICE CONDITIONS WHICH
*                   IS GOVERNED BY THE OPENING AND
*                   CLOSING LOGICS.
*
```

```
FREE    DP      0.
RES     DP      RO*Q*Q/(2.*CD*CD*AV*AV)
CTAP    DP      RO*Q*Q/(2.*CD*CD*(AV+ACX)*(AV+ACX))
OTAP    DP      RO*Q*Q/(2.*CD*CD*(AV+AOX)*(AV+AOX))
CFRTP   F       -0.785*D1*D1*DP
CRES    F       -0.785*(D1*D1-D2*D2)*DP
OFRTP   F       0.785*D1*D1*DP
ORES    F       0.785*(D1*D1-D2*D2)*DP
*
*               OPENING LOGIC
*
        OPEN    FSW(DTETA1,TRUE,FALSE,FALSE)
        XLO1    FSW(X-O1,TRUE,FALSE,FALSE)
        XGEO1   NOT(XLO1)
        XLO12   FSW(X-O1-O2,TRUE,FALSE,FALSE)
        XGEO12  NOT(XLO12)
        OFREE   AND(OPEN,XGEO12)
        OTAP    AND(OPEN,XGEO1,XLO12)
        ORES    AND(OPEN,XLO1)
        OFRTP   AND(OPEN,XGEO1)
*
*               CLOSING LOGIC
*
        CLOSE   NOT(OPEN)
        XLC3    FSW(X-C3,TRUE,FALSE,FALSE)
        XGEC3   NOT(XLC3)
        XLC23   FSW(X-C2-C3,TRUE,FALSE,FALSE)
        XGEC23  NOT(XLC23)
        CFREE   AND(CLOSE,XLC3)
        CTAP    AND(CLOSE,XGEC3,XLC23)
        CRES    AND(CLOSE,XGEC23)
        CFRTP   AND(CLOSE,XLC23)
*
*               FREE OF ORIFICE CONDITIONS
*
        FREE    IOR(CFREE,OFREE)
*
*               RESTRICTED BY ORIFICE CONDITIONS
*
        RES     IOR(CRES,ORES)
*
*               OUPUT CONTROL
*
        DT      0.05
        DTMAX   0.0005
        DTMIN   0.0005
                OUT(T,DTETA1,TETA)
                PLO(T,TO,DTETA1,TETA)
                FIN(T,4.9)
                END
```

1.750	0.625	0.3125	0.437	2.5000	
0.875	0.875	0.875	0.8750	0.8750	0.875
4.0	10.00	1.0	12.0	4.500	0.523
0.00078	0.6	0.0123			
1.0472	0.				
0.	0.				
1.00	0.				
1.5	500.				
2.5	500.				
3.00	0.				
10.	0.				
0.	0.57325				
1.7883	0.				
0.	-0.13240				
2.625	0.30170				
0.	1.0472				

APPENDIX E

Component Detailed Drawings

of

the Test Rig

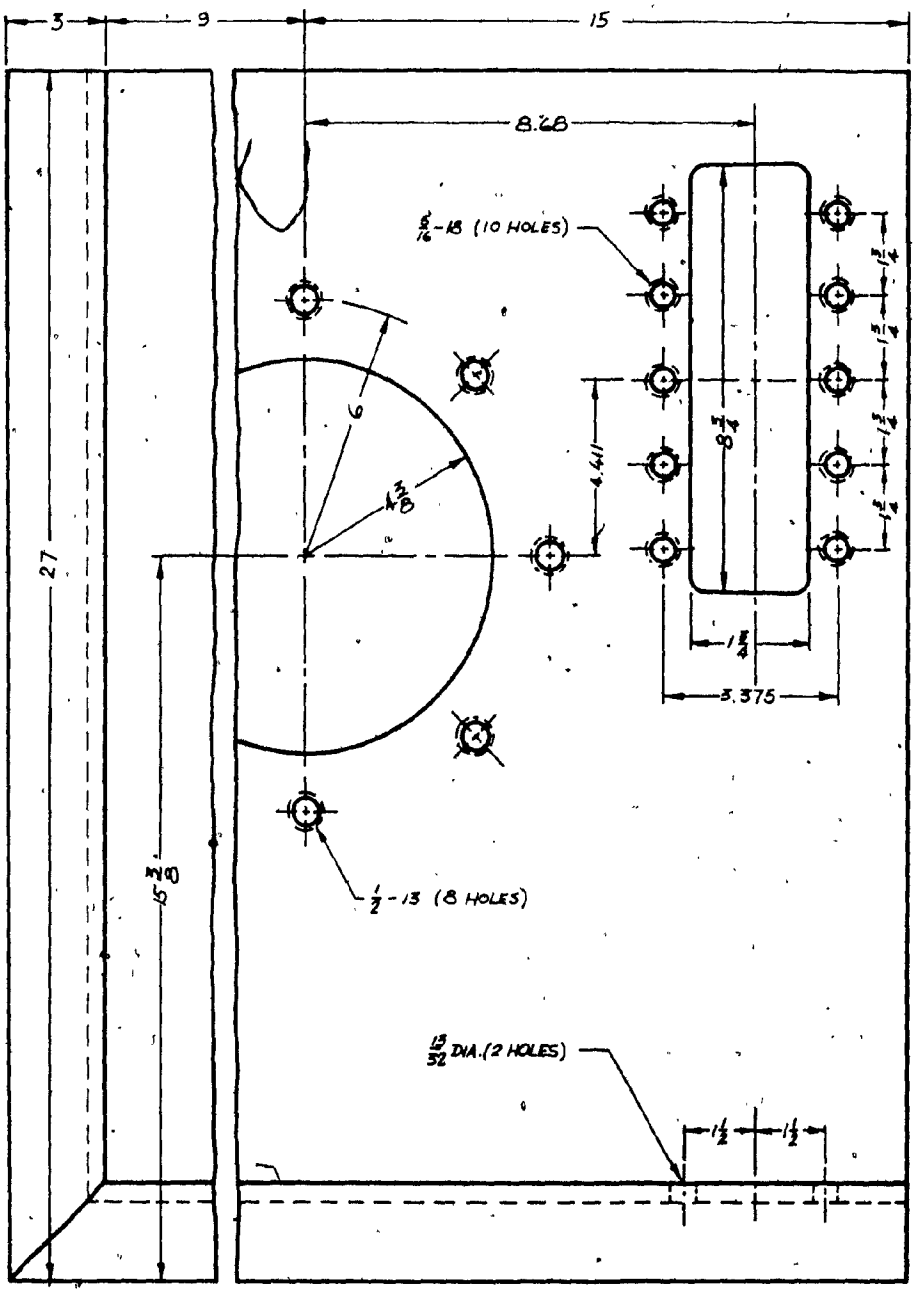

Figure E-1 Front View of Test Rig Base

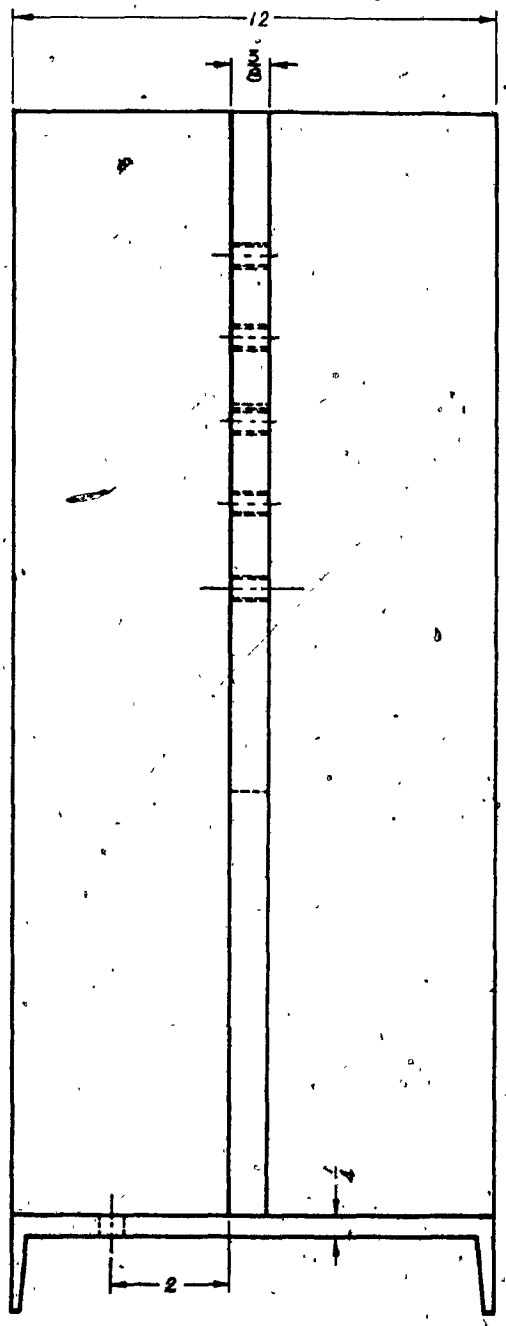

Figure E-2 Side View of Test Rig Base

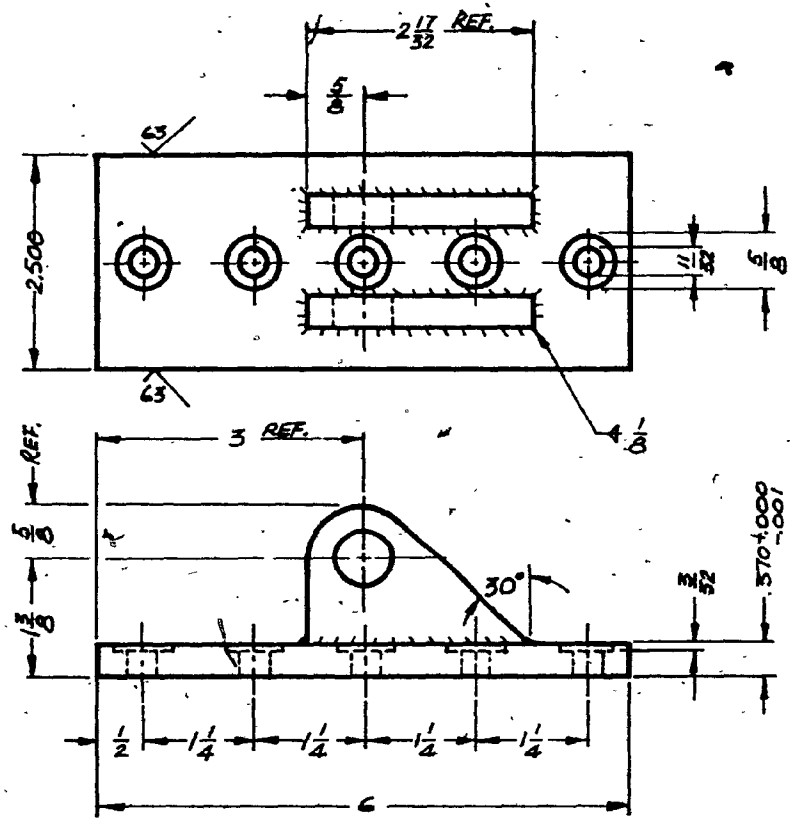

ITEM NO. 2.

MATERIAL: AISI C-1018/C-1020

REQ'D: 1

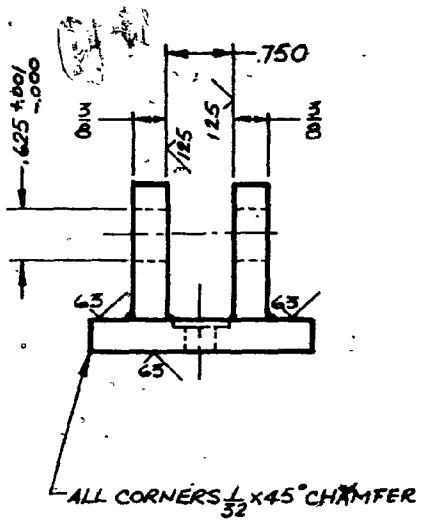

Figure E-3 Rack Clevis

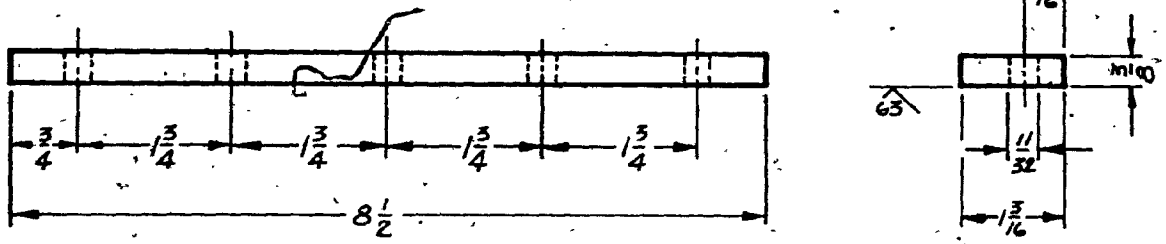

ITEM NO. 3

MATERIAL: AISI C-1018/C-1020

REQ'D: 2

Figure E-4 Rack Guide Clamp

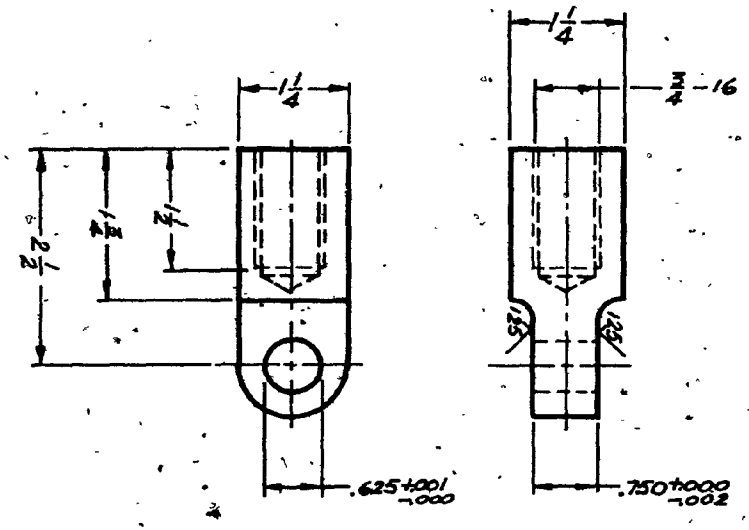

ITEM NO. 4

MATERIAL: AISI C-1018/C-1020

REQ'D: 1

Figure E-5 Actuator Clevis

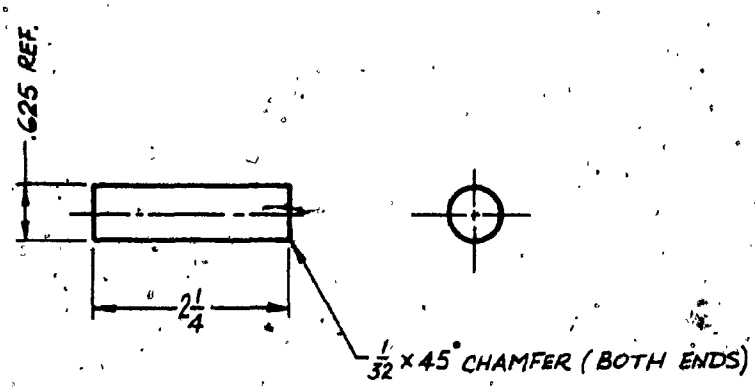

ITEM NO. 5

MATERIAL: AISI C-1018/C-1020

REQ'D: 1

Figure E-6 . Rack Clevis Pin

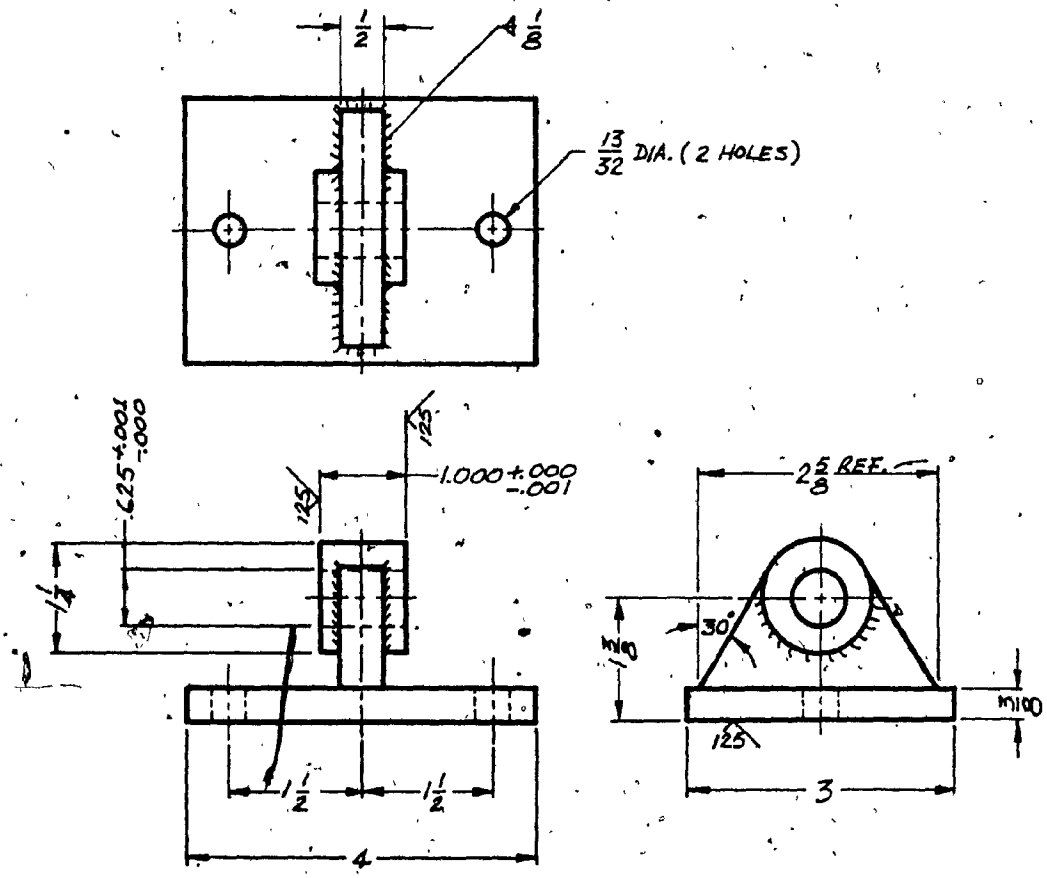

ITEM NO. 6

MATERIAL: AISI C1018/C-1020

REQ'D: 1

Figure E-7 Test Rig Base Clevis

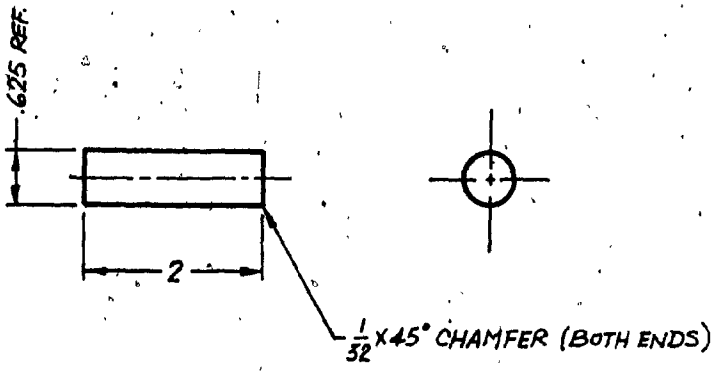

ITEM NO. 7

MATERIAL: AISI C-1018/C-1020

REQ'D: 1

Figure E-8 Actuator Clevis Pin

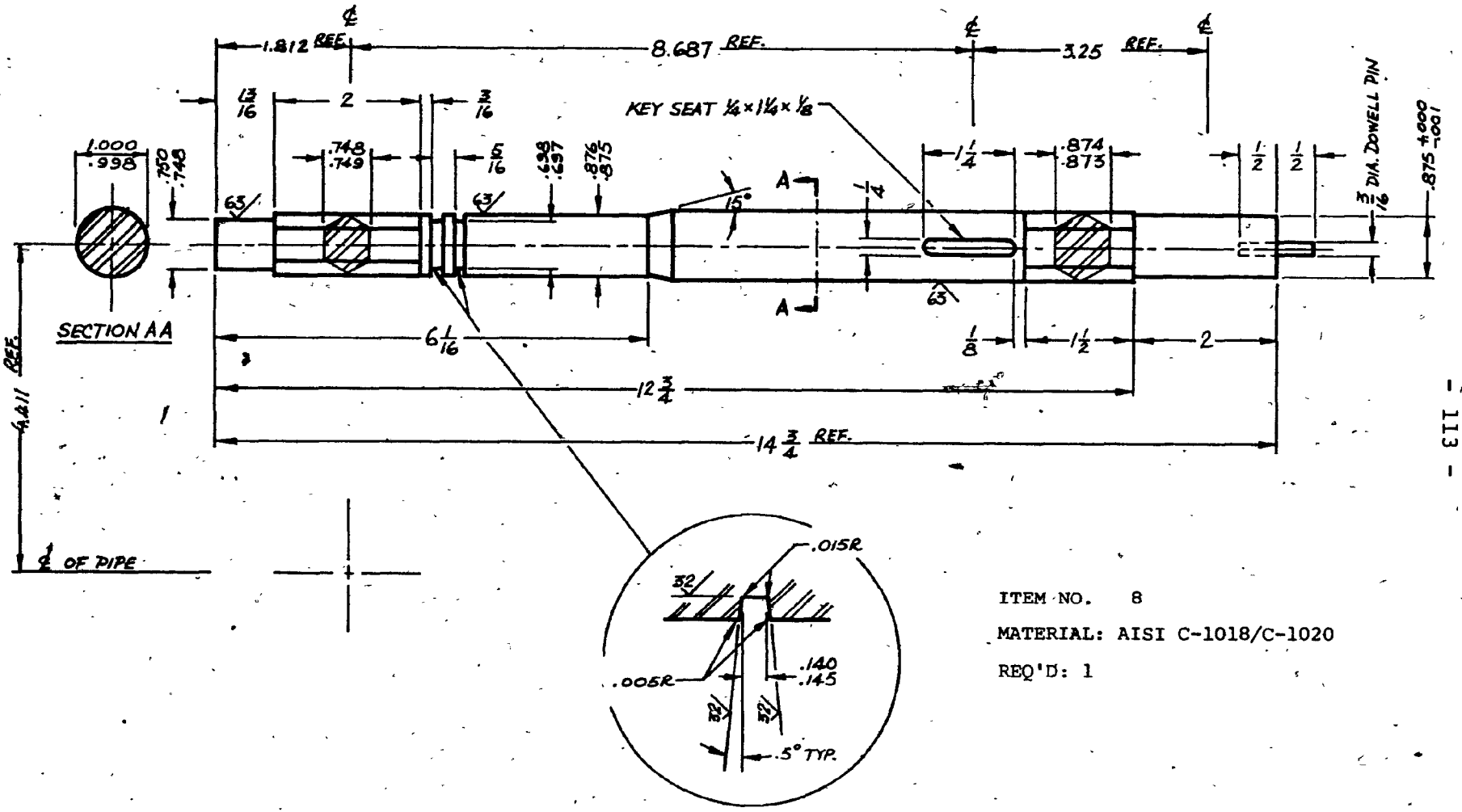

ITEM NO. 8

MATERIAL: AISI C-1018/C-1020

REQ'D: 1

Figure E-9 Wafer Shaft

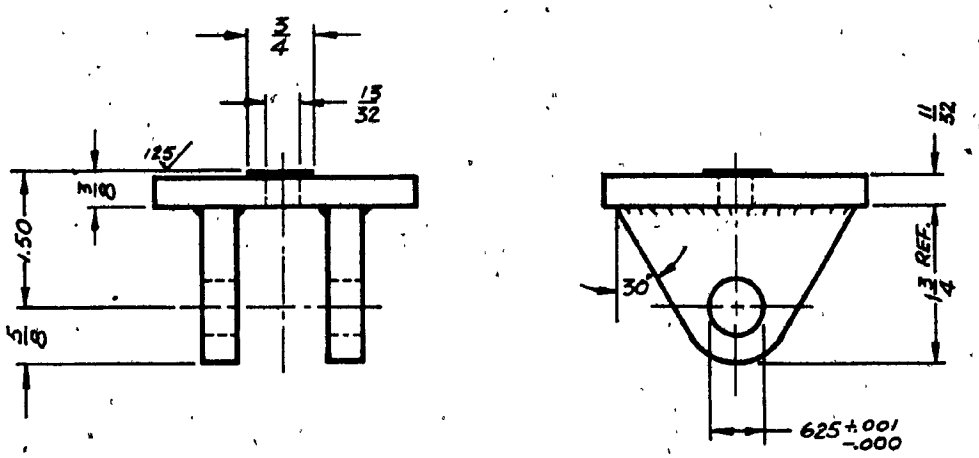

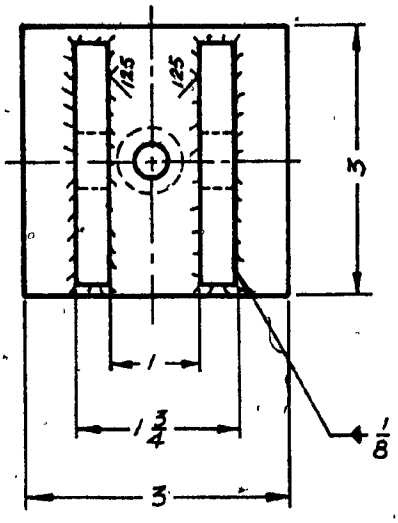

ITEM NO. 9

MATERIAL: AISI C-1018/C-1020

REQ'D: 1

Figure E-10 Load Cell Clevis

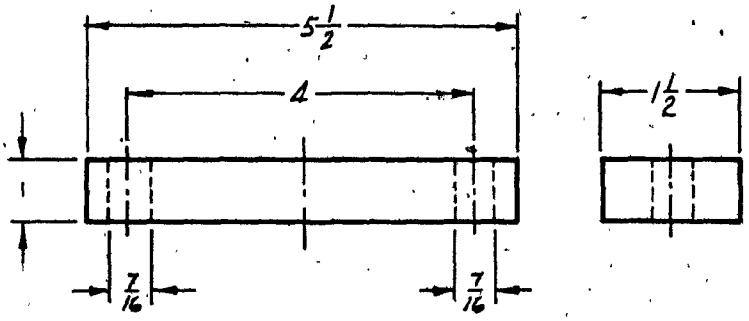

ITEM NO. 10

MATERIAL: AISI C-1018/C-1020

REQ'D: 1

Figure E-11 Bearing Spacer

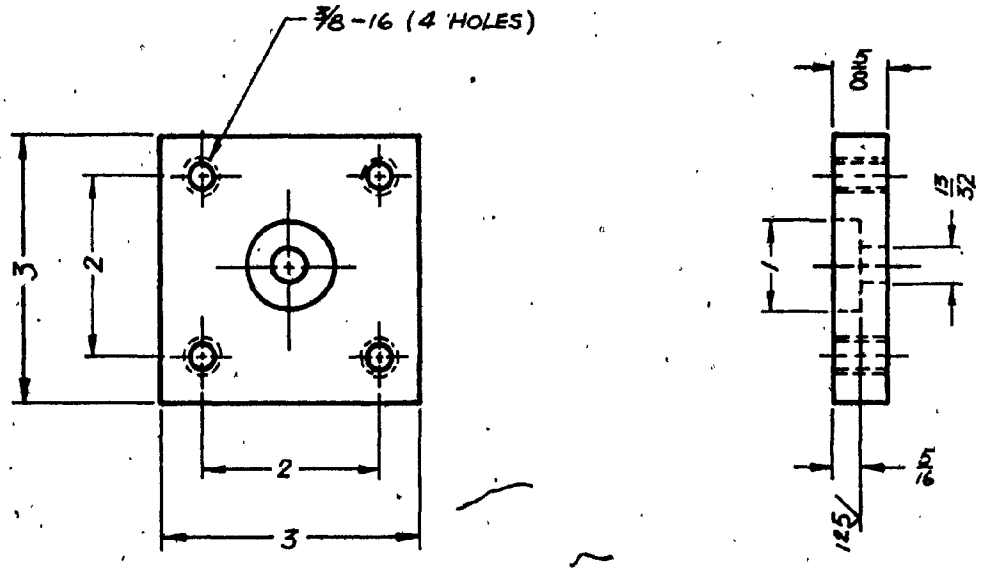

ITEM NO. 11

MATERIAL: AISI C-1018/C-1020

REQ'D: 1

Figure E-12 Load Cell Adapter

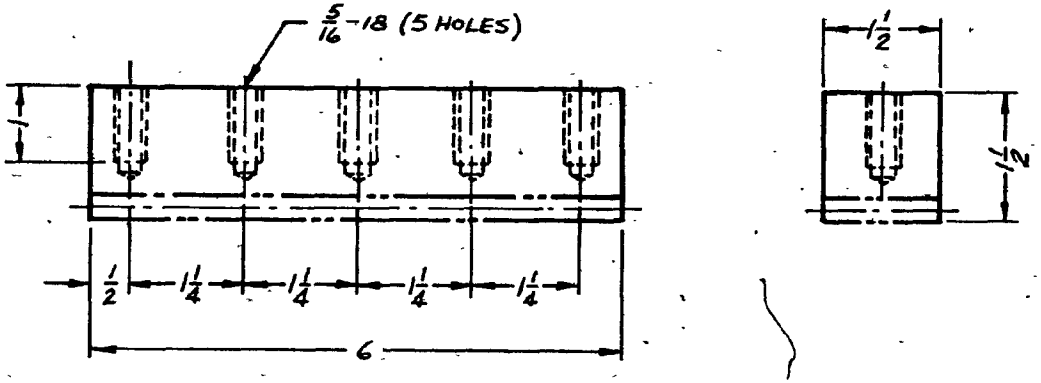

ITEM NO. 12

BOSTON GEAR: MODEL L208

REQ'D: 1

Figure E-13 Rack

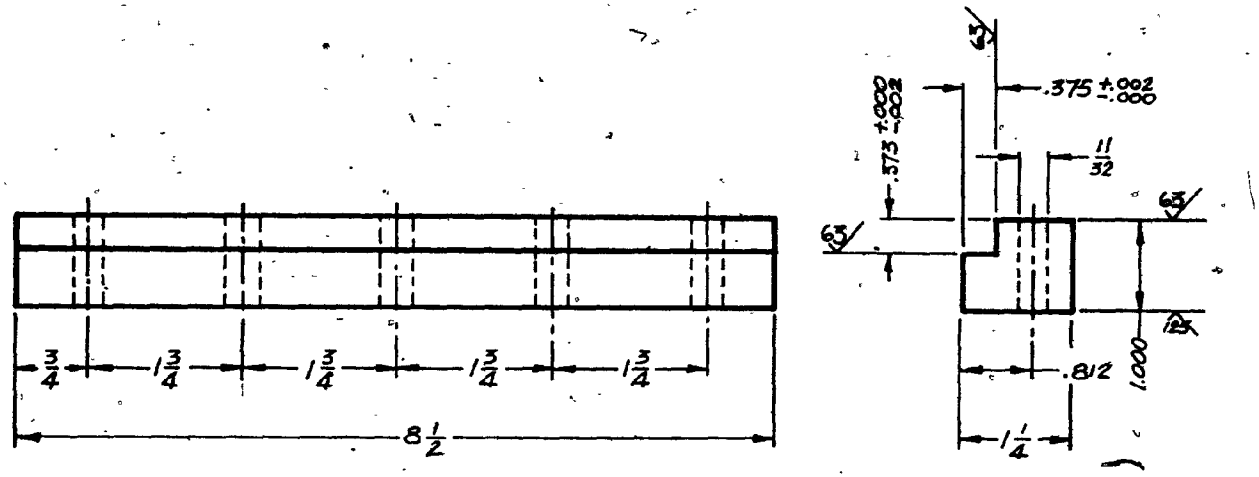

ITEM NO. 13

MATERIAL: AISI C-1018/C-1020

REQ'D: 1

Figure E-14 Sliding Guide

APPENDIX F

Equipement Description and Calibrations

Equipement Description and Calibrations

Rack and Pinion

The combination of rack and pinion is used for the generation of torque on the wafer shaft. Both of them are Boston Gear products and the specifications are

Gear Model	:	YH36
Diametral Pitch	:	8
Pressure Angle	:	20^{0}
Pitch Diameter	:	4.5"
Rack Model	:	L208
Diametral Pitch	:	8
Pressure Angle	:	20^{0}

Hydraulic Actuator

A hydraulic actuator force output is used for the simulation of flow force on the valve disk. The actuator chosen is manufactured by Parker Hannifin and the specifications are

model	:	2-H-2H142
max. pressure	:	3000 psi
Bore	:	2"
Stroke	:	2"

Cushioned on both sides

Hydraulic Power Supply

The hydraulic power supply used in this experiment is a variable displacement piston pump which is manufactured by Sperry Rand Vickers, and the specifications are

Theoretical Displacement	:	0.843 in^3/rev
Operating Speed	:	1800 rpm
Delivery at 1800 rpm	:	6.5 GPM
Operating Pressure	:	1000 psi max.
Case Pressure	:	5 psi
Minimum Inlet Pressure	:	12 psi

Servo Controller

The feed back controller, Moog model 122-105, is used to ensure the force generated by the actuator is the desired one. The schematic of the controller is shown in Figure F-1. Moog 122-105 controller contaips an operational amplifier input stage A_1, an operational amplifier current drive stage A_2, and a complimentary pair I F transformers Q_1, Q_2 for current boost. The input stage will accept multiple signals (terminals 2, 3, 4). Input stage A_1 may be used to provide either proportional or integral control. The output of stage A_1 is summed with an additional input, terminal 1, at the current drive stage A_2. This additional input allows an

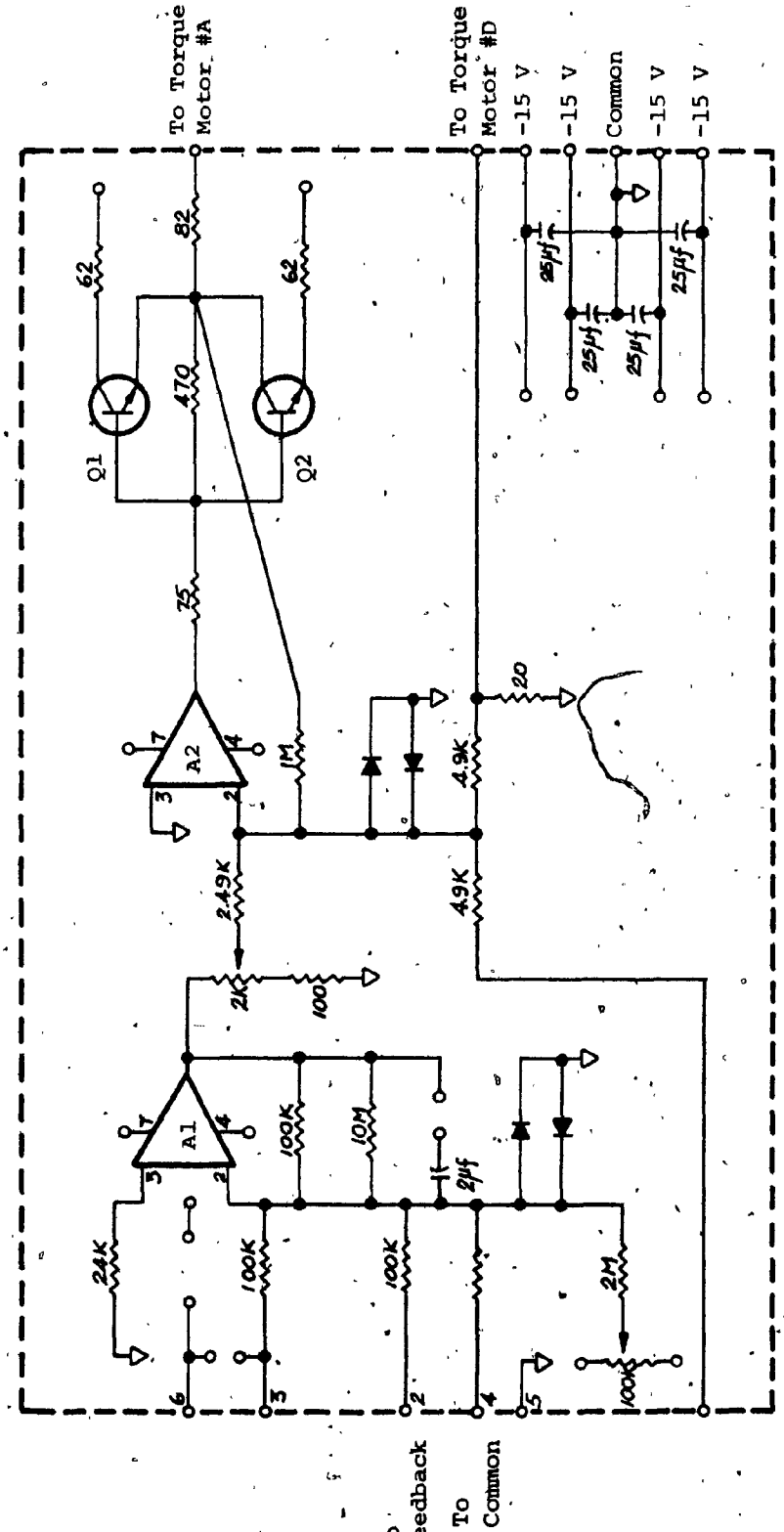

Figure F-1 Moog 122-105 Servo-Controller Schematic

inner loop feedback independent of outer loop gain and signal shaping. Terminals 7 and 8 are used for external connections and in this case, connected to the servo-valve.

Servo-Valve

A two-stage electro-hydraulic servo-valve, Moog 62-105, is used to control the input actuator. Servo-valves convert electric signal into a hydraulic output which controls the acceleration, velocity and position of the actuator. Figure F-2 shows the sectioned view of the servo-valve. A current difference (i_1,i_2) causes the speed to a new position directly proportional to the input current.

The hydraulic characteristics of the servo-valve can be described by the rate flow curves and the flow-load characteristics which are illustrated in figure F-3. Control flow rate to the load will change with load pressure drop and electrical input. The characteristics follow closely with the theoretical square-root relationship for a sharp edge orifice which is

$$Q_L = Ki\sqrt{P_v} \qquad (F.1)$$

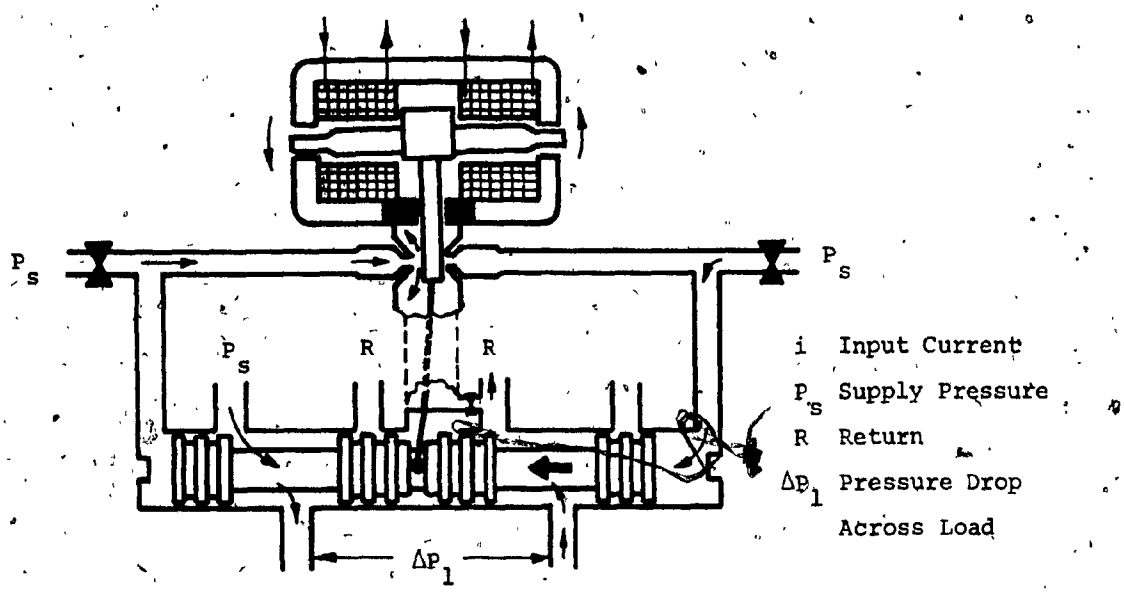

Figure F-2 Sectional View of Servo-Valve

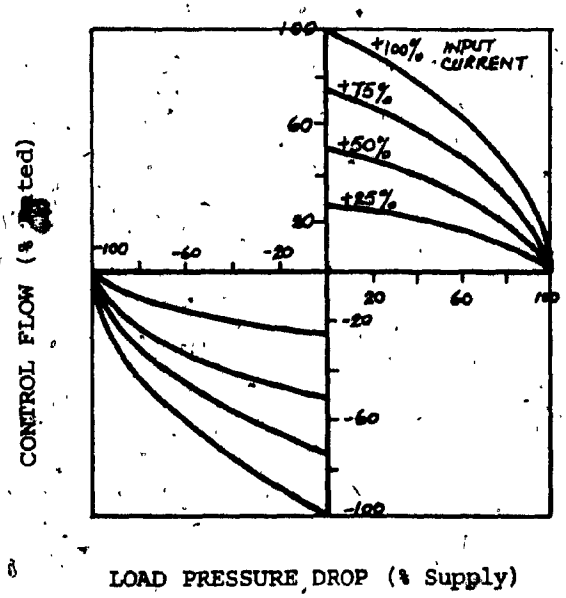

Figure F-3 Servo-Valve Flow-Load Characturistics

where Q_L = control flow

K = valve size constant

i = input current

P_v = valve pressure drop

The static performance of the valve can be shown by the flow plot figure F-4. The performance of the valve can be expressed by the frequency-response curve as shown in figure F-5. Generally, the dynamic response of servo-valves can be approximated by a second order transfer funtion with a damping ratio between 0.5 and 0.7. The Moog 62-105 servo-valve specifications are

Supply Pressure	:	200 psi minimum
		2000 psi maximum
Operating Temoerature	:	0 ^{o}F minimum
		200 ^{o}F maximum
Rated Flow	:	5.0 GPM @1000 psi valve drop
Internal Leakage	:	<0.4 GPM
Hysteresis	:	<6% @1000 psi
Linearity	:	<7%
Threshold	:	<2% @1000 psi
Pressure Gain	:	>20% supply 1% input

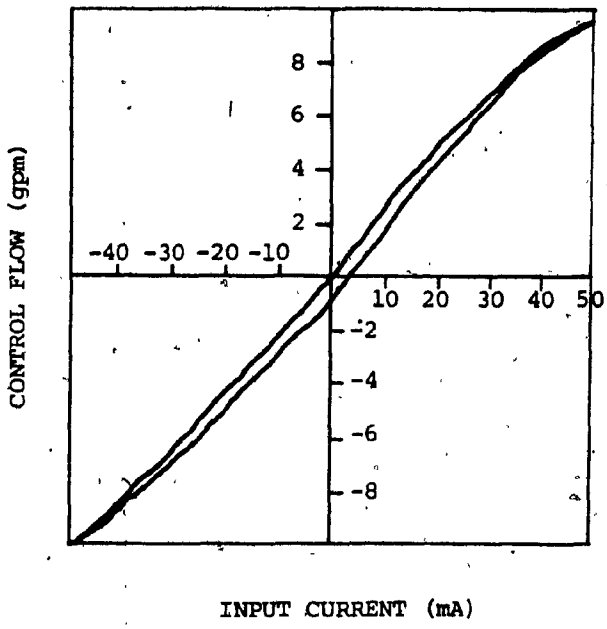

Figure F-4 Servo-Valve Flow Plot at 1000 psi supply

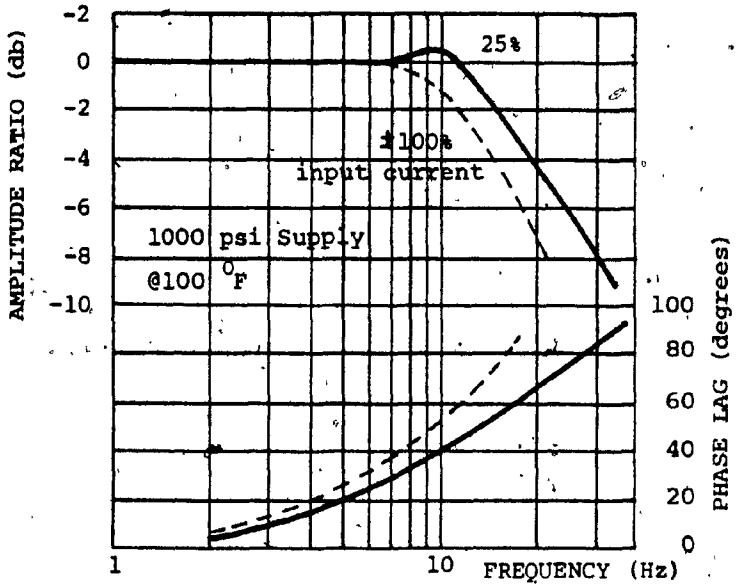

Figure F-5 Servo-Valve Frequency Response

Force Transducer

A strain gage load cell is used in this experiment as a force measuring device. A stain gage based transducer is a unit converting weight or force into an electrical output by virtue of the internal strain gage installation. The electrical output is then connected to different types of measuring instruments for indication.

Figure F-6 shows the simplified form of the strain gage transducer and its schematics. This type of load cell is capable of both steady and dynamic load measurements. The deformation of the load column of the transducer results in a strain at its surface. This strain is transmitted to the wire via the bonding cement, changing their resistance in accordance with the following relationship.

$$\frac{\Delta R}{R} = K\lambda = K\frac{\Delta L}{L} \qquad \text{(F-2)}$$

where ΔR = change in resistance of gage

R = original gage resistance

K = gage factor

λ = elogation per unit length

The force transducer used in this experiment is manufactured by Kulite Semiconductor Inc, model TC-3000 and the specifica-

Force Transducer

A strain gage load cell is used in this experiment as a force measuring device. A stain gage based transducer is a unit converting weight or force into an electrical output by virtue of the internal strain gage installation. The electrical output is then connected to different types of measuring instruments for indication.

Figure F-6 shows the simplified form of the strain gage transducer and its schematics. This type of load cell is capable of both steady and dynamic load measurements. The deformation of the load column of the transducer results in a strain at its surface. This strain is transmitted to the wire via the bonding cement, changing their resistance in accordance with the following relationship.

$$\frac{\Delta R}{R} = K\lambda = K\frac{\Delta L}{L} \qquad \text{(F-2)}$$

where ΔR = change in resistance of gage
R = original gage resistance
K = gage factor
λ = elogation per unit length

The force transducer used in this experiment is manufactured by Kulite Semiconductor Inc, model TC-3000 and the specifica-

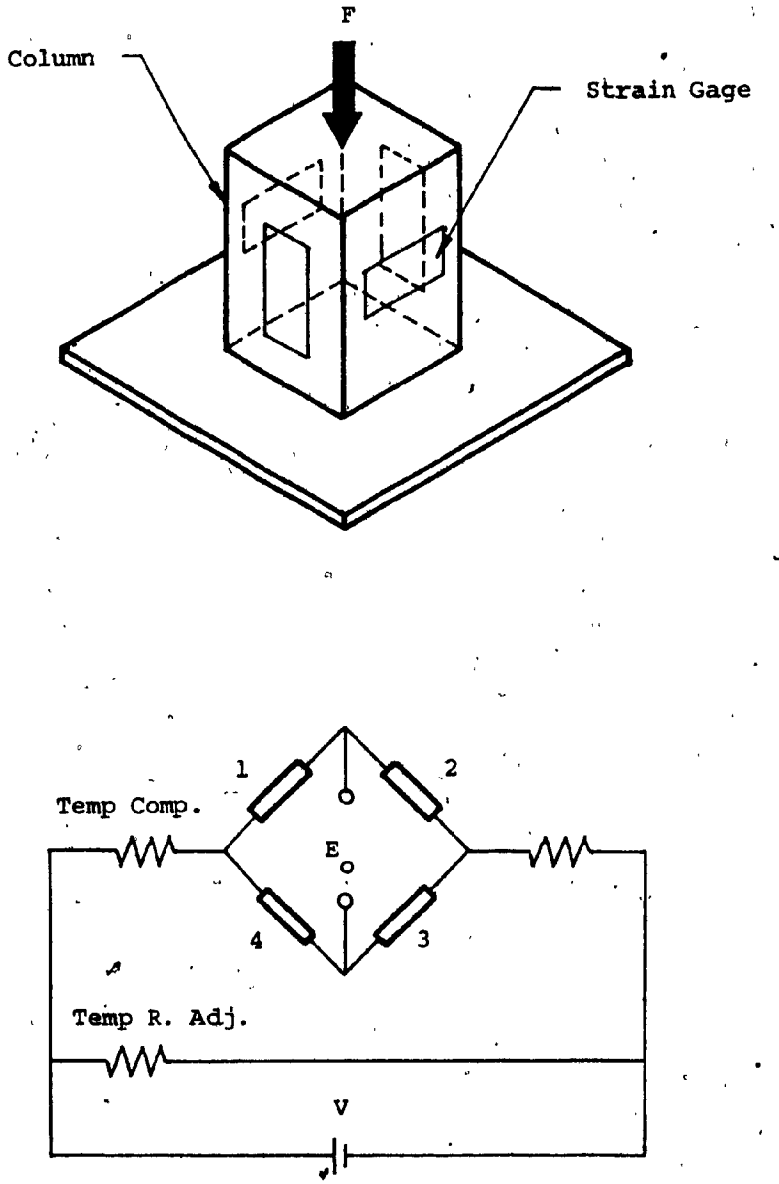

Figure F-6 Simplified Strain Gage and its Schematics

tions are

Rated Load	:	3000 lbs max 4500 lbs
Diaphram Thickness	:	0.160"
Nominal deflection	:	0.0001"
Natural frequency	:	30 KHz
Over load	:	150%
Operational mode	:	tension and compression
Rated electrical excitation	:	10 VDC/AC (RMS)
Input resistance	:	1535 ohms
Full scale output	:	138 mV FSO (nominal)
Output resistance	:	676 ohms
Residual Unbalance	:	±2%
Non-linearity	:	0.5%
Hysteresis	:	0.1%
Repeatability	:	0.1%
Temperature range	:	-40° F to 250° F

Differential Input Amplifier

The input signal from the force transducer is amplified by a Burr-Brown 3620 differential input amplifier. Figure F-7 shows the amplifier schematics. It is used to adjust the gain of the feed back signal for the servo-controller. The amplifier gain is governed by the equation

$$E_o = (1 + \frac{25 \times 10^3}{R}) E_d \qquad (F-3)$$

$$E_o = \left(1 + \frac{25K}{R}\right)(E_{d_1} - E_{d_2})$$

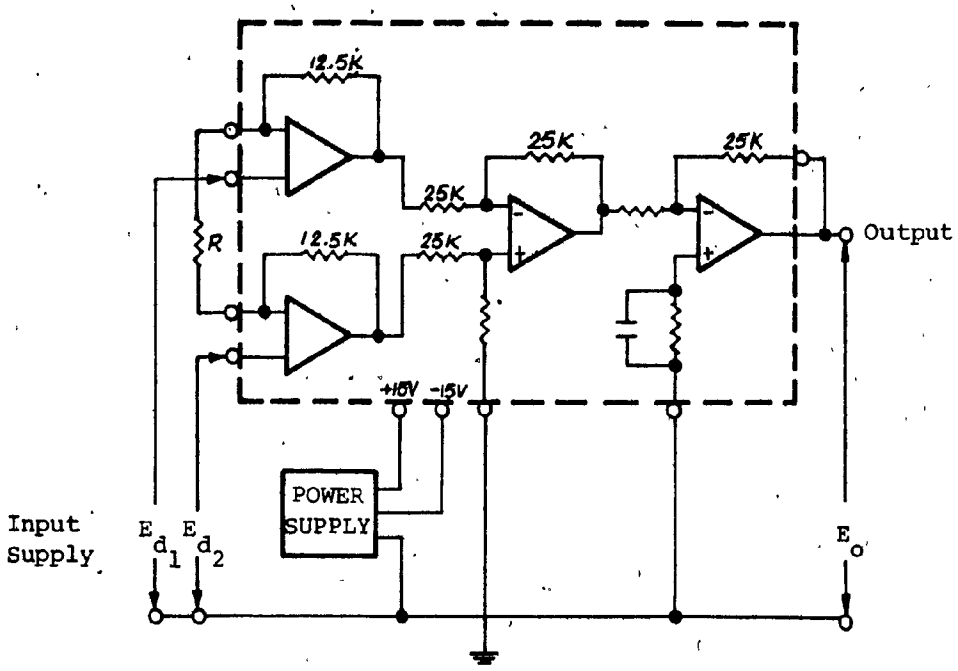

Figure F-7 Schematic Diagram of Differential Input Amplifier

where E_o = output voltage, mV

E_d = input differential voltage, mV

R = resistance, ohms

The specifications are

Rated output	:	$\pm$10 V, $\pm$10 mA
Input	:	$\pm$10 V
Dynamic response	:	5 KHz
Power supply	:	$\pm$15 VDC
Operating temperature	:	-40° C to 85° C

Calibration of the Force Transducer

A tensile testing machine with the capacity 60,000 lb by Tinius Olsen is used as standard in the calibration of the force transducer. Figure F-8 shows the pictorial view of the calibration set-up.

A zero reference point is taken when no load is applied to the transducer. A minimum scale reading is obtained on the recorder when the transducer is subject to a 2000 lb compression load. This can be done by adjusting the recorder gain while load increases gradually from 0 to 2000 lb. The suitable recorder gain is found to be 2.5 mV/cm. The calibra-

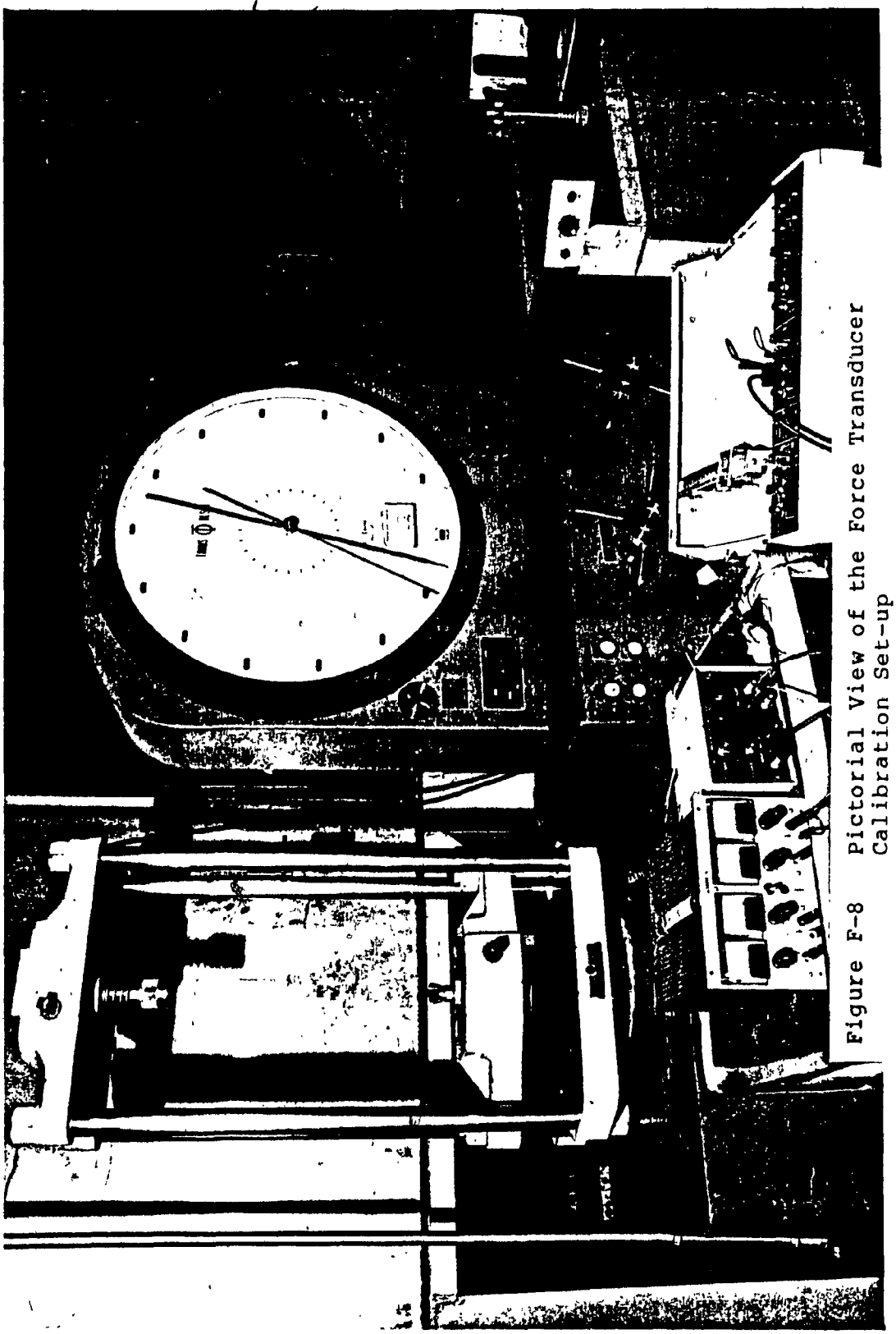

Figure F-8 Pictorial View of the Force Transducer Calibration Set-up

tion data, as shown in table F-1, are obtained by gradually increasing compressive load from 0 to 2000 lbs. The calibration curve plotted according to the data is shown in figure F-9 and the static gain K is found to be

$$K = \frac{50}{2000} \text{ mV} = 0.025 \text{ mV/lb} \qquad \text{(F-4)}$$

Calibration of the Differentiator

Differentiation is the process of finding instantaneous rates of change by finding the slope of a line tangent to the point of interest on the graph of a function. Figure F-10 shows a simple electronic differentiator using an operational amplifier.

The output amplitude of the valve disk which is operating from close, (0 rad) to open (1.0472 rad) is 4.45 V, as shown in figure F-11. A saw-tooth function of 4.45 V amplitude is used as an input of the differentiator. By varying the saw-tooth function frequency, the differentiator output characteristics can be obtained. Figures F-12, F-13 and F-14 show the effect of various input frequencies on the differentiator output. The differentiator calibration curve is shown in figure F-15.

lb_f	200	400	600	800	1000	1200	1400	1600	1800
mV	5.2	10.1	15.0	19.9	24.9	30.0	35.1	39.8	45.0

Table F-1 Force Transducer Calibration Data

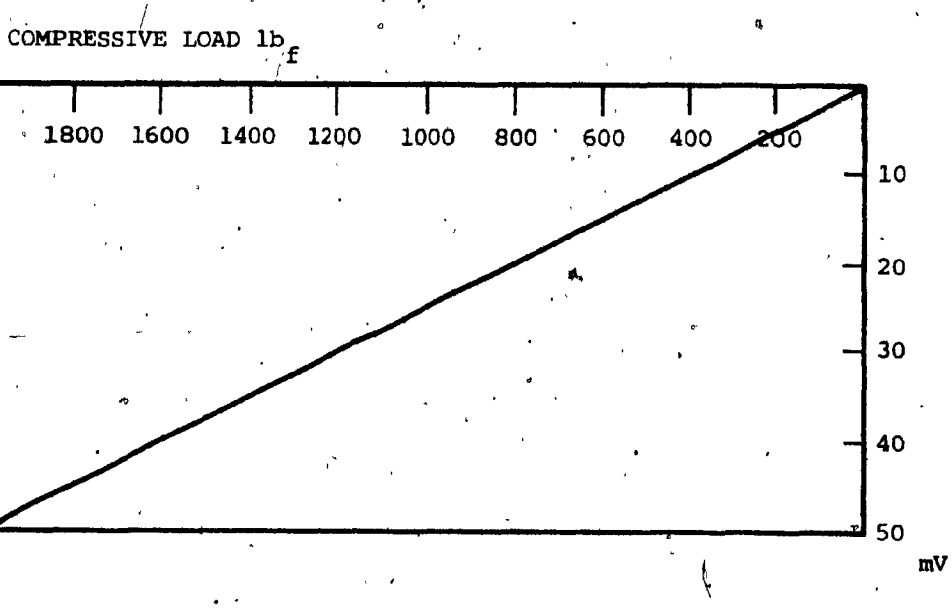

Figure F-9 Force Transducer Calibration Curve

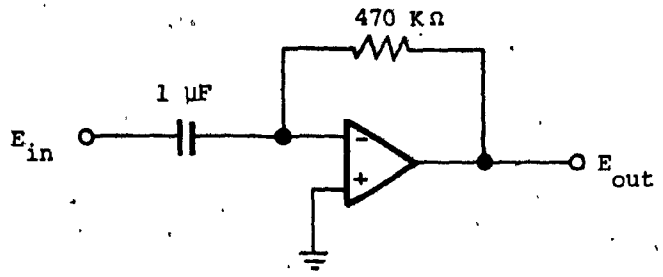

Figure F-10 Schematic of Differentiator

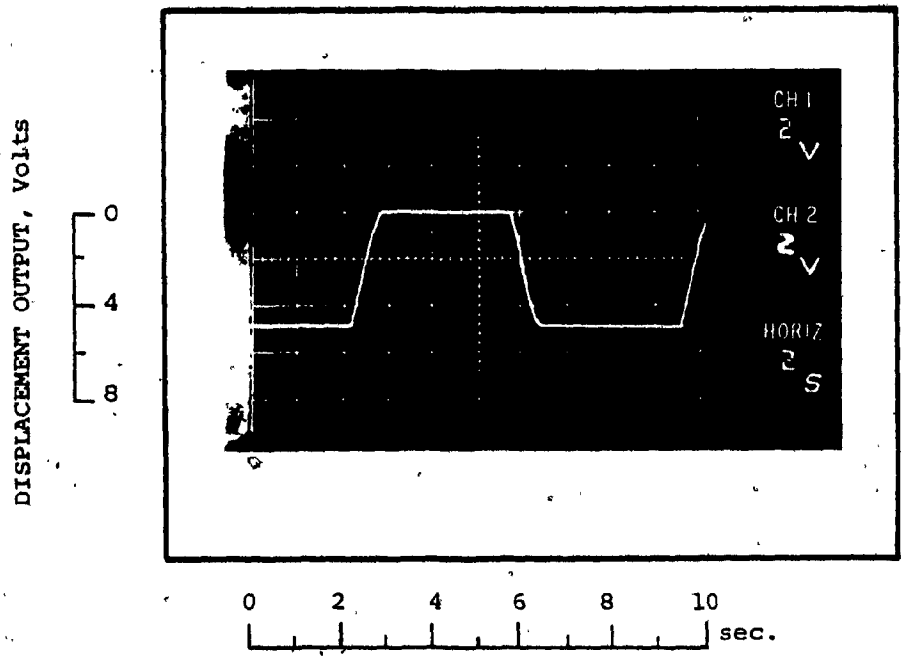

Figure F-11 Valve Disk Displacement Output Voltage

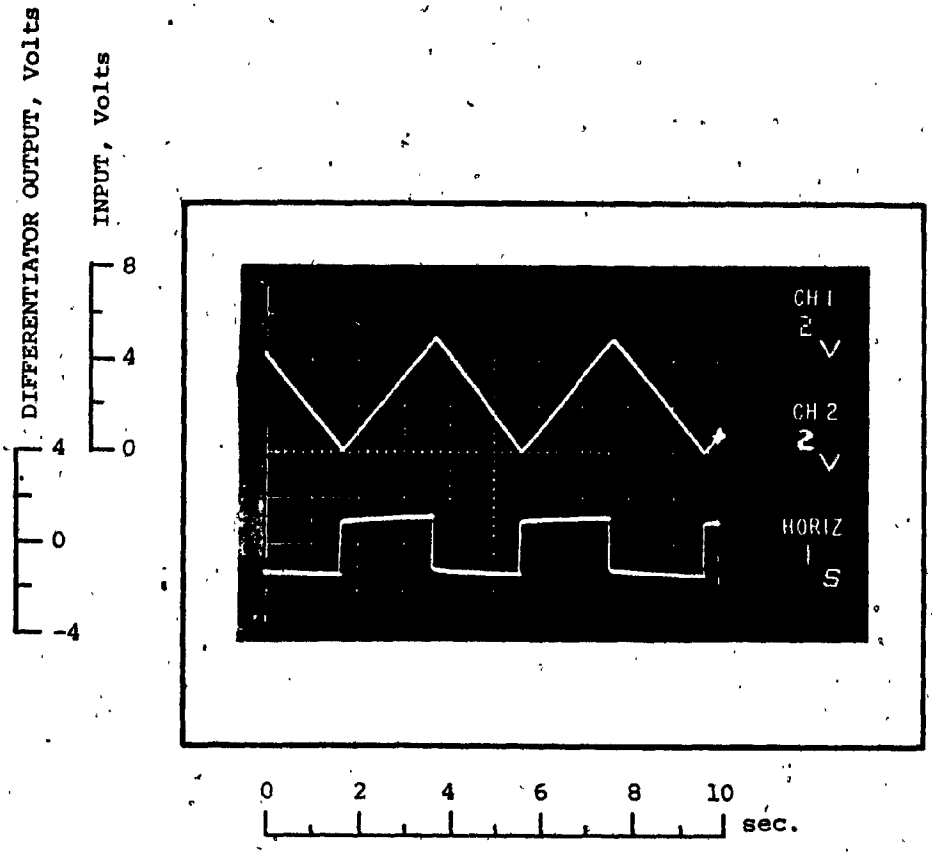

Figure F-12 Differentiator Output at 0.5236 rad/sec

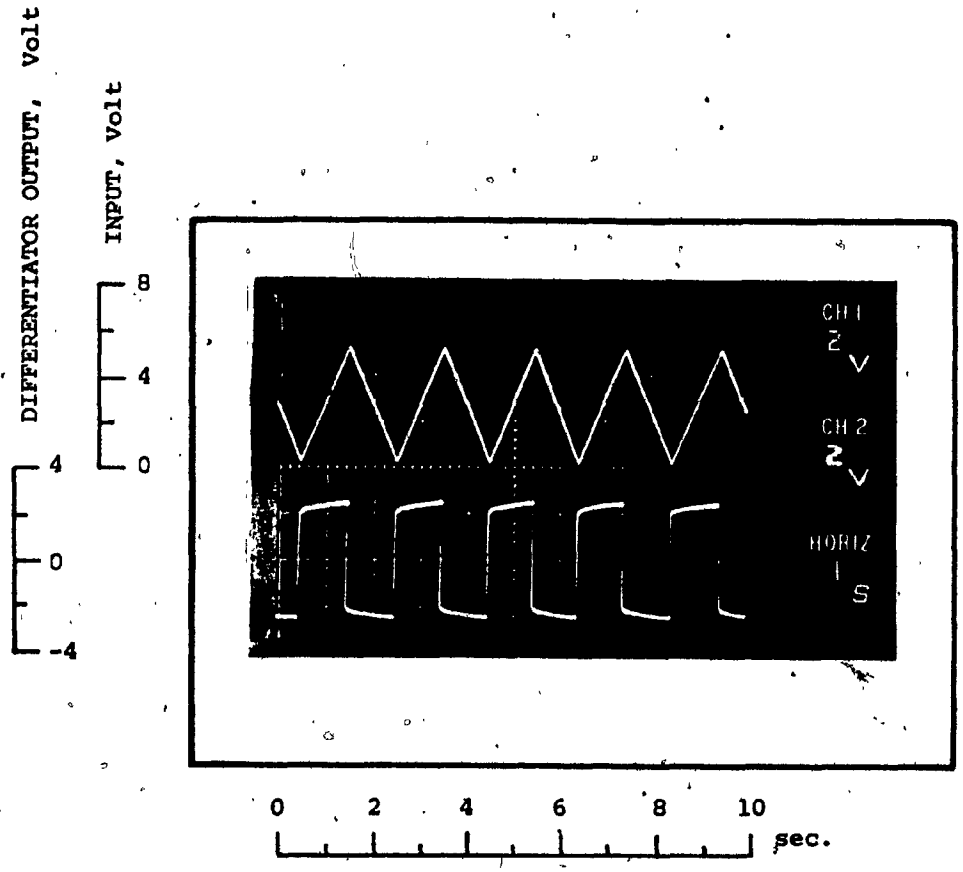

Figure F-13 Differentiator Output at 1.0472 rad/sec

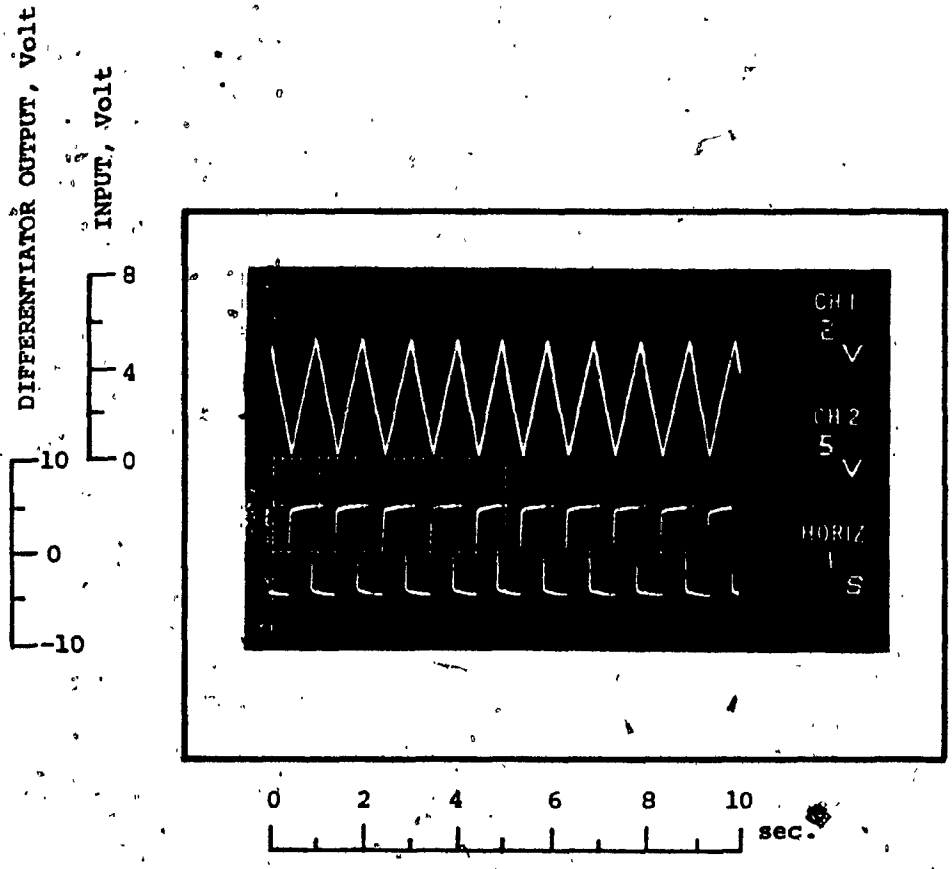

Figure F-14 Differentiator Output at 2.0944 rad/sec

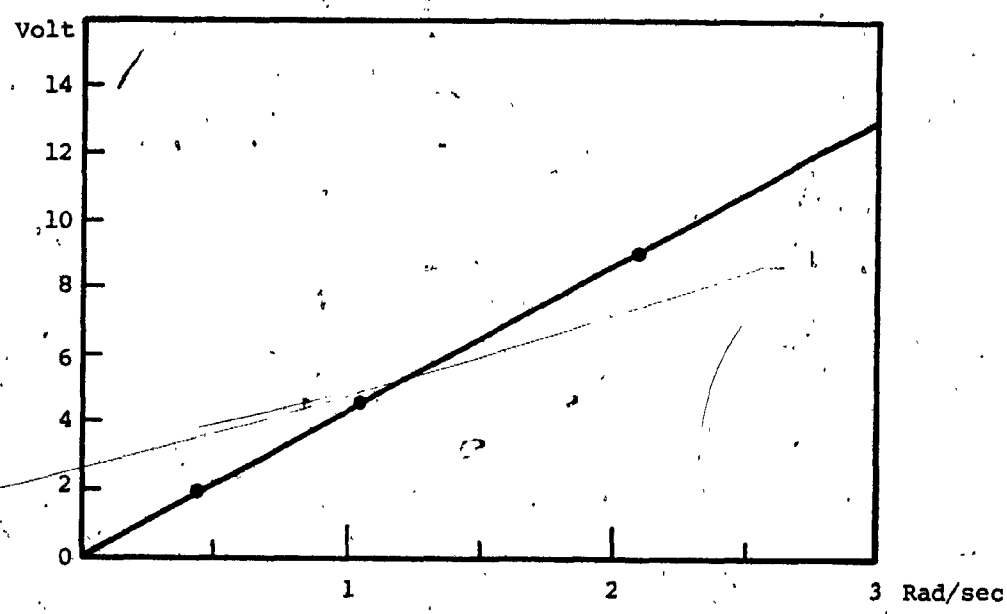

Figure F-15 Differentiator Calibration Curve

APPENDIX G

MIMIC Model of Hydro-Pneumatic Closing Valve with Experimentally found Cushioning Condition

```
*
*               DYNAMICS SIMULATION OF HYDRO-PNEUMATIC CLOSING
*               VALVE WITH EXPERIMENTAL FOUND CUSHIONING
*               CONDITION
*
*
*               INPUT FUNCTION GENERATOR
*
      FN1       CFN(6.)
*
*               INITIAL CONDITIONS
*
*               PAR(DTETA,TETA,ALFA,DY)
*
*               SYSTEM PARAMETERS
*
      VA0       30.
      PA0       85.
      A1        3.68
      A2        4.9
      J         1.
      RV        0.4
      RC        0.3
      RU        0.85
      RL        0.85
*
*               INPUT TORQUE FUNCTION
*
      TIN       FUN(FN1,T)
*
*               HYDRAULIC CYLINDER TORQUE AT ANGLE ALFA
*
      TCY       (P2*A2-P1*A1)*SIN(ALFA)*4.0
*
*               DISK ANGULAR ACCELERATION IS OBTAINED
*               FROM DIVIDING TORQUE DIFFERENCE BY INERTIA
*
      TDIFF     (TCY-TIN)/J
*
*               MAXIMUM ANGULAR DISPLACEMENT WHICH IS 1.0472 RAD.
*
      TEMAX     FSW(TETA-1.0472,FALSE,TRUE,TRUE)
*
*               MINIMUM ANGULAR DISPLACEMENT WHICH IS 0. RAD.
*
      TEMIN     FSW(TETA,TRUE,TRUE,FALSE)
*
*               POSITIVE ANGULAR VELOCITY
*
      PDTETA    FSW(DTETA,FALSE,FALSE,TRUE)
*
*               NEGATIVE ANGULAR VELOCITY
*
      NDTETA    FSW(DTETA,TRUE,FALSE,FALSE)
*
*               PHYSICAL LIMITATIONS
*               FIRST LIMITATION IS MAX. DISPLACEMENT
```

```
*                       AND POSITIVE ANGULAR VELOCITY
*                       SECOND LIMITATION IS MIN. DISPLACEMENT
*                       AND NEGATIVE ANGULAR VELOCITY
*
          LIMIT         IOR(AND(TEMAX,PDTETA),AND(TEMIN,NDTETA))
          RANGE         NOT(LIMIT)
*
*                       WHEN LIMIT CONDITION IS SATISFIED
*                       THE ACCELERATION IS SET TO ZERO
 LIMIT    TDIFF1        0.
 RANGE    TDIFF1        TDIFF
*
*                       TO FIND ANGULAR VELOCITY BY INTEGRATING
*                       ACCELERATION
*
 LIMIT    DTETA         0.
 RANGE    DTETA         INT(TDIFF1,0.,LIMIT,FALSE)
*
*                       TO FIND ANGULAR DISPLACEMENT BY INTEGRATING
*                       ANGULAR VELOCITY
*
          TETA1         INT(DTETA,TETA)
*
*                       THE ACCEPTABLE ANGULAR DISPLACEMENT VALUE
*                       IS FROM 0. TO 1.0472 RAD.
*
          SET1          FSW(TETA1,TRUE,TRUE,FALSE)
          SET2          FSW(TETA1-1.0472,FALSE,TRUE,TRUE)
          SET3          NOT(IOR(SET1,SET2))
 SET1     TETA          0.
 SET2     TETA          1.0472
 SET3     TETA          TETA1
*
*                       HYDRAULIC ACTUATOR DISPLACEMENT
*
          Y             SQR(76.999-62.482*(COS(.5877+TETA)))
*
*                       TO FIND ANGLE ALFA
*
          FN            (Y*Y-45.)/(8.*Y)
          ALFA          ACS(FN)
*
*                       HYDRAULIC ACTUATOR VELOCITY
*                       WITH PHYSICAL LIMITATIONS IN CONSIDERATION
*
 LIMIT    DY            0.
 RANGE    DY            62.482*SIN(0.5877+TETA)*DTETA/(2.*Y)
*
*                       ROD END FLUID FLOW RATE
*
          Q1            A1*DY
*
*                       PISTON END FLUID FLOW RATE
*
          Q2            A2*DY
*
*                       ACCUMULATOR FLUID FLOW RATE
```

```
            QA          Q2-Q1
*
*                       THE COMPRESSED GAS VOLUME IS OBTAINED
*                       BY INTEGRATING THE ACCUMULATOR FLUID FLOW RATE
*
            VA          INT(QA,30.)
*
*                       INSTANTANEOUS ACCUMULATOR PRESSURE
*
            PA          PA0*VA0/VA
            P1          PA
*
*                       POSITIVE ACTUATOR VELOCITY
*
            PDY         FSW(DY,FALSE,FALSE,TRUE)
*
*                       UPPER CUSHION REGION IS .75 IN. FROM THE END OF
*                       STROKE
*
            UPCU        FSW(Y-8.25,FALSE,FALSE,TRUE)
*
*                       THE P2 VALUE DEPENDS ON THE FLUID RESTRICTION
*
 PDY        P2          LSW(UPCU,P1-RU*Q2*Q2,P1-RV*Q2*Q2)
*
*                       NEGATIVE ACTUATOR VELOCITY
*
            NDY         FSW(DY,TRUE,FALSE,FALSE)
*
*                       LOWER CUSHION REGION IS .75 IN. FROM THE END OF
*                       STROKE
*
            LOCU        FSW(Y-5.75,TRUE,FALSE,FALSE)
            CU          EOR(UPCU,LOCU)
 UPCU       R1          RU
 LOCU       R1          RL
            R           LSW(CU,R1,RC)
*
*                       THE P2 VALUE DEPENDS ON THE FLUID RESTRICTION
*
 NDY        P2          P1+R*Q2*Q2
*
*                       FOR ZERO ACTUATOR VELOCITY P2=P1
*
            ODY         FSW(DY,FALSE,TRUE,FALSE)
 ODY        P2          P1
*
*                       OUTPUT TIME INTERVAL AND INTEGRATING TIME INTERVAL
*
            DT          0.05
            DTMAX       0.0005
            DTMIN       0.0005
*
*                       OUTPUT FORMAT
*
                        OUT(T,DTETA,TETA)
                        OUT(DY,Y,PA)
```